CIRCULATION COPY
SUBJECT TO RECALL
IN TWO WEEKS

UCID- 21328

Simulation of the Richtmyer-Meshkov Instability and Turbulent Mixing in Shock-Tube Experiments

Karnig O. Mikaelian
Lawrence Livermore National Laboratory
Livermore, California 94550

January 1988

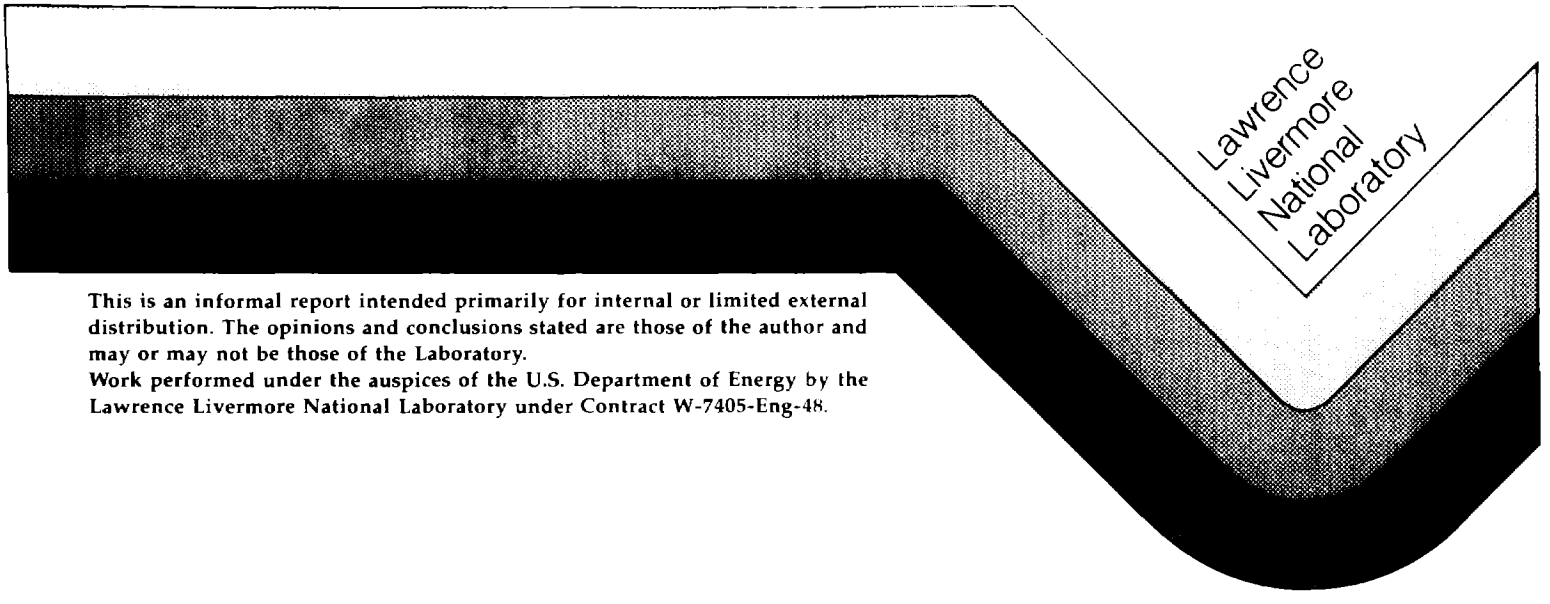

This is an informal report intended primarily for internal or limited external distribution. The opinions and conclusions stated are those of the author and may or may not be those of the Laboratory.
Work performed under the auspices of the U.S. Department of Energy by the Lawrence Livermore National Laboratory under Contract W-7405-Eng-48.

DISCLAIMER

This document was prepared as an account of work sponsored by an agency of the United States Government. Neither the United States Government nor the University of California nor any of their employees, makes any warranty, express or implied, or assumes any legal liability or responsibility for the accuracy, completeness, or usefulness of any information, apparatus, product, or process disclosed, or represents that its use would not infringe privately owned rights. Reference herein to any specific commercial products, process, or service by trade name, trademark, manufacturer, or otherwise, does not necessarily constitute or imply its endorsement, recommendation, or favoring by the United States Government or the University of California. The views and opinions of authors expressed herein do not necessarily state or reflect those of the United States Government or the University of California, and shall not be used for advertising or product endorsement purposes.

Printed in the United States of America
Available from
National Technical Information Service
U.S. Department of Commerce
5285 Port Royal Road
Springfield, VA 22161

Price Code	Page Range
A01	Microfiche
Papercopy Prices	
A02	001 - 050
A03	051 - 100
A04	101 - 200
A05	201 - 300
A06	301 - 400
A07	401 - 500
A08	501 - 600
A09	601

SIMULATION OF THE RICHTMYER-MESHKOV INSTABILITY AND TURBULENT MIXING IN SHOCK-TUBE EXPERIMENTS

Karnig O. Mikaelian
Lawrence Livermore National Laboratory
Livermore, California 94550

CONTENTS

I. INTRODUCTION

This is a report on our code calculations in support of shock-tube experiments that are now in progress at CalTech. The primary purpose of the experiments is to study the evolution of perturbations and the subsequent mixing when a shock passes through the interface between two gases. The Richtmyer-Meshkov[1,2](RM) instability causes initial, i.e. pre-shock perturbations at an interface between two fluids to grow after the passage of the shock, much the same way as the Rayleigh-Taylor[3](RT) instability acts in a constant gravitational field.

The compressible nature of the RM problem makes analytic treatment difficult. An "incompressible" theory, in which the shock is treated as an instantaneous acceleration, was given by Richtmyer[1] for the linear regime where the amplitude of the perturbation is much smaller than its wavelength. Direct numerical simulations and experiments are necessary to understand the fully compressible and non-linear nature of the problem.

The code that we have used is an Arbitrary Lagrangian-Eulerian (ALE) code in which rezoning is done automatically in zones satisfying certain requirements of skewness, etc. It also allows for mixed zones across an interface. An artificial viscosity is used for numerical stability in shock problems. More details about the code are given in Ref. 4

In the simulations we treat the walls as reflecting boundaries (free slip), hence we do not include any of the boundary layer effects which may be present in the experiments. Also, we simulate the full width of the tube, without imposing any symmetry around the center of the tube. Problems that start symmetric develop some asymmetry at late times, but not much.

In Fig. 1 we show a schematic of the shock tube and of the types of problems that we considered. A shock, of strength M_s=1.2 - 1.3, moves from air into a test gas which can be

helium, freon (or refrigerent R_{22}) or SF_6 . Helium is about 7 times lighter than air, while freon and SF6 are 4 and 5 times heavier than air respectively. The cross-section of the tube is 11.3cm × 11.3cm. We have also done calculations for a 9cm wide tube because an earlier shock-tube was approximately 9cm × 9cm. The length of the test-gas section can be varied, and of course it controls the time when the reflected shock crosses the interface. In practically all our calculations we considered a 60cm long helium section and a 30cm long freon or SF_6 section (a longer helium section is chosen because the shock is faster in that case). In a very recent experiment with SF_6 the length of the test section was 10cm - the simulation of that experiment is discussed in Sect. V.

The velocities of the air/helium and air/freon interfaces are shown in Fig. 2. In the 60cm long helium case it takes about 1ms for the reflected shock to hit the interface, while in the 30cm long freon case it takes about 2.4ms. We continue our calculations for approximately 1ms beyond the reflected shock.

We expect to carry out more detailed calculations in the future when experiments become available. Rather than concentrate on a few problems, we have here looked at a variety of possible experiments that can be done on a shock tube. It is important to understand this spirit in which the calculations reported here were carried out - to suggest ideas to experimentalists in this area. Of course we expect some, at least qualitative, agreement between future experiments and our calculations. As such, this report must be viewed more as work-in-progress than a finished effort. Once the experimental results become available we are prepared to do a much more detailed calculation . The one comparison discussed in Sect. V suggests that the code is doing a reasonable job.

Fig. 1 is also an outline of this paper. In Sect. II we treat single-scale perturbations where several identical bubbles are set up next to each other. Experiments of this type were performed in an earlier shock-tube at CalTech, but the initial conditions were not well-characterized, in particular the initial amplitudes were not measured ; they will be repeated in the new shock-tube. The single-scale perturbations may be set up at the air/helium, air/freon, or air/freon/air interfaces. In Sect. III we consider double-scale experiments in which a large bubble is set up

next to smaller ones. The idea here is to measure and compare the growth of different size bubbles, particularly in the non-linear regime. In Sect. IV we consider multi-scale and random perturbations at various interfaces. Here we want to measure how the mixing evolves from very small perturbations. In Sect. V we simulate a recent experiment[5] and discuss variations of it; both large and small scale perturbations at a diffuse air/SF_6 interface were involved in this experiment. Finally, in Sect. VI, we present a few conclusions and remarks.

II. SINGLE-SCALE PERTURBATIONS

A. Air/Helium

Fig. 2(a) shows the velocity of the air/helium interface as a shock of Mach number $M_S = 1.2$ passes from air into helium, reflects off the end wall, and recrosses the interface. For the 60cm long test section, this takes approximately 1ms, and we follow the motion of the interface for another millisecond, and then stop the calculation, just as a second reflected shock is about to cross the interface.

The gross features of perturbations at the air/helium interface are easy to predict: since helium is approximately 7 times lighter than air, the Atwood number A, where

$$A = (\rho_{testgas} - \rho_{air}) / (\rho_{testgas} + \rho_{air}) \qquad (1)$$

is -0.75. Upon the passage of the first shock, perturbations will change phase and then grow, which happens whenever a shock "sees" a negative Atwood number. The reflected shock, moving from helium to air, sees a positive Atwood number and simply adds to the growth rate without causing a phase change.

The evolution of a single cosine perturbation is shown in Fig. 3, with the arrows indicating the incident and reflected shocks.. The initial amplitude $\eta(0)$ was 0.2cm, i.e. peak-to-valley distance was 0.4cm. These snapshots confirm the expected gross features of phase reversal and subsequent growth.

More quantitatively, we plot in Fig. 4(a) the following variables: R_{1D}, the position of the interface with no perturbations; R_B, the position of the bubble; and R_S, the position of the spike, as functions of time. In Fig. 4(b) we plot the bubble amplitude $\eta_B = R_B - R_{1D}$ and the spike amplitude $\eta_S = R_S - R_{1D}$. Note that cross-over time, when $\eta_S = \eta_B = 0$, is about 0.2ms, corresponding to the second snapshot in Fig. 3. The spike, i.e. the heavy air "falling" into

helium, continues to grow after each shock. The bubble, i.e. the light helium "rising" towards the heavier air, also grows after each shock, albeit at a slower rate than the spike. It is interesting that the general shape of bubbles and spikes is strongly reminiscent of the classic Rayleigh-Taylor instability.

The interface assumes this non-linear shape after the reflected shock crosses the interface. Up to that time it preserves its cosine shape, i.e.

$$\eta(x,t) = \eta(t)\cos(kx) \qquad (2)$$

with $\eta(t)$ given approximately by Richtmyer's formula

$$\eta(t) = \eta(0)(1 + Ak\Delta vt). \qquad (3).$$

This equation ignores compressional effects because it is derived from incompressible Rayleigh-Taylor theory(see Ref. 1), and we will see that it overestimates the growth rate. At issue is the value of the initial amplitude $\eta(0)$ and, to a lesser degree, of the Atwood number A: should one use their pre-shock or post-shock values, or, as suggested in Ref. 6, an average over their pre-shock and post-shock values? Either prescription is phenomenological, but it is clear that compression will reduce $\eta(0)$. Let us point out that the cross-over time, i.e. the time when $\eta(t) = 0$, is independent of $\eta(0)$ and, from Eq.(3),

$$t_{cross\text{-}over} = -(Ak\Delta v)^{-1}$$

To compare with our 2D calculations, we will replace Δvt by Δy, the distance travelled by the interface after the first shock; hence

$$\Delta y_{cross\text{-}over} = -\lambda/(2\pi A) . \qquad (4)$$

We have checked this relation by changing the initial amplitude by factors of 2 and 4 and noticing that the cross-over time or distance is indeed the same in all three cases. For the case shown in Fig. 3, i.e. λ = 10cm, Eq.(4) gives $\Delta y_{cross\text{-}over}$ = 2.1 cm, in fair agreement with the 2.5 cm seen in Fig.3(b).

Between the incident and reflected shock the interface covers a distance of 14.5 cm. Writing Eq.(3) as

$$\eta(\Delta y) = \eta(0)(1 + Ak\Delta y) \qquad (5)$$

we obtain $\eta(14.5) = 0.2 \times (1 - 0.75 \times 2 \times \pi \times 14.5/10) = -1.17$. From Fig. 3(d) we see that $\eta_B = 0.75$cm and $\eta_S = -0.90$cm, somewhat smaller, presumably because of compression, than calculated. The asymmetry between bubble and spike is a well-known non-linear effect.

That asymmetry is further amplified after the passage of the reflected shock, as we see in Fig. 3(e) and 3(f). By the end of the problem, $\eta_B \approx 1.6$cm while $\eta_S \approx -3.4$cm. This "saturation" of the bubble amplitude is reflected in its slower growth rate as seen in Fig. 4.

We now study the dependence on the initial amplitude $\eta(0)$. Just as the asymmetric evolution of bubbles and spikes is an indication of non-linear effects, an even clearer indication is when our results stop being proportional to the initial amplitude. Fig. 5 shows the air/helium interface at t=1.9ms as it evolves from three different initial amplitudes: $\eta(0)$=0.2cm, 0.4cm, and 0.8cm. While the initially larger perturbations do evolve into larger bubbles and spikes, the results are far from being proportional to $\eta(0)$: as we double and quadruple $\eta(0)$, the bubble amplitude at 1.9ms increases only by a factor of 1.3 and 1.6, while the spike amplitude increases by a factor of 1.5 and 2 respectively. Note that the asymmetry between bubble and spike increases as we increase $\eta(0)$.

Instead of varying the magnitude of $\eta(0)$, one might change its phase, i.e. let $\eta(0) \rightarrow -\eta(0)$ (This is experimentally easy to do). Of course one merely interchanges the location of the bubbles and the spikes. Since there is a large asymmetry between bubbles and spikes in the non-linear regime, the visual effect can be quite impressive. In Fig. 6 we compare the late time isodensity contours for two problems one of which started with $\eta(0) = 0.2$cm and the other with $\eta(0) = -0.2$cm.

From the variations in $\eta(0)$ we now turn to study variations in λ . Wavelengths shorter than the tube width are set up by a set of wires across the thin membrane. This procedure gives a bowed membrane shaped more like a parabola than a cosine. While there are differences between these two shapes at early times,we find that at late times the differences are rather small. We have checked this by running several examples with a cosine or a parabola whose peak-to-valley distances were the same. For example, in Fig. 7 we show the interface at 1.9ms for these two cases. The parabolic shape evolves somewhat slower than the cosine and the spike is wider, suggesting that the effective λ for a parabola of width D is somewhat larger than D, but not by much. Of course, in comparing with experiments we will use parabolas.

The case shown in Fig. 7 was for the longest wavelength, i.e. the width of the tube. For the higher harmonics the difference between a cosine and a parabola is even less because the shorter wavelengths get more quickly to the non-linear regime where the exact shape of the initial perturbation matters less. In discussing the higher harmonics we will show only the parabolic cases.

Figs. 8 and 9 show the evolution for 2 and 4 parabolas respectively. The times chosen for these snapshots match those of Fig. 3. As expected from linear theory, the early growth of shorter wavelengths is faster because $d\eta/dt \sim 1/\lambda$, but note that they saturate earlier and by t=1.9ms the differences between 1,2 or 4 parabolas , all starting with the same peak-to-valley amplitude of 0.4cm, are rather small. In Fig. 10 we show isodensity contours of these three cases.

Finally, we ran a couple of calculations with a stronger shock: M_s=1.5. The purpose was to check the scaling w.r.t. the jump velocity Δv, which approximately doubles by going to this faster shock. The problems were single cosine perturbations as in Fig. 3, one with $\eta(0)$=0.2cm and the other with $\eta(0)$=0.4cm. First, we checked that the cross-over distance was the same, ~2.5cm, in fair agreement with Eq.(4), in all cases Second, we compared the interface after it had travelled a distance of 14.5cm and again the shapes were similar between a Δv=14cm/ms and a Δv= 30cm/ms shock. We ran the faster shock problem a little beyond the time where a second reflected shock goes through the interface, inducing further growth. In Fig. 11 we show the evolution of this faster shock

problem which started with $\eta(0)$=0.4cm. Note that the vertical distance (12cm) in these snapshots is twice the distance in the earlier ones.

B. Air/Freon

We now replace the test gas by freon, 30cm long. The velocity of the air/freon interface was shown in Fig. 2(b): after passing through the interface the shock takes about 2.4ms to reflect off the end wall and re-cross the interface. Since $\Delta v_{interface}$=7.5 cm/ms, the interface travels approximately 18cm during this time.

The gross features of the perturbations are once again easy to predict: freon being heavier than air, the first shock merely increases the perturbations as in the classical RT instability: light fluid (air in this case) pushing on heavier fluid(freon in this case). During the 2.4ms that it takes for the shock to come back the perturbations may evolve into the non-linear regime depending on their initial amplitude and wavelength. In any case the reflected shock, going from heavy-to-light, will change the phase of the perturbations. If by that time they have reached the non-linear regime then the phase-reversed perturbations can look quite different from the initial perturbations and only the periodicity of the pattern will be preserved.

The evolution of a single wave is shown in Fig. 12. The initial amplitude was 0.2cm, and it grows to about 1.2cm by the time the reflected shock arrives there. This growth by a factor of 6 is somewhat smaller than the 7-8 fold increase predicted by Eq.(2), where we take $\Delta vt = \Delta y$ = 17cm, $k=2 \times \pi/10 cm^{-1}$, and A=0.6. The discrepancy is probably due to the compression of the initial amplitude, as suggested by Richtmyer.

The bubble-and-spike formation in the non-linear regime is similar to the air/helium case: bubbles grow slower than spikes (note that in this problem the spikes are near the walls). In Fig.13(a) we show the 1D position of the interface and the locations of the tips of the bubble and the spike as functions of time. The amplitudes are shown in Fig. 13(b).

There are differences between the air/helium and air/freon cases stemming primarily from the different densities of helium and freon. The first order difference is obviously in the jump velocity Δv, which to some extent can be taken care of by scaling time proportionally, i.e. using $\Delta y = \Delta v t$ as the independent variable instead of time. Better yet, use $A\Delta y$. To account for the sign of A, allow a distance of $2\Delta y_{cross\text{-}over}$. These prescriptions are exact in the linear regime : Eq. (5) is invariant under $A \rightarrow -A$, $\eta(0) \rightarrow -\eta(0)$, and $\Delta y \rightarrow \Delta y - 2\Delta y_{cross\text{-}over}$. While Eq.(5) obviously fails in the non-linear regime, the scaling it suggests may be used to compare the evolution of perturbations in different gases or fluids.

One difference not predicted by this scaling law is the difference in the shape of the interface - there is more mushrooming at lower Atwood numbers. By mushrooming we refer to the spreading and roll-up of the wings of the spike; a clear example is seen in Fig.11(d). The existence of mushrooming, and its inverse correlation with Atwood number, reinforces the similarities between RT and RM instabilities.

To illustrate this point, we show in Fig. 14 the air/helium and air/freon interfaces for the cases when they started with identical perturbations, and moved about 12cm after the first shock (According to the scaling arguments above, this distance should slightly favour the air/helium case because the ratio of the Atwood numbers 0.75/0.60 times Δy more than compensates for the difference $2\Delta y_{cross\text{-}over}$). In Figs. 14(a) and 14(b), λ= 5cm, and the peak-to-valley distances are about 2cm in both cases, and the shapes are not too dissimilar, though one can observe the beginning of mushrooming in Fig. 14(b). The mushrooming is highly obvious in the shorter wavelength case, λ=2.5cm. Though total peak-to-valley or bubble-to-spike distances are roughly the same in both cases(about 2.5cm), the shapes are quite different. The air/helium case also also developes mushrooms as shown in Fig.9, but it happens much later.

Finally, we turn to the possibility of "freeze-out". As discussed in Ref.7, in a two-shock system it is possible to freeze the amplitude. In a shock tube, where the second shock is a reflected shock, it is clear that freeze-out is extremely difficult in the air/helium combination (the reflected shock must come before the initial amplitude changes phase - see Fig. 3(n) in Ref.7), but it is possible, in principle , in the air/freon combination where the

amplitude, instead of reversing its phase and overshooting after the passage of the second shock, merely stops growing (this is the case indicated by Fig. 3(c) in Ref.7). Applying that analysis here, we see that freeze-out will not occurr in shock tubes with solid end walls because the reflected shock is stronger than the first, i.e. $|\Delta v_2| > |\Delta v_1|$, where $\Delta v_{1,2}$ refers to the jump velocity of the interface induced by the first and second shocks respectively (in the case considered here Δv_1 = 7.5cm/ms and Δv_2 = 10cm/ms, as shown in Fig.2(b)). The reason why a weaker second shock is required for freeze-out is simple: freeze-out occurs when the growth rate induced by the second shock cancels exactly the growth rate induced by the first shock. Since the growth rate is proportional to the product of the jump velocity and the amplitude at the time the shock passes thru, one must have a weaker second shock to compensate for the fact that the amplitude grows in-between shocks (changes in Atwood number are small). Of course if $|\Delta v_2| < |\Delta v_1|$ the interface will keep moving, albeit slower, in the same direction as the original shock. Such a situation may be possible with some kind of a shock absorber instead of a solid wall at the end of the tube. Even then a delicate timing, achieved by a judicious choice of the length of the test section, is needed:

$$\Delta t = \frac{|\Delta v_1| - |\Delta v_2|}{|A\, k\, \Delta v_1 \Delta v_2|} \qquad (6)$$

where Δt is the time between the 1st and 2nd shocks. For the present set up we have Δv_1=7.5cm/ms, A=0.6, and $k=2\pi/10 cm^{-1}$ for a single wavelength across the tube. If $|\Delta v_2|$ can be reduced to 2cm/ms, then we find $\Delta t \approx 1$ms. This would freeze the amplitude after it has grown to about 4 times its initial value. The timing is independent of the actual value of that amplitude.

C. Air/Freon/Air

While there are only 2 basic possibilities in 2-fluid experiments (positive and negative Atwood numbers) there are 4 basic combinations in 3-fluid experiments which have two interfaces: ++, --, -+, and +-, where ± refers to the Atwood number at each

interface. For example, air/freon/helium would be the +- combination. We have simulated a special case of the +- combination, air/freon/air because of its symmetry and because this combination is similar to a heavy shell in ICF capsules which is surrounded by lighter fluids (a staging fluid on one side and fuel gas on the other).

Another parameter that is introduced by going to 3-fluid experiments is the thickness of the middle layer. Finally, one can impose perturbations on either one or both interfaces. Clearly, a large variety of experiments can be done in this category.

To be specific, we chose a 4cm thick layer of freon which is 60cm away from the end of the tube, a section taken to be filled with air as shown in Fig. 15(a) (The width in these calculations was taken to be 9cm). The shocked layer of freon is compressed to 3cm and travels at about 10cm/ms. The shock takes 2.5ms to return, so the freon layer travels about 25cm before it meets the reflected shock. The calculations are stopped approximately 1ms after this time. In Fig. 15(b) we show the positions of the upper and the lower surfaces of freon as functions of time.

In Fig. 16 we show the evolution of the freon layer which starts with a single cosine perturbation of amplitude 0.2cm on its upper surface. This is clearly the simplest case of 3-fluid experiments which may be analytically treated, as discussed below. We are particularly interested in the phenomenon of feed-thru, whereby a perturbation from one interface feeds through to another interface. In Fig. 16 we see the lower interface, which starts perfectly flat, acquiring some perturbations as a result of feed-thru from the upper surface. As expected, this secondary perturbation is further amplified upon the return of the reflected shock.

Before we turn to other variations, of which there are many, let us discuss simple analytical approaches to this problem We will limit ourselves to the linear regime because, as far as we know, there is no analytic treatment of the non-linear regime even for the case of a single interface, let alone two interfaces. This is not a bad assumption for a good period of time because the amplitude stays small relative to the wavelength, at least until the reflected shock comes through.

The simplest approach would have been to treat each interface separately. While this may be acceptable for the

initially perturbed upper interface, it clearly fails for the lower interface where the whole effect comes from feed-thru or interface-coupling (we use these terms interchangeably). The coupling serves to seed perturbations at the lower interface which grow "on their own" after the second shock.This is not to say that there is no interface coupling after the second shock (in fact there is more of it-see Fig. 16), but the point is that an independent treatment of the interfaces would predict absolutely no perturbations at the initially flat lower interface and miss the necessary seed that fuels the later growth.

An analytic treatment of interface coupling in RM instabilities was given in Ref.7, again treating the shock as an instantaneous acceleration. The simplest case is that of a fluid layer immersed in a "massless" gas, which is somewhat similar to the freon layer in air considered here. To leading order in $e^{-k\Delta l}$, where Δl = thickness of the fluid layer, we obtain

$$\eta_{upper} = \eta(0)(1 + k\Delta vt) \tag{7}$$

$$\eta_{lower} = 2\eta(0)e^{-k\Delta l}k\Delta vt \tag{8}$$

We dropped higher order corrections to these equations because $e^{-k\Delta l}$ = (6-12)% when we take $k=2\pi/9cm^{-1}$ and Δl=(3-4)cm. Complete expressions are given in Ref.7.

To this order, Eq.(7) describes the perturbation at the upper interface evolving independently. Interface coupling is of order $e^{-k\Delta l}$. One must remember that to obtain simple expressions the upper and lower surfaces are assumed to have $A = \pm 1$. Nevertheless, we will compare the ratio $\eta_{lower}/\eta_{upper}$ at Δvt=20cm. Eqs.(7) and (8) predict 0.7cm/3cm = 0.2 , while from the 2D calculation shown in Fig. 16 we obtain 0.3cm/1.6cm = 0.2. Eqs.(7) and (8) predict too large a value for the individual values of the amplitudes which is not surprising because the actual Atwood number is 0.6, but the ratio $\eta_{lower}/\eta_{upper}$ seems to be given fairly accurately. This ratio is the same whether we use the pre-shock or post-shock amplitude $\eta(0)$, but it does depend on the thickness Δl used in $e^{-k\Delta l}$. The ratio 0.2 is obtained by using the post-shock vaue Δl=3cm. It goes down to about 0.1 if the pre-shock value Δl=4cm is

used. Clearly, there is less interface coupling across a thicker layer, but it is not clear if the exponential drop-off with thickness is correct. We have to study these and related questions elsewhere.

The choice of an initially 4cm thick layer was motivated by the following: to see interface coupling the ratio $\Delta l/\lambda$ must not be too large, i.e. the layer must not be too thick relative to the wavelength. Higher harmonics, as discussed below, have shorter wavelengths and therefore require thinner layers for this purpose. On the other hand, to survive the shocks the layer must be relatively thick. We found that 4cm of freon fulfilled both requirements in our calculations.

In Fig. 17 we show the case where both upper and lower interfaces of the freon layer are bowed initially in the same direction (these shapes are parabolic). By the end of the problem, approximately 1ms after the reflected shock, we see the freon layer has turned into a bubble that is breaking off the side walls.

In Fig 18 we show another case: the lower interface is flat (as in Fig.16), but the upper interface has two wavelengths of perturbations. Experimentally, this would be done by trapping freon gas between two membranes, the upper membrane having a thin wire running through the middle, and by slightly increasing the pressure in the upper air layer to bow the upper membrane into the shape shown in Fig. 18(a). The opposite case, where the lower membrane is bowed with the opposite phase, is shown in Fig. 19.

The reflected shock is not much weaker than the first shock, so the freon layer almost comes to rest in all cases. This has obvious experimental advantages: the layer of interest remains within the detector window for a long time. Also, since there is almost no net flow, we expect that wall/boundary effects will be suppressed. To the extent that the shocks are the same, the difference between the two cases where the perturbations are on the upper or on the lower layer reflects the difference between a perturbation first growing then phase reversing and vice versa.

Comparing Fig. 18 and 19 one may conclude that the side which starts with an initial perturbation ends up having larger perturbations than the side with no initial perturbations. This is probably true in systems subjected to shocks only. In systems

where shocks and constant accelerations are combined, as in ICF capsules, one can find cases where it is no longer true that the surface which starts smoother ends up smoother. Several examples are given in Ref. 7.

Figs. 16,18 and 19 show an unbroken, albeit curved, layer of freon up to 3.5ms after the first shock. Only when perturbations of the same amplitude (0.2cm) are set up on both interfaces, as in Fig. 17, do we see the layer beginning to break up. We will find the same feature in Sect. IVC when we set up random perturbations at these interfaces.

III. DOUBLE-SCALE PERTURBATIONS

Double-scale perturbations can be set up experimentally in a straightforward manner using the same technique of laying wires across the thin membrane that separates the two gases. By placing wires which are not equidistant from each other or from the walls of the shock tube, one can set up perturbations which have two or more scales. In this Section we report our numerical experiments of this type.

These calculations were done with helium as the test gas, 60cm long. The initial interface consists of 3 bubbles, with the central bubble twice as long as the two side bubbles(see Fig. 20). The bubbles all have the same height: 0.4cm peak-to-valley.

By having a long and a short wavelength perturbation next to each other we can see how differently they evolve. As shown in Fig.20, shortly after the passage of the shock the shape of the interface is reversed with the larger central bubble lagging behind the two smaller side bubbles. This is expected from the linear theory- larger wavelengths move slower than shorter wavelengths. What is more interesting is that as the bubbles get into the non-linear regime, and in particular after the reflected shock, the wider bubble catches up with the shorter ones and after that they advance together into the test gas. The shorter side bubbles appear to have broken off, but their heads are in line with that of the wider, mushrooming central bubble.

The same qualitative features were seen when we made the central bubble 4 times larger than the side bubbles. Alternatively, we made the central bubble 2 times smaller than the side bubbles, and again we saw the initially larger bubbles catch up with the smaller one and then all three advance with a fairly uniform front into the test gas.

An interesting variation on the problem shown in Fig. 20 is the case where the central bubble is not only 2 times wider but also 2 times higher than the side bubbles. We find in this case that the increased height makes up for the larger width at early times, so that the central bubble no longer lags behind the other two.

This is shown in Fig. 21. At late times, the central bubble now leads the two adjacent ones.

A logical limit in this class of problems is the case where there are no side bubbles but only a central bubble with flat extensions to the walls of the shock tube. This problem is shown in Fig. 22- the central bubble is the same as in Fig. 20, but the two side bubbles are missing(this may be experimentall difficult but not impossible to set up). It is interesting that with the side bubbles absent there is a little more penetration into the test gas (helium) than with the side bubbles present. In general, however, the late time total penetration width is a relatively weak function of the initial interface, ranging between 6.2cm and 8.0 cm in Figs. 20-22.

The problems discussed so far were symmetric about the center line of the shock tube, at least initially.The left-right asymmetry about the central line seen at late times, in particular in Fig. 21, is a measure of numerical diffusion occurring in the code and, of course, should not appear experimentally as long as the initial conditions are set up symmetrically. We also ran a problem which initially was not symmetric: a large bubble next to a small one - i.e. a single wire laid off to one side instead of the center of the shock tube membrane. The evolution of such a problem is shown in Fig. 23, where the large bubble to the right is 3 times wider than the one one on the left (the amplitudes are the same). At late times we see the larger bubble expanding to choke-off the smaller bubble.

In this Section we have covered what we believe to be the simplest double-scale experiments, symmetric and asymmetric. They give us an insight into how perturbations, of different wavelengths and/or amplitudes interact with each other. In the next Section we consider multi-scale and random perturbations, as these match more closely actual surface conditions.

IV. MULTI-SCALE AND RANDOM PERTURBATIONS

A. Air/Helium

From single and double-scale perturbations we proceed directly to multi-scale and random perturbations. Multi-scale perturbations are generated by adding a large (10-15) number of sine-waves with different amplitudes and wavelengths, an example of which is shown in Fig. 24. In addition to the sum, the functions defining the air/helium interface had a quadratic envelope of the form x(1-x) which ensured that the perturbations vanished near the walls (x is the position across the shock tube in units of the width of the tube, so that x=0 and x=1 define the left and right walls respectively). The evolution of a typical multi-scale perturbation, shown in Fig. 24, indicates that some memory of this long wavelength perturbation is retained, along with the four prominent features that are present from the beginning (t=0) to the end (t=1.9ms) of the problem.

One question of interest is the effect of initial conditions on the late time evolution of the mixing zone. We carried out a number of calculations with different interfaces, some of which are shown in Fig. 25. Cases A, B, and C have the same combination of wavelengths but with amplitudes multiplied by 2 and 4 respectively.(The evolution of case B was shown in Fig. 24). Case D is similar to case B except that the signs of the various amplitudes are reversed and, in addition, we do not suppress the perturbations near the walls. In Fig. 26 we show how these 4 cases have evolved by the end of the problem.

Fig. 26 suggests that while the detailed shapes of the interfaces differ in these 4 cases, the total width of the mixing region is a relatively weak function of initial conditions. Some of this dependence comes from our highly restricted definition of L, which we take to be the maximum distance over which one of the gases has penetrated the other. For example, in Fig. 26(d) helium has penetrated to a height of 43.5cm, while we find air bubbles all the way down to 34.0cm, so L=9.5cm, while for Fig. 26(a), which started with an amplitude 4 times smaller than case D, we find L=5.2cm. The

advantage of this definition for L is that it is well-defined and easily obtained from interface plots. An alternative definition for the mixing width is to average laterally over the concentration fraction (CF) of the two gases and take the vertical distance over which the CF of one of the gases falls from say 95% to 5%, instead of the 100% to 0% used in our definition of L. The choice of ±5% CF may appear arbitrary and will ultimately be dictated by the experimental resolution with which average concentration fractions can be determined. Of course the disadvantage of using our 100% - 0% definition is that it includes all bubbles, no matter how small, down to the resolution of the grid. One might argue, for example, that the air bubbles in Fig. 26(d) carry so little mass that the penetration into helium reaches down only to 36cm and the effective mixing width should be taken to be about 7cm.

To set up a sharp interface between two gases a thin membrane will be needed. This is not included in our simulations. While the relatively large single and double scale perturbation experiments are not expected to be too sensitive to the presence of a very thin membrane which disintegrates as the shock passes through it, small multi-scale or random perturbations may be substantially affected by the presence of a membrane. In Refs. 8 and 9 a thin flat membrane with no imposed perturbations was used to separate the gases. This is probably as close as one can get to 1D motion, though small random perturbations on the membrane will eventually seed perturbations large enough to grow upon subsequent shocks. Our present computational capabilities, however, do not allow us to simulate such experiments: the membranes are 0.5-1.0μm thick, so that the initial seeds are probably of order 0.1μm. Our grid resolution is about 0.1cm, 4 orders of magnitude larger.Such a coarse mesh is required to finish the problems within reasonable CPU time, i.e. 10 - 15 hours. We are forced to considering relatively large amplitudes. The conclusions derived from such large amplitude simulations may be valid in experiments where shocks generate vigorously turbulent flows.

From multi-scale perturbations we now turn to random perturbations. The position of the interface at each (lateral) zone is varied randomly around the nominal position, which is 60cm for the air/helium combination discussed in this subsection. The variations are done by pulling out a random number between 0 and

1, multiplying it by a constant amplitude , typically 0.1cm, and adding the product to the 60cm. This is repeated for each of the 80-100 lateral zones that we use in our simulations.

The evolution of a random interface is shown in Fig. 27. It is a complex evolution characterized by two apposite trends: on the one hand we see bubbles merging together and forming larger structures of the order of 1-2cm, on the other hand very small air bubbles, about 0.1cm which is the resolution of the grid, separate from the large bubbles and "fall" into the helium gas.

Before studying how the mixing width evolves as a function of time, we address the issue of how it depends on initial conditions. In Fig. 28we show 4 different shapes at t=0 labelled A, B, C and D, and in Fig. 29 we show them at t=1.9ms. Interfaces A, B, C were generated with the same sequence of random numbers multiplied by 0.05cm, 0.1cm, and 0.2cm respectively. Interface D also had an amplitude of 0.2cm, but in this case we used the squares of the random numbers multiplied by -1.

The two opposite trends mentioned above, very large bubbles next to very small ones, are present in all cases. Comparing C and D, the shapes of the two interfaces at late times are different, but the total mixing length is not too different. Comparing A, B, and C, we see that there is more sensitivity to the amplitude of the initial perturbations than to their detailed shape. Again some of this sensitivity comes from our definition of L which includes the smallest resolvable bubbles determined by the resolution of the grid.

In Fig. 30 we show the evolution of L for the two cases where the initial amplitudes are 0.1cm and 0.2cm. Also shown in Fig. 30 are two additional curves, for the same initial conditions, where we increased the shock strength to M_s=1.7. As expected, the mixing increases as the shock gets stronger. The 1D motion of the interface for each shock is shown in Fig. 31. Since the test gas was kept the same, viz. 60cm of helium, the air/helium interface sees many more reflected shocks in the M_s=1.7 case.

Fig. 30 suggests that L(t) grows approximately linearly with time in between shocks. As a shock goes through the mixed region it compresses it and immediately after the passage of the shock L(t) grows with time. Since the first shock sees a negative

Atwood number, there is a phase reversal whereby hills and valleys turn into valleys and hills respectively. The reflected shock(s) see a positive Atwood number so there is no phase reversal, and the drop in L(t) is caused only by shock compression. Of course the opposite sequence occurrs with a heavier test gas as discussed in the following subsection on air/SF_6, and there the phase reversal which takes place upon the passage of the reflected shock is much more dramatic.

A stronger shock generates more mixing. If we assume that L(t) grows linearly with time, then we can compare the growth rate dL/dt for a fast and slow shock: with the same initial conditions, Fig. 30 suggests that the growth rate triples as we go from M_s=1.2 to M_s=1.7. Since the jump velocity Δv also triples (from 14cm/ms to 42cm/ms, see Fig. 31), it is consistent to assume that $L(t) \sim (\Delta v t)^n$ with $n \sim 1$.

There is a qualitative change in going from the weaker to the stronger shock. When the shock is weak we see that L(t) depends on the initial amplitude L(0), particularly before the second shock arrives. With the stronger shock there is less sensititvity to L(0). It will be interesting to investigate this trend experimentally and with further calculations.

B. Air/SF_6

Multiscale and random perturbations were set up the same way as described above, except that the test gas was replaced by SF_6, 30cm long. Since SF_6 is about 5 times heavier than air, the first(second) shock sees a positive(negative) Atwood number, exactly the opposite case from helium. Again we see that perturbations grow following each shock.

Fig. 32 shows the evolution of a random set of perturbations with a peak-to-valley amplitude of 0.1cm. The reflected shock hits the interface approximately 2.3ms after the first shock, by which time the interface has moved about 22cm. The 1D motion of the air/SF_6 interface for this shock (M_s=1.3) and a stronger shock(M_s=1.7) are shown in Fig. 33, along with dashed lines showing the extent of mix for the case where the amplitude was doubled to 0.2cm.

To study the dependence on initial conditions, we show 4 interfaces in Fig. 34 labelled A through D. The first three cases are random perturbations with total amplitudes of 0.05cm, 0.1cm, and 0.2cm (the evolution of case B was shown in Fig. 32),while case D is a multi-scale perturbation of maximum amplitude 0.2cm. Fig. 35 shows how these four cases have evolved by t=3ms. There is some dependence on the amplitude and shape of the initial perturbations, but not a strong one.

It is interesting to compare Figs. 29 and 35, the helium and SF6 cases respectively. There is clearly more finger-like structures in Fig. 35 than in Fig. 29. This is related to the fact that shocks going into a lighter gas tend to create finger-like structures, while shocks going into a heavier gas generate mushrooms. This characteristic of shocks, already noted in Sect. II, is perhaps best illustrated in the evolution of multi-scale perturbations in SF_6 which we show in Fig. 36. The mushrooms are quite clear after the first shock; after the reflected shock, they evolve into fingers, as seen in the last snapshot.

Another difference between the helium and SF_6 cases emerges when we study the time evolution of the total mixing width L, which we again define as the maximum distance of interpenetration. In Fig. 37 we plot L(t) as a function of time for two different shocks (Ms=1.3 and 1.7), and two different initial L(0) in each case: 0.1cm and 0.2cm. There is again some dependence on initial conditions, and the growth is not quite linear in time, particularly for the weak shock. As expected, the growth rate is larger for the faster shock. If we again assume that L scales as $(\Delta vt)^n$, then the power n is less than 1 and close to 2/3, as suggested by C. Leith[10].

These two differences, mushrooming and the late time slowing of the growth, may be connected - clearly, air that is mushrooming, i.e. expanding laterally into the heavier SF_6 will penetrate less than fingers of air pushing through the lighter helium gas. We must remember, however, that mushrooming and fingering are essentially large scale phenomena and their appearance in our random perturbations may be a result of the coarseness of our grid. For the same reason we feel that these calculations must be refined

using a much finer grid before drawing any detailed conclusions about L(t).

As the second shock passes through the interface, L(t) drops just before it resumes a more vigorous growth. The drop is caused by the combined effects of shock compression and phase reversal, signalling that there are large scale structures in the calculation. At present we have no simple analytic description of how L evolves after the second shock. The compression of the mixed region, and more importantly the minimum width L_{min} it attains because of phase reversal, depend on the scales that are present in the mixed region. If both large and small scales evolve from initially random perturbations, as suggested in our calculations, then the description can become quite complicated. If the mix is "atomic", i.e. all scales are much smaller than the width L, then phase reversal may be ignored and a simple description like a power-law may be possible.

There are two further differences between the helium and SF_6 cases. Comparing Fig 30 with Fig. 37, we see that a reflected shock has less of an effect on the growth rate in the case of helium than in the case of SF_6. The main reason is that in helium the reflected shock is about 50% weaker, as measured by Δv, than the first shock, while in SF6 the reflected shock is about 40% stronger than the first. Even after taking into account this Δv effect, it appears that somewhat more mix is generated by a shock moving into a lighter medium than into a heavier medium, at least for the Atwood numbers of -0.75 and +0.67 considered here. Further calculations are needed to determine if this difference in A is enough to account for the residual difference between helium and SF_6.

C. Air/Freon/Air

We consider the same set up as in Sect.IIC: 4cm thick layer of freon gas whose lower interface is 60cm away from the end of the shock tube. The layer is surrounded by air both above and below. A Mach 1.2 shock accelerates first the upper interface, then the lower interface, passes into the lower air section, reflects off the end wall, and crosses the freon layer a second time. In Sect. IIC we discussed the evolution of single scale perturbations on either or

both interfaces; here we describe the evolution of random perturbations.

Fig. 38 shows the case where only the upper interface had initial random perturbations with peak-to-valley amplitudes of 0.1cm. Fig. 39 shows the case with perturbations only at the lower interface, and Fig.40 shows the case where both upper and lower interfaces are perturbed Unlike the case of large scale perturbations, small scale perturbations on either interface appear to evolve independently of the other interface, which is expected because the random perturbations have extremely short wavelengths, much smaller than the average width of the freon layer, so interface coupling is less effective here.

Another observation concerning these calculations is the following: while early on the perturbations at each interface evolve differently, after the reflected shock both interfaces develop similar perturbations. This is clearly seen in Fig. 40; in the last snapshot the total mixing width at both the upper and lower interface is about 2.7 cm. Note that the freon layer is almost completely intermixed with air, in the sense that one cannot draw a horizontal line across the shock tube without intercepting some pockets of air.

This intermixing increased somewhat by doubling the initial amplitudes to 0.2cm. In Fig. 41 we compare this case with the other three cases discussed above.

A three fluid experiment was reported[11] in a constantly accelerating system, and the evolution of the mixing layers with initially random perturbations at each interface was well described as being independent of each other until the middle layer was completely penetrated. In those experiments an intermediate layer of density ρ_2 was chosen so as to minimize mixing across the two adjacent fluids with a high density ratio ρ_1/ρ_3. The density ρ_2 of the intermediate fluid was chosen by $\rho_2 = (\rho_1\rho_3)^{1/2}$ as suggested by a linear analysis[12]. It will be interesting to see if the same stabilizing mechanism of density gradients is effective for shocks. In fact, in the next Section we will describe an experiment in which a continuous density gradient is set up and the growth of the small scale scale perturbations appears to be suppressed.

As mentioned earlier, there is a large variety of experiments that can be carried out by using different densities in the three fluids. We plan to pursue them at a later date.

V. COMPARISON WITH A RECENT SHOCK-TUBE EXPERIMENT

We hope that most, if not all, of the numerical experiments reported in this paper will be carried out experimentally in the near future. In this Section we describe a recent shock-tube experiment[5] carried out at CalTech and our simulation of it. The test section consists of SF_6 gas 10cm long with a cross-sectional area of 11.3cm×11.3cm . A metal plate, which initially separates the test gas from the upper section of the shock tube filled with air, is pulled out to the left, as viewed by the camera, just before the arrival of the shock. As a consequence, the gases are premixed to a thickness of about 1.2cm, and two gravity waves are set up: one on the side of air and one on the side of SF_6, the first one travelling faster than the second. In our simulations, shown in Fig. 42, we set up a premixed layer in which concentration fractions of the gases change linearly over the 1.2cm distance, plus two bumps, each 2mm high and 3cm long, at the air/premix interface and the premix/SF_6 interface, representing the two gravity waves. The upper(lower) bump is 1.5cm(1.0cm) away from the left wall . There are small amplitude(0.2mm) random perturbations throughout the premix layer.

Fig. 42 shows our initial set up and its evolution as a Mach 1.3 shock impinges on the diffuse interface. The isodensity contours shown in this figure are in good agreement with the shadowgraphs reported in Ref. 5. In particular, the structures near the left hand wall are fairly well reproduced in our simulation. In the experiments another structure appears near the right wall which is not found in our simulations, and it is not clear if it is a boundary layer effect or a 3D effect . Another possibility is that the concentration fractions are not identical near the two walls: because the metal plate is drawn to the left, the gases near the right hand wall have had more time to premix than the ones near the left wall.

In Fig. 43 we show a comparison of the experiment and our simulation.

From the last snapshot shown in Fig. 42 we see that the total mixing region is about 6.4cm thick, extending from 2cm

to 8.4cm. If there were no perturbations, i.e. no bubbles and no random perturbations, the thickness of the 1.2cm premix layer would end up only 0.5cm. A calculation with only random perturbations but no bumps reached a mixing width of 3cm. Interestingly, when we doubled the initial width of the premix layer to 2.4cm in this last calculation , the final thickness was somewhat less: 2.8cm. It appears that the longer density gradient has such a stabilizing effect that an initially wider premix layer can end up thinner than an initially thinner premix layer.

In Fig. 44 we show isodensity contours, at t=5.7ms, of the three problems discussed above: 1.2cm premix width with bumps(Fig. 44(a)), 1.2cm premix width with no bumps(Fig. 44(b)), and 2.4cm premix width with no bumps(Fig. 44(c))

Let us point out an interesting, albeit small effect on the mixing length near the right wall in our calculations. Comparing Fig. 44(a) with Fig. 44(b), we see that L near the right wall is 20% smaller in Fig. 44(a) than in Fig. 44(b), being 2.4cm and 3cm respectively. It appears that the vortex motions created by the large bubbles in Fig. 44(a) have robbed, by entrainment or otherwise, some of the mixed mass near the right wall.

Figs. 44(b) and 44(c) illustrate the stabilizing effect of density gradients mentioned above. It is somewhat surprising that this effect, well known in the linear RT problem, appears to suppress also the highly non-linear process of mixing at a shocked interface .

Measurements are in progress at this time to determine the concentration fraction of gases across the premix layer. This was assumed to be a linear function of positon in our simulation. Although we have not verified explicitly, we feel that small deviations from the assumed linear profile would have little effect on the evolution at late times. Of more importance may be the assumption that the concentration fraction was *uniform* across the shock tube, in particular near the right and left walls. Even after waiting for the gravity waves to die out a left-right asymmetry may persist due to the fact that the separating plate leaves the right wall before it leaves the left wall.

VI. REMARKS AND CONCLUSIONS

In this paper we have studied some of the rich phenomena that arise at shocked interfaces with various initial perturbations. The complexity of those phenomena, and in particular the fact that we are dealing with compressible fluids, practically rule out analytic approaches and hence require direct numerical simulations. We believe our calculations will be useful in planning future experiments, both physical and computational, out of which we hope to get insight into the physical processes that occurr at shocked interfaces, and insight into numerical techniques for solving problems in shock hydrodynamics.

Here we mention some of the tests that we carried out. The artificial viscosity introduced in the code for numerical stability also slows down the fluid motion to some extent. This is particularly severe in regions of the problem where physical scales are resolved only by a few grid zones. For example, in Fig. 45 we show the air/freon/air problem (Fig. 19) with a resolution of 0.14cm and 0.07 cm. Not only there is more small-scale structure in the case of high resolution, but the mushrooming freon heads extend deeper into air, and the necks are thinner. It could well be that, with even higher resolution, the necks will snap and the heads will separate.

We carried out similar zone-doubling studies for the random perturbations also. As expected, the mixing region increased, but most of the increase was due to a few narrow jets which penetrated deeper into the lighter fluid. The penetration into the heavier fluid was much less affected because that side consisted of wider bubbles (see, e.g., Fig. 32). Keeping the same number of zones (about 100×250), we varied the shape of the initial random perturbations, and found that it was again the mixing into the lighter fluid which changed (by about 16%) ,while the mixing into the heavier fluid remained practically the same.

The above exercises suggest that the mixing into the heavier side may obey some simple scaling law, while the mixing into the lighter side is more susceptible to changes in initial conditions, etc. As observed by Andronov et al.[8], the mixing

into the lighter fluid is wider than the mixing into the heavier fluid, and our calculations also show the same effect (see Fig. 31).

The overall mixing length L is the crudest description of the mixing process. At the next level one may set $L = L_1 + L_2$, where L_1 and L_2 are the mixing widths into the heavier and lighter fluids respectively. The only drawback to this decomposition is that it requires computing the unmixed, i.e. 1D position of the interface because it cannot be measured experimentally (this is not a problem for incompressible fluids - see, e.g., Ref. 13). This is an acceptable price to pay because the 1D positions can be computed accurately. We analyzed some of our random perturbation results in terms of L_1 and L_2 , and found that indeed $L_2 > L_1$, and that L_2 was more sensitive to initial conditions. In the future we hope to carry out calculations with higher resolution to see what scaling laws, if any, describe L_1 and L_2.

Going beyond this decomposition into L_1 and L_2, the description of turbulent mix quickly becomes extremely complex: eddies of all sizes appear to be present, and the velocity field is quite complicated. The usual description of turbulence is in terms of the spectrum of turbulent energy, but the code at present cannot readily extract that information.

As an example of highly developed turbulence generated by shocks, we show in Fig. 46 isodensity contours and velocity vectors for the 60cm long helium test gas, 1.9ms after it is first hit by a M_s=1.7 shock. Several reflected shocks have passed by this time, and the total mixing width is about 13 cm, i.e. 130 time larger than L(0) which was 0.1cm (the evolution of L for this case was shown in Fig. 30). Several vortices are clearly seen in this mixture of air and helium; large scale motion, almost as wide as the shock tube, is accompanied practically everywhere by very small islands of dense air bubbles floating through the mixture. Even with the relatively crude 1mm wide zoning, the code took 16500 cycles and close to 6 hours on the CRAY/XMP to get to this time.

In 1D, i.e. without any perturbations, the sharp air/helium interface at t=1.9ms is about 17cm away from the end of the shock tube. Since the mix extends from about 9cm to 22cm (see Fig. 46), we conclude that L_1 = 5cm and L_2 = 8cm.

Finally, let us mention a few problems that we ran primarily as a check on the code. With no imposed perturbations, the interface remained flat well into the times that we were interested in. Imposing perturbations between two identical gases, i.e. setting $\rho_{test\text{-}gas} = \rho_{air}$ and $\gamma_{test\text{-}gas} = \gamma_{air}$, we saw no growth - nor did the code diffuse the perturbations.

To study the dependence on the Atwood number A, we made a few runs where A was reduced by a factor of 2. The adiabatic index γ was not changed. We saw approximately linear behaviour with A, although in one case (helium test gas with random perturbations) the suppression was more than a factor of 2, suggesting a stronger dependence on A.

Density gradients can be viewed as effectively reducing the Atwood number at an interface. For a definitive proof one must compare experiments on the same system, one with a diffuse interface and one with a sharp interface. Such experiments have not yet been carried out (they soon will be), but we did a simulation and found at late times the mixing width was indeed somewhat larger when the initial interface was sharp. This may be a clue to understanding how the late time evolution of L may be independent of initial conditions: perturbations grow slower in the large premix case, giving time for the faster growing perturbations in the small premix case to catch up.

As mentioned in the Introduction, this is essentially a work-in-progress report. We have simulated a variety of possible experiments in a shock tube such as the one at CalTech. These experiments require either a thin membrane or a separating plate between two gases, and the CalTech facility is equipped with both. New experimental results will soon become available. We are encouraged by the good agreement between our simulation and the reported air/SF_6 experiment which we discussed in Sect. V. Future experiments and simulations will shed much more light on how perturbations evolve and how two fluids mix across a shocked interface.

ACKNOWLEDGMENT

During the course of this work I have benefited much from discussions with Gene Burke, Vivian Rupert, Brad Sturtevant and Martin Brouillette. Bob Tipton has often helped me run the code.

REFERENCES

1. R. D. Richtmyer, Commun. Pure Appl. Math. 13, 297(1960).

2. E. E. Meshkov, Izv. Akad. Nauk. SSSR, Mekh. Zhidk. Gaza 5 , 151(1969) .

3. S. Chandrasekhar, Hydrodynamic and Hydromagnetic Stability, (Oxford University Press, London, 1968).

4. Energy and Technology Review. UCRL-5200-83-3, March 1983,p. 38.

5. B. Sturtevant, to be published in "Shock waves and Shock Tubes", ed. H. Gronig, RWTH, Aachen, Germany(1988).

6. K. A. Meyer and P. J. Blewett, Phys. Fluids 15, 753(1972).

7. K. O. Mikaelian, Phys. Rev. A31, 410(1985).

8. V. A. Andronov et al, Sov. Phys. JETP 44, 424(1976).

9. S. G. Zaitsev et al, Sov. Phys. Dokl. 30, 579(1985).

10. C. E. Leith, "Acceleration-Induced Turbulent Mixing: Model One", LLNL working paper, August 1985.

11. K. D. Burrows, V. S. Smeeton and D. L. Youngs, AWRE Report O22/84, 1984.

12. K. O. Mikaelian, Phys. Rev. Lett. 48, 1365(1982).

13. K. I. Read, Physica 12D, 45(1984); D. L. Youngs, *ibid* 12D, 32(1984).

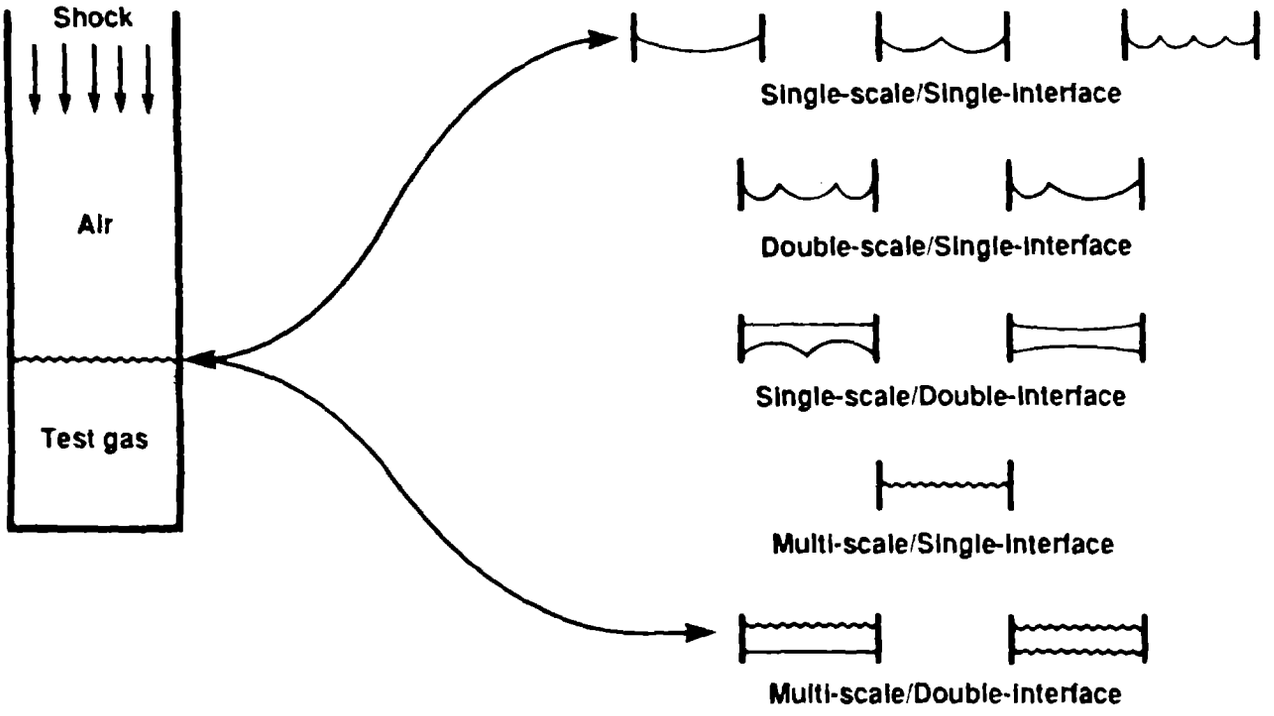
Shock
Air
Test gas
Single-scale/Single-Interface
Double-scale/Single-Interface
Single-scale/Double-Interface
Multi-scale/Single-Interface
Multi-scale/Double-Interface

Fig. 1

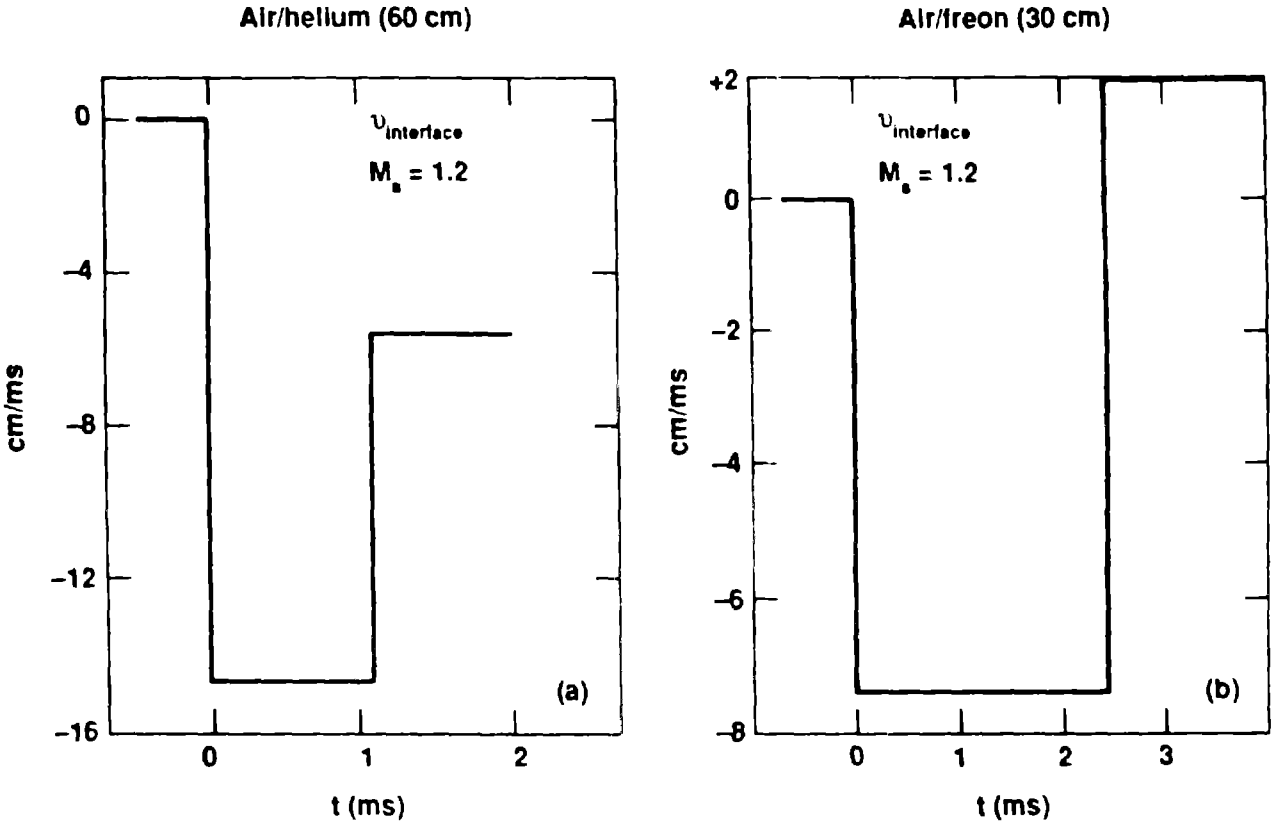
Air/helium (60 cm)
Air/freon (30 cm)
$v_{interface}$
M_s = 1.2
cm/ms
t (ms)
(a)
(b)
0
-4
-8
-12
-16
+2
-2
-6
1
2
3

Fig. 2

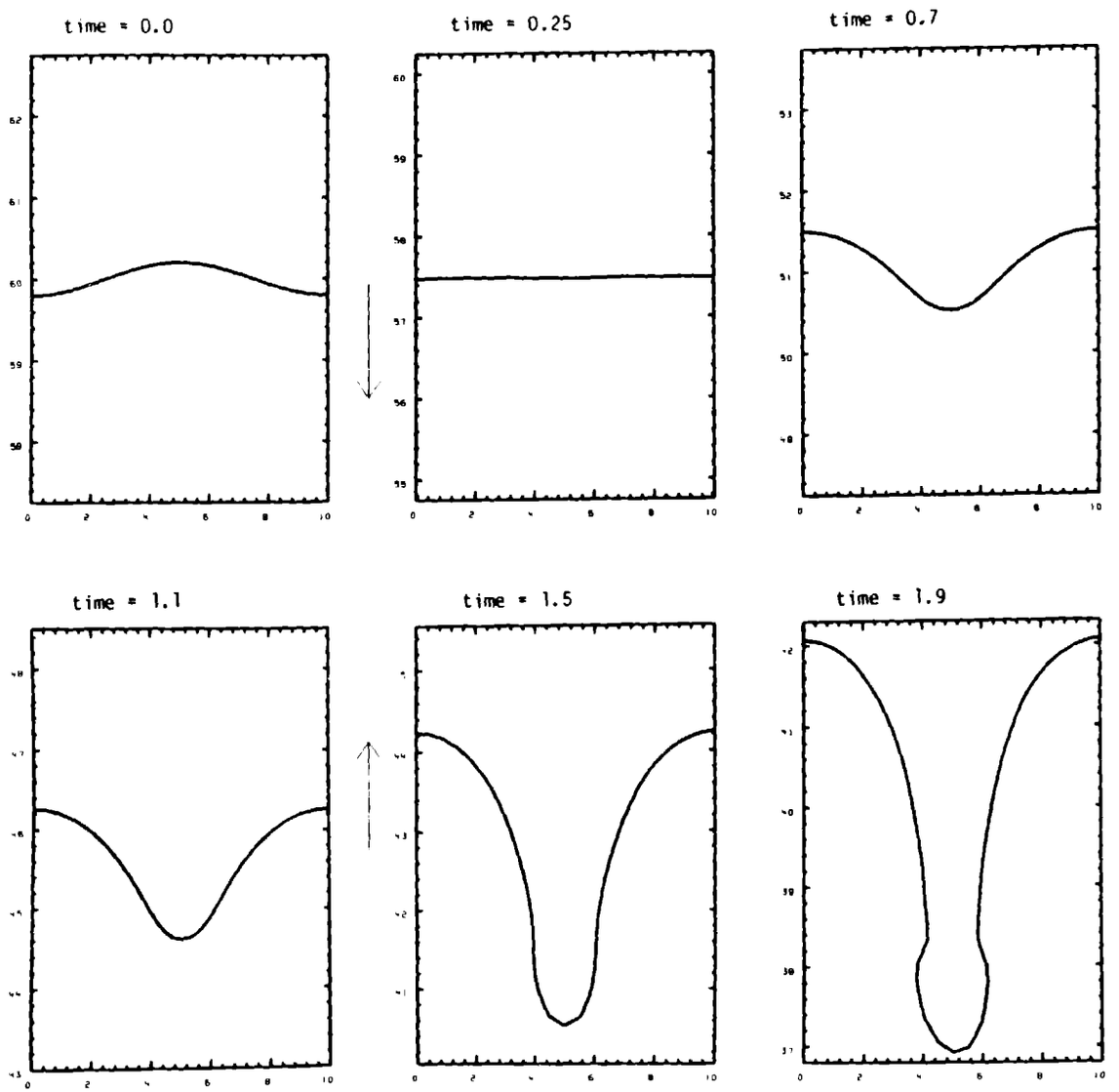

Fig. 3

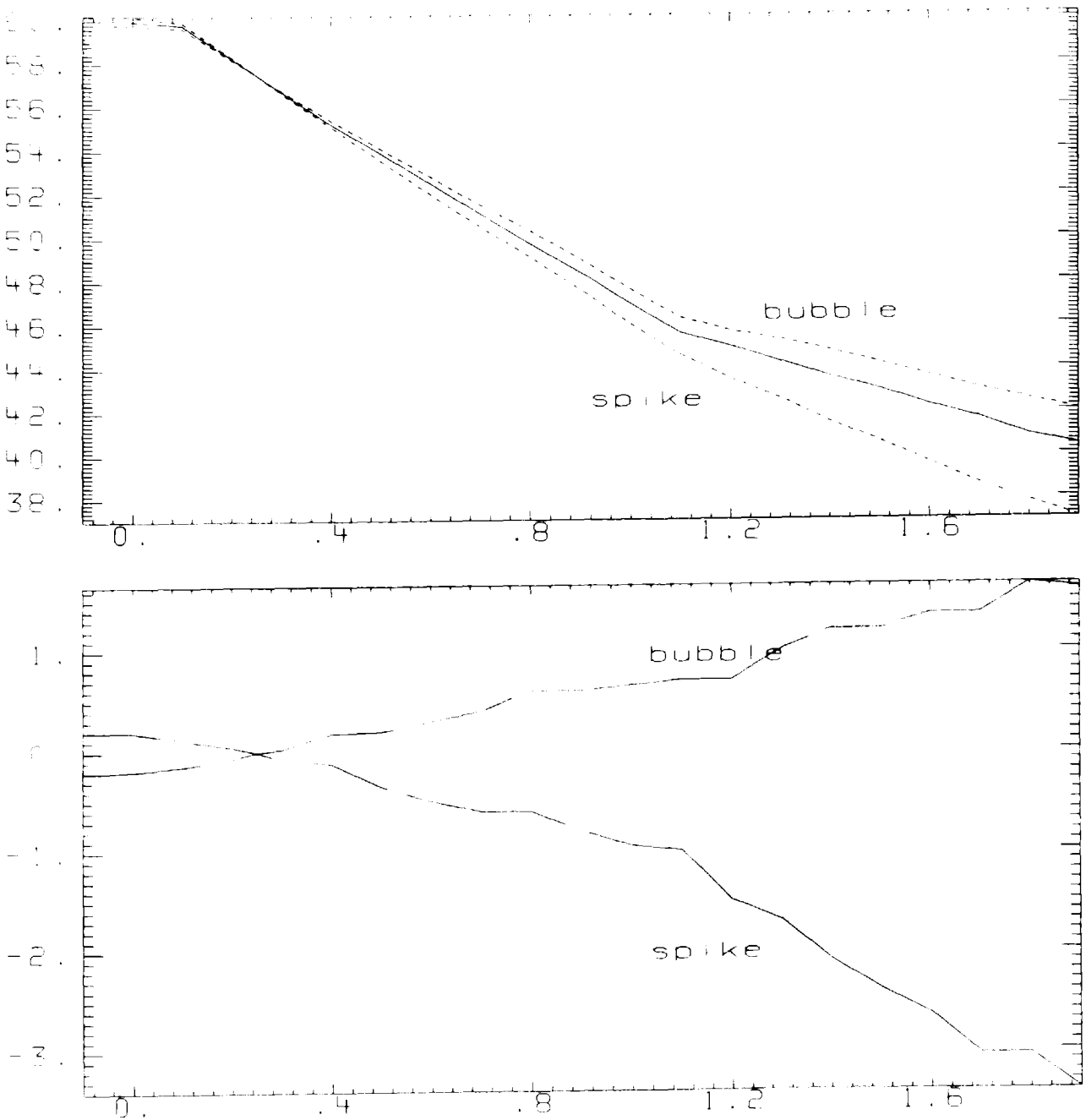

Fig. 4

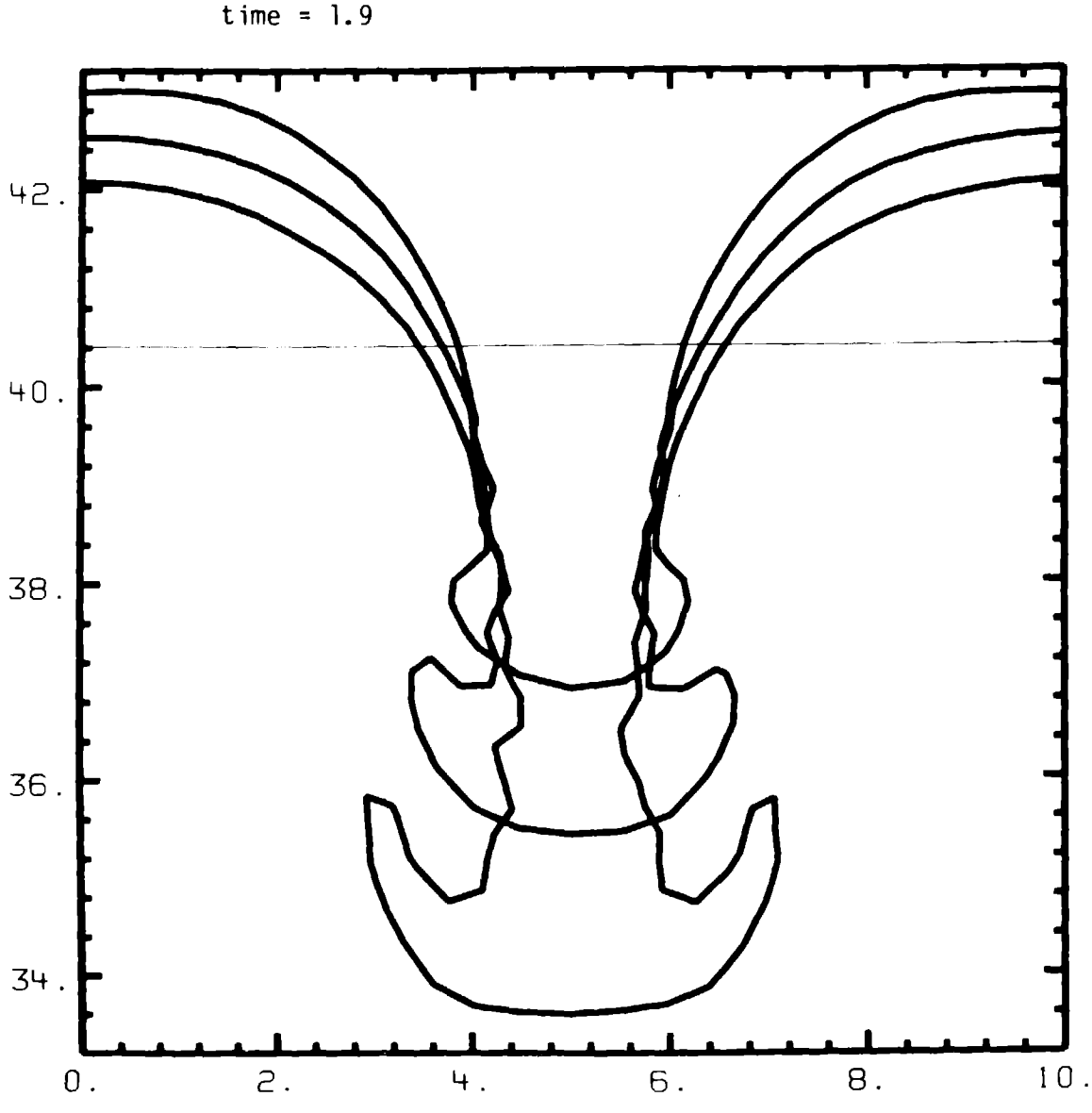

Fig. 5

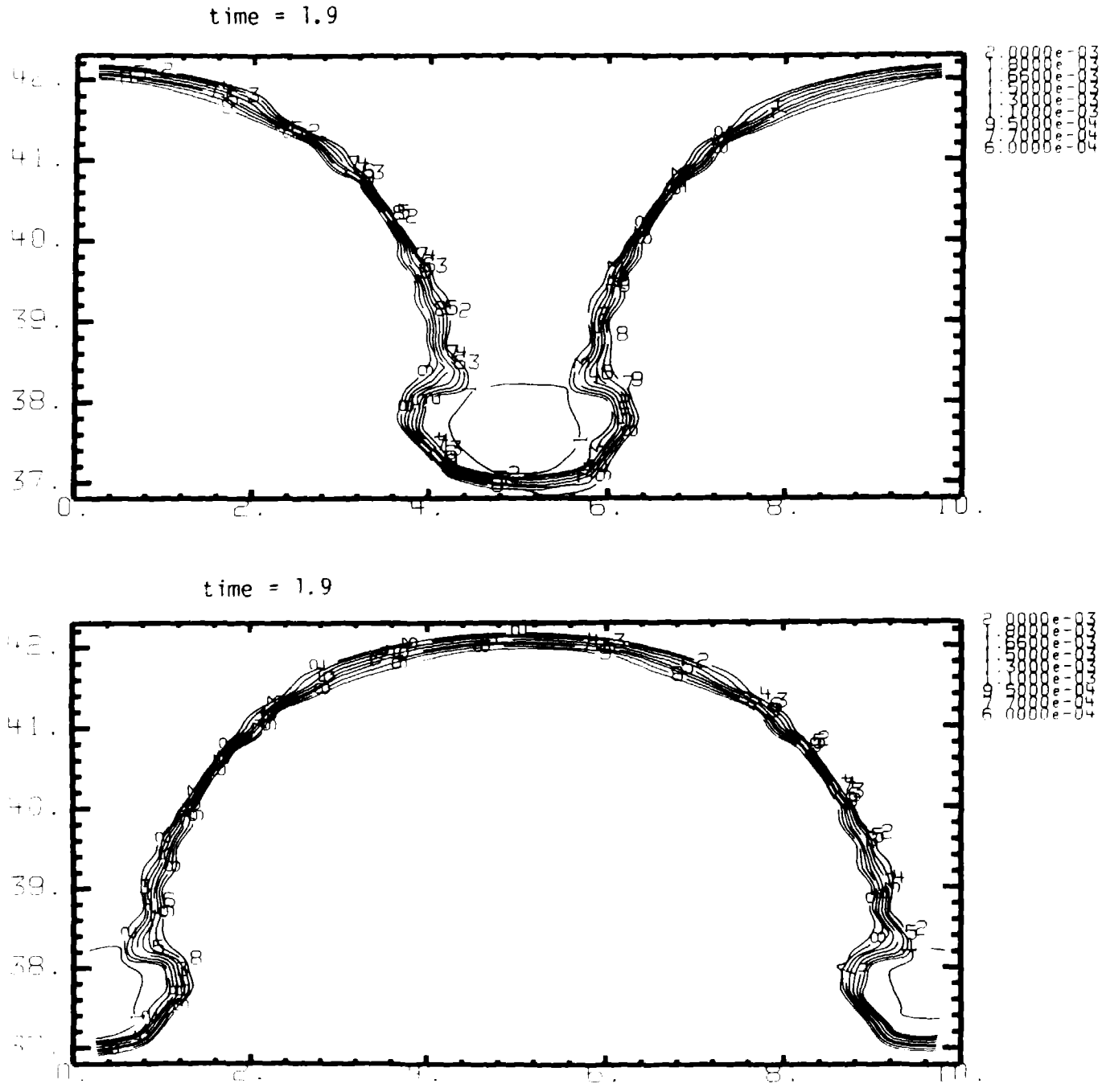

Fig. 6

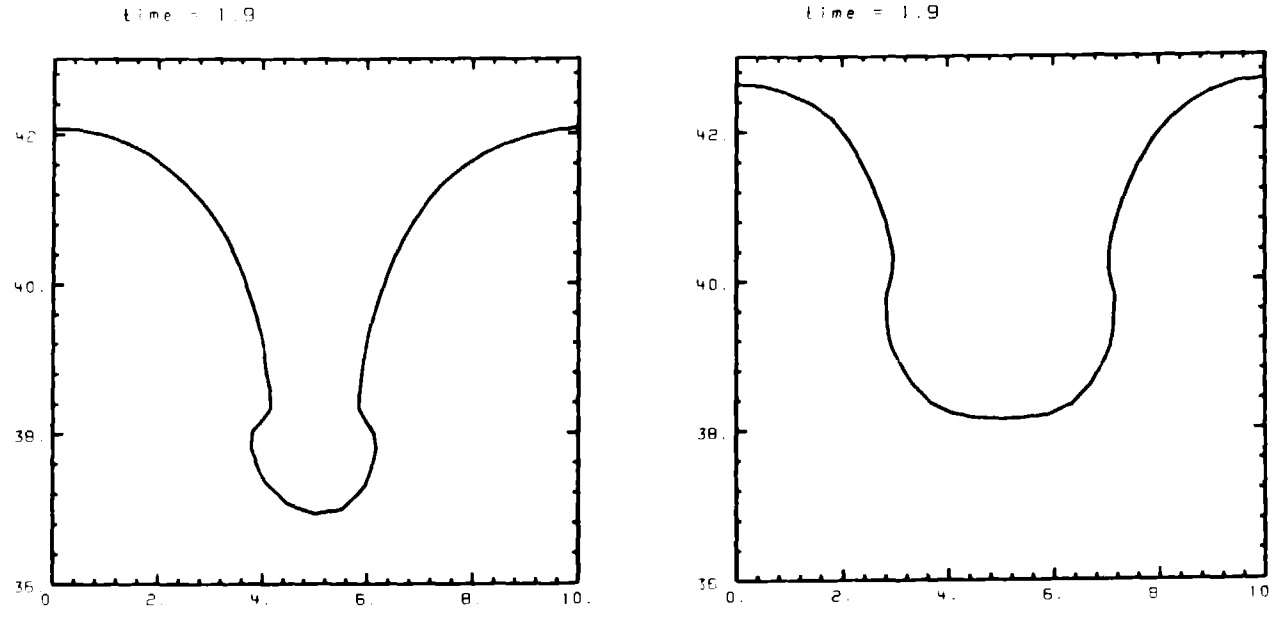

Fig. 7

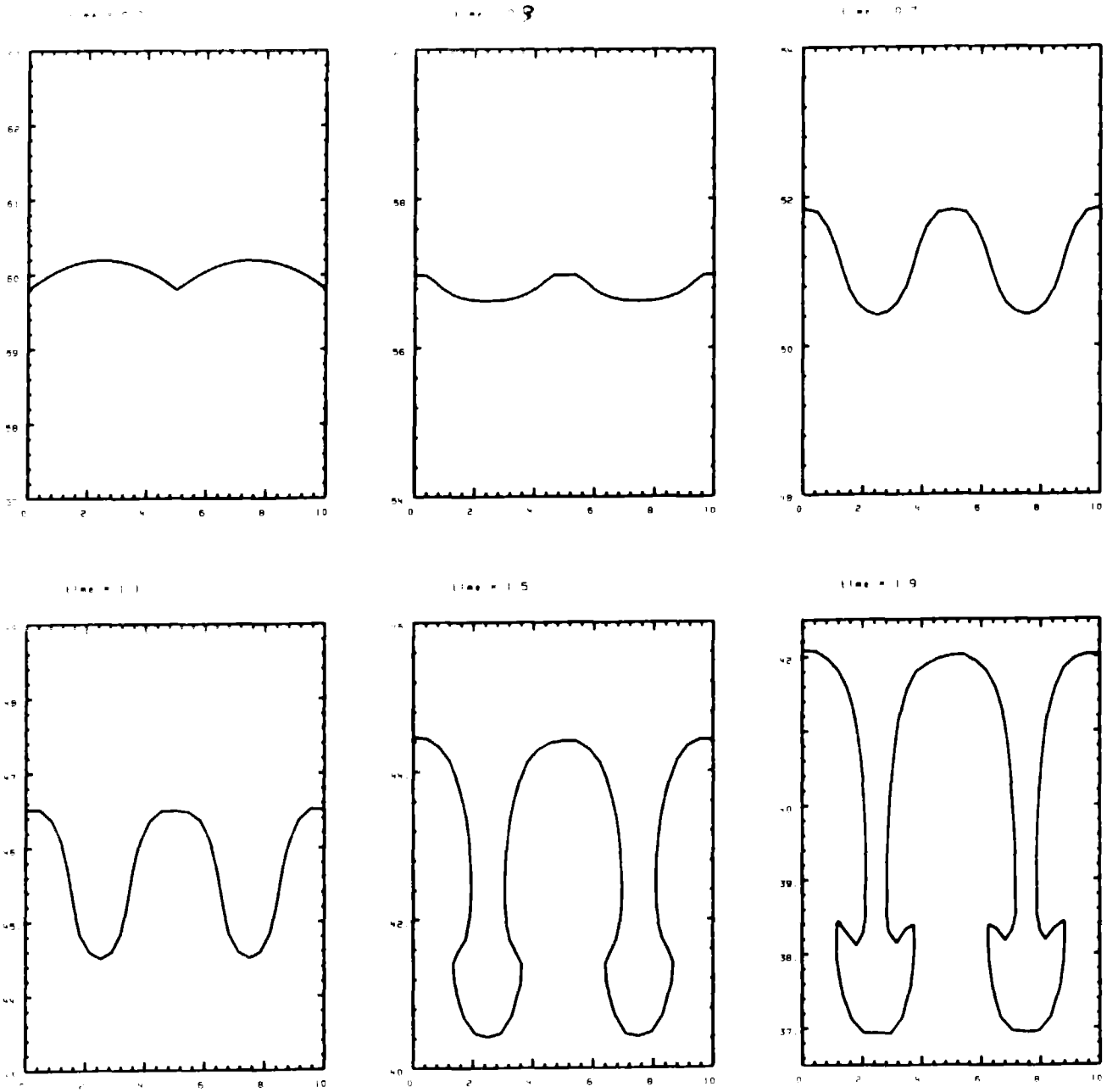

Fig. 8

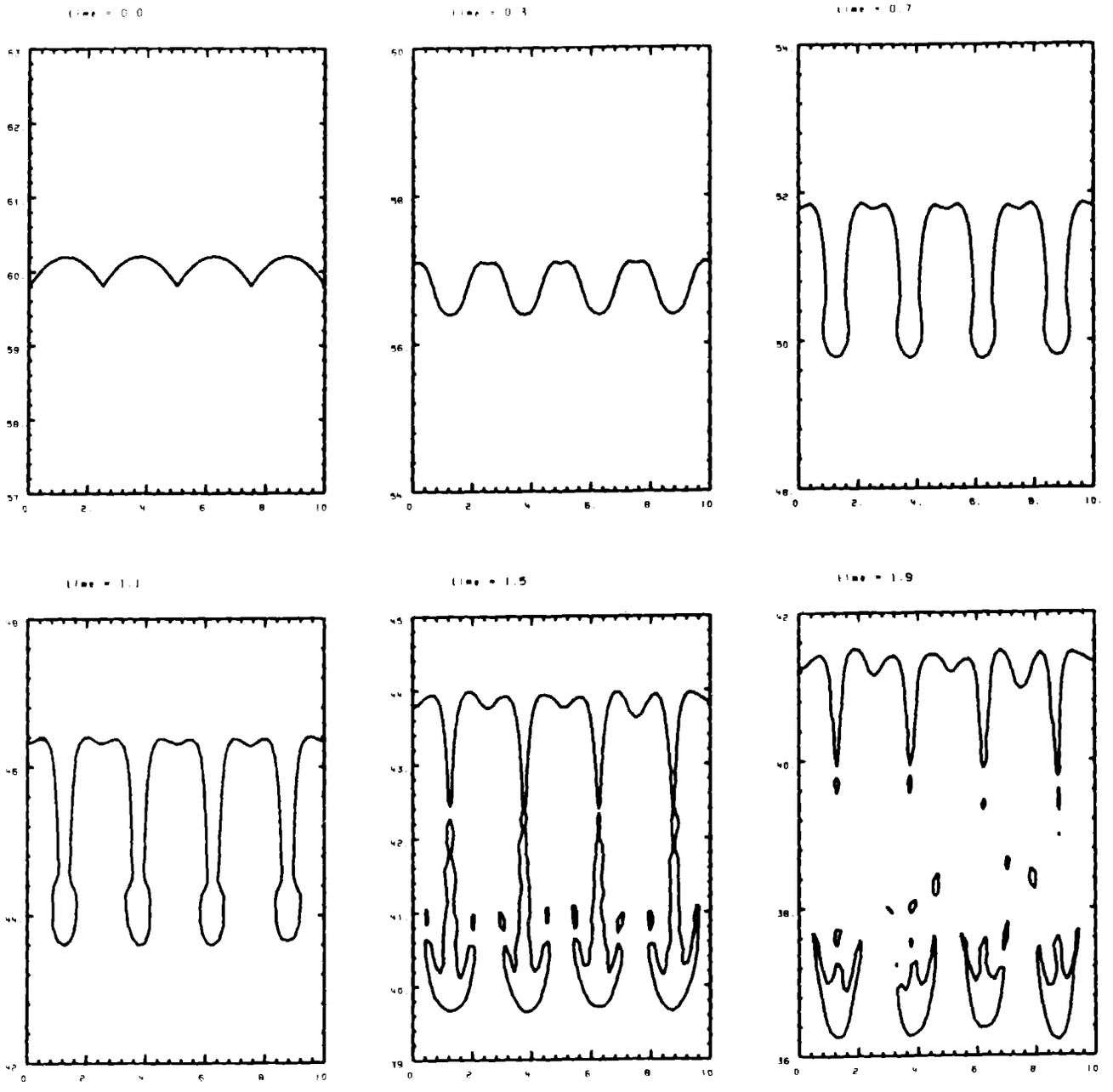

Fig. 9

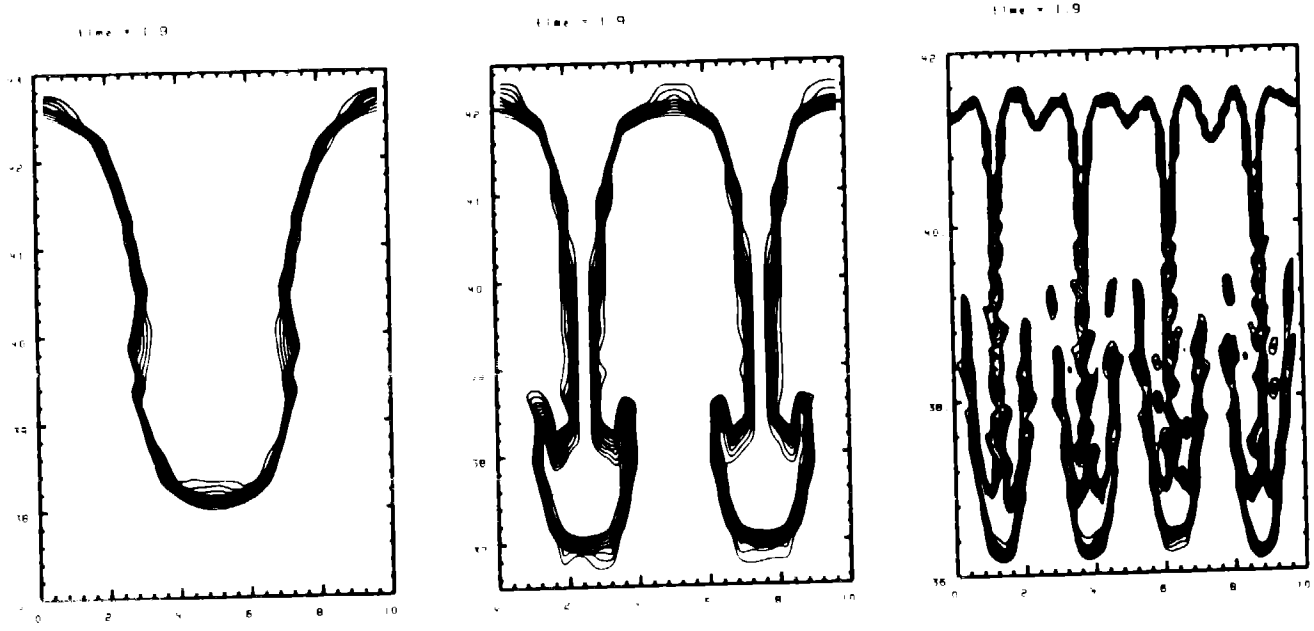

Fig. 10

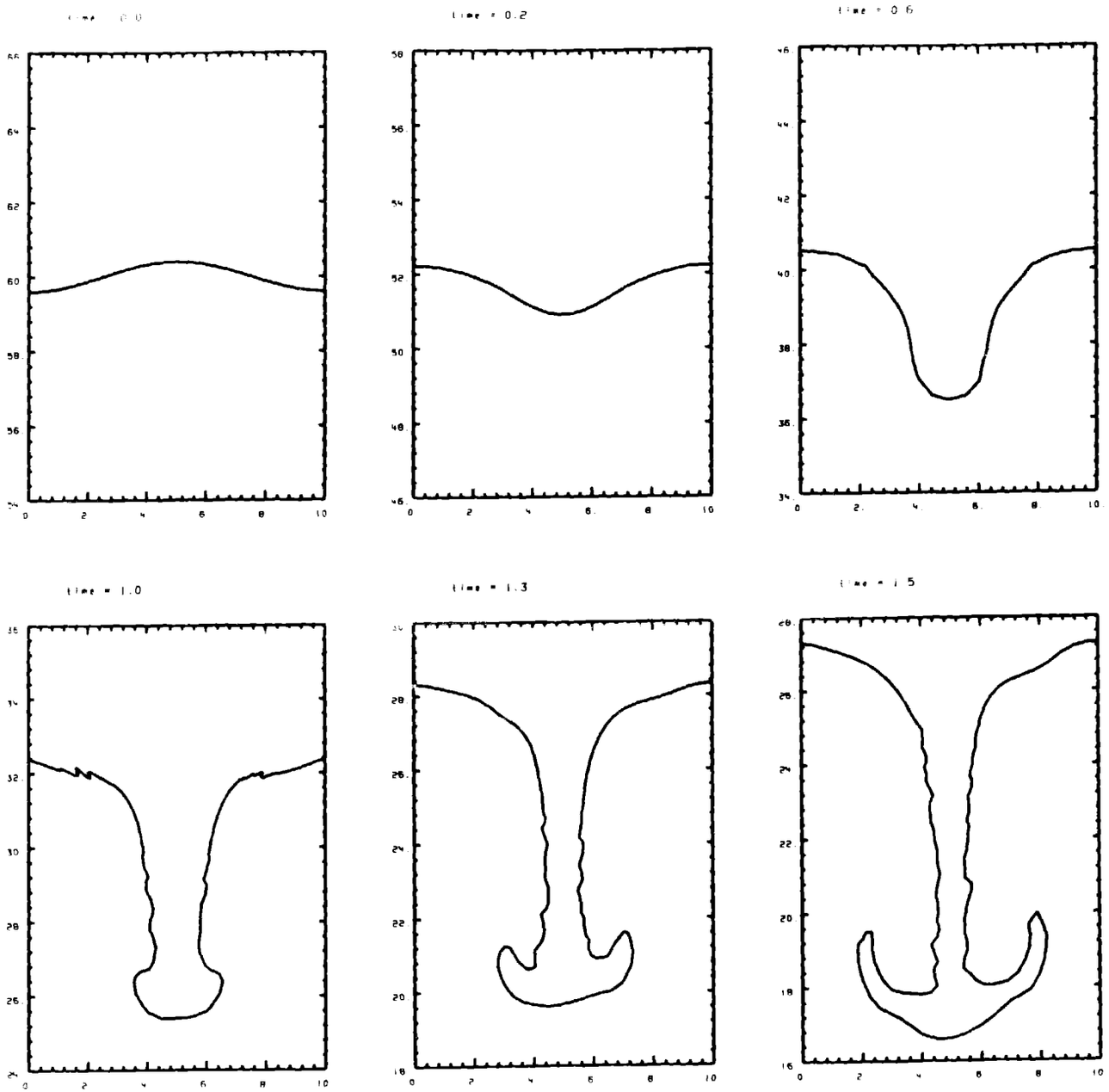

Fig. 11

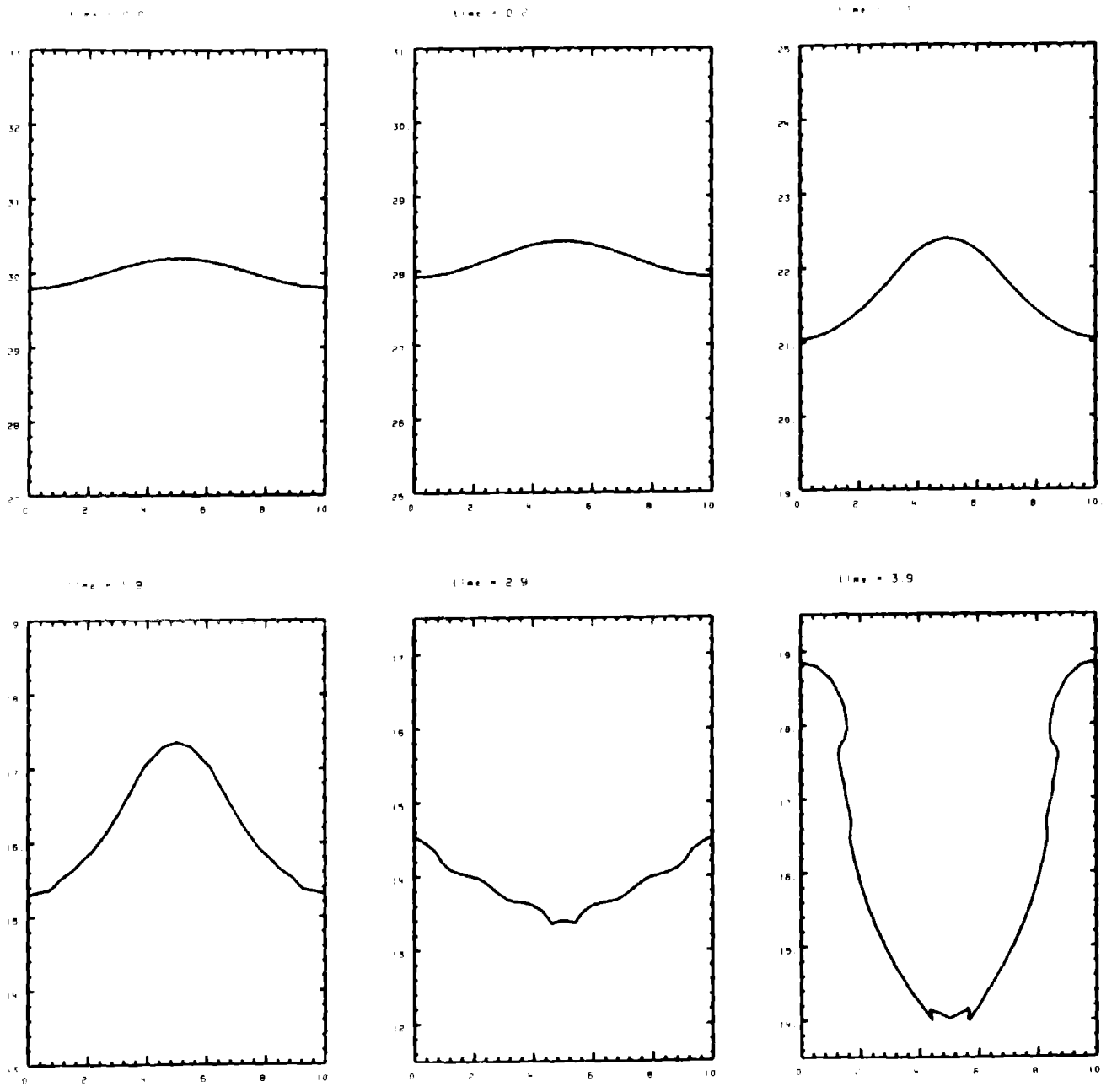

Fig. 12

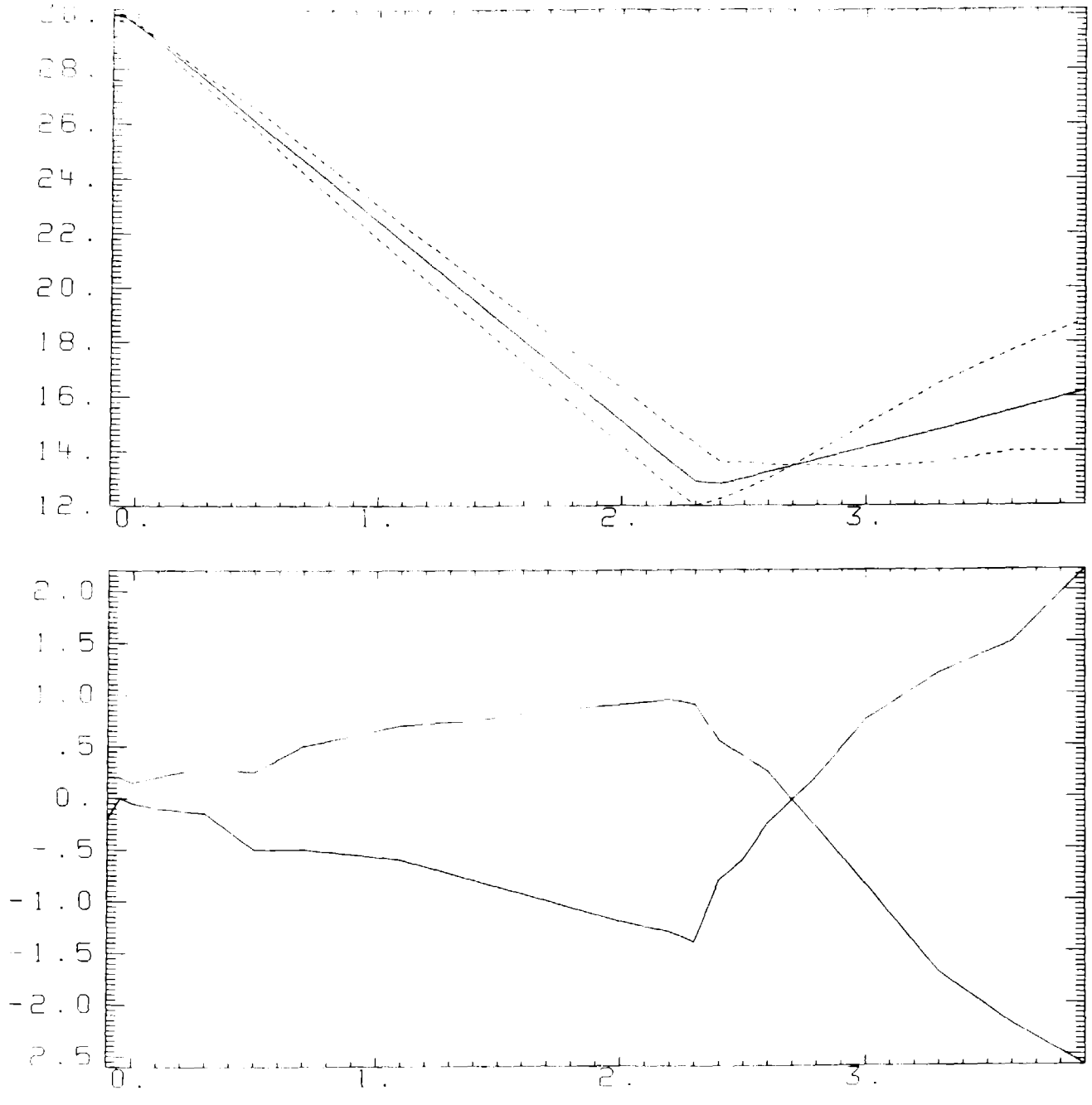

Fig. 13

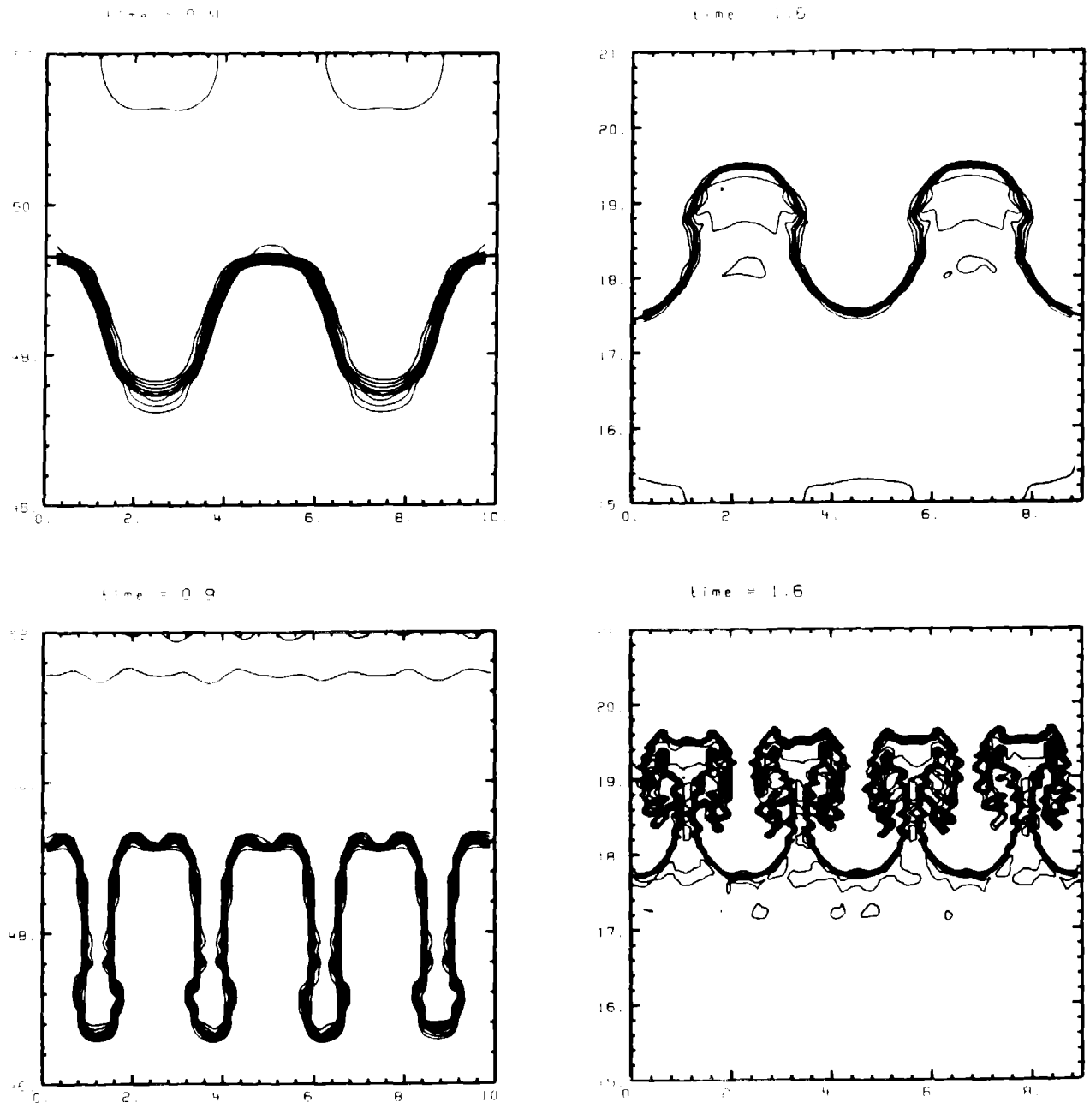

Fig. 14

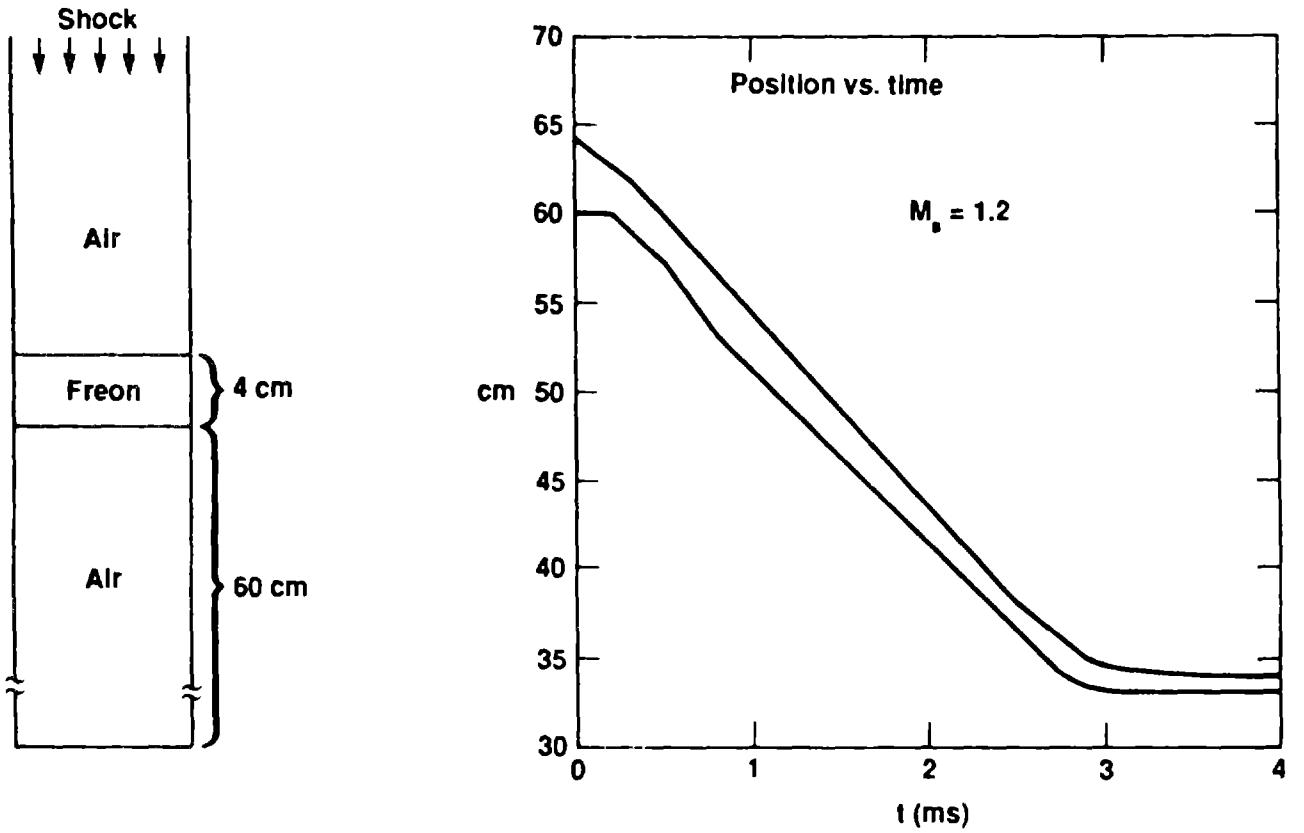
Shock
Air
Freon
4 cm
Air
60 cm
Position vs. time
M_s = 1.2
cm
70
65
60
55
50
45
40
35
30
0
1
2
3
4
t (ms)

Fig. 15

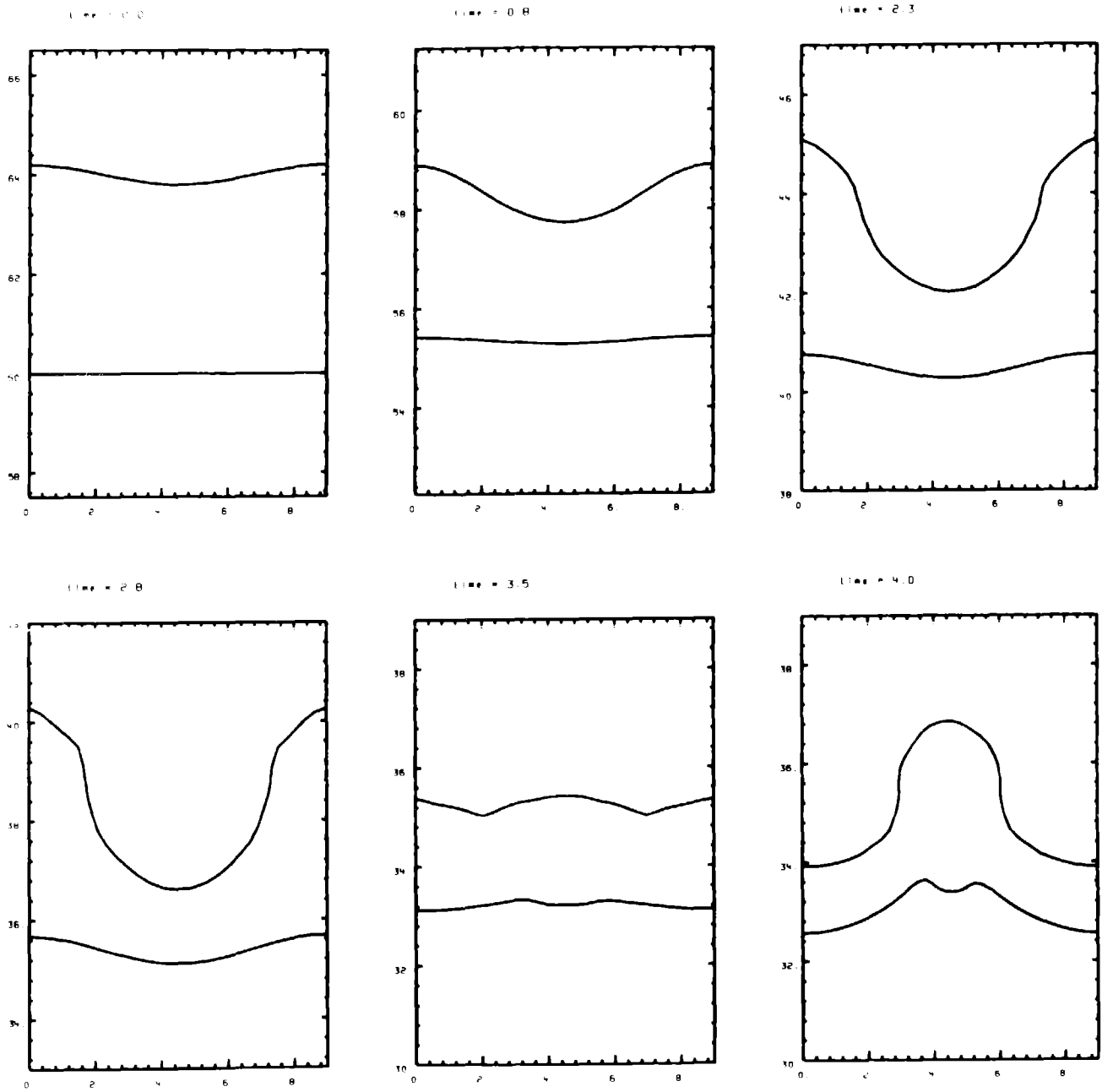

Fig. 16

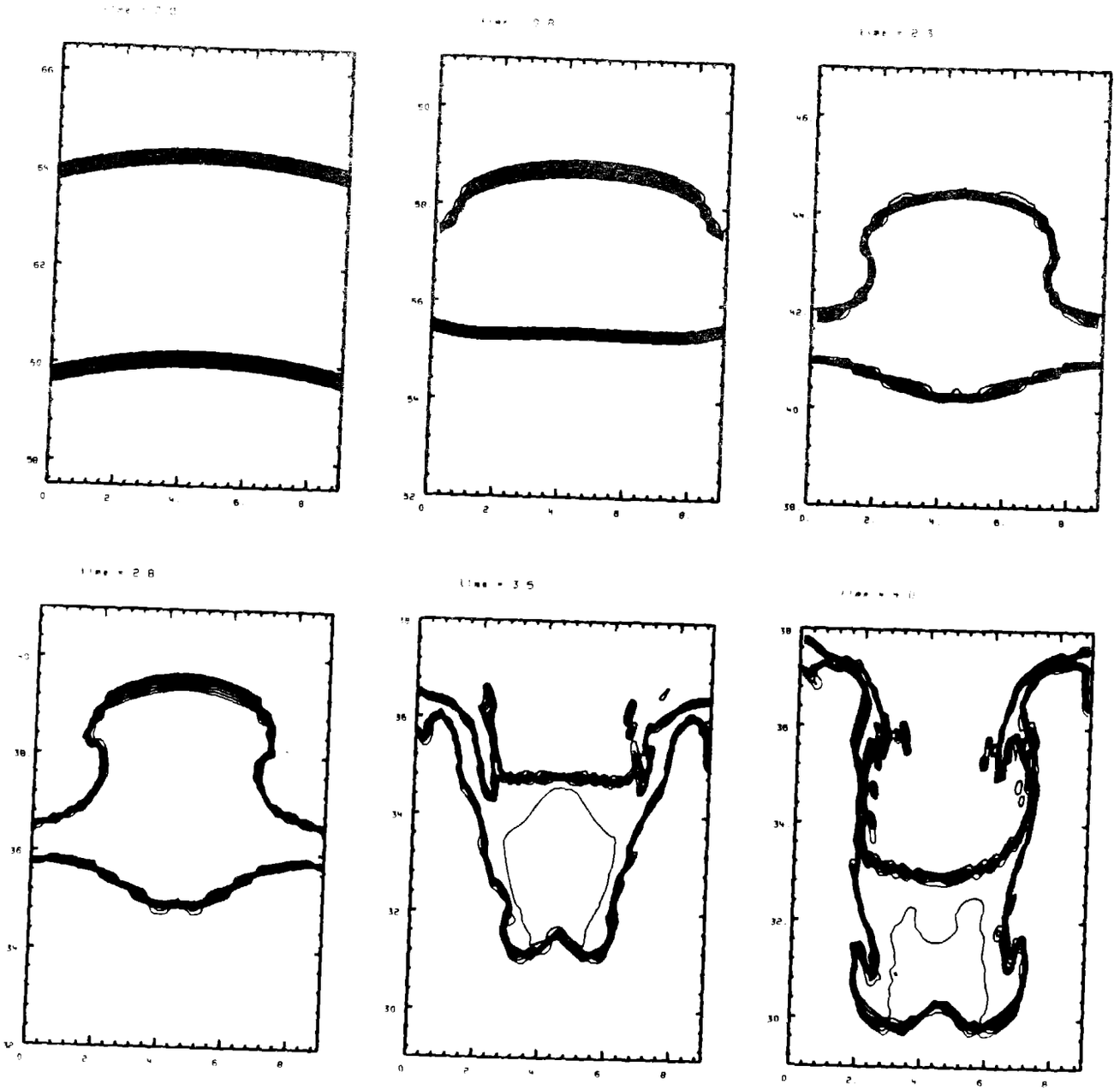

Fig. 17

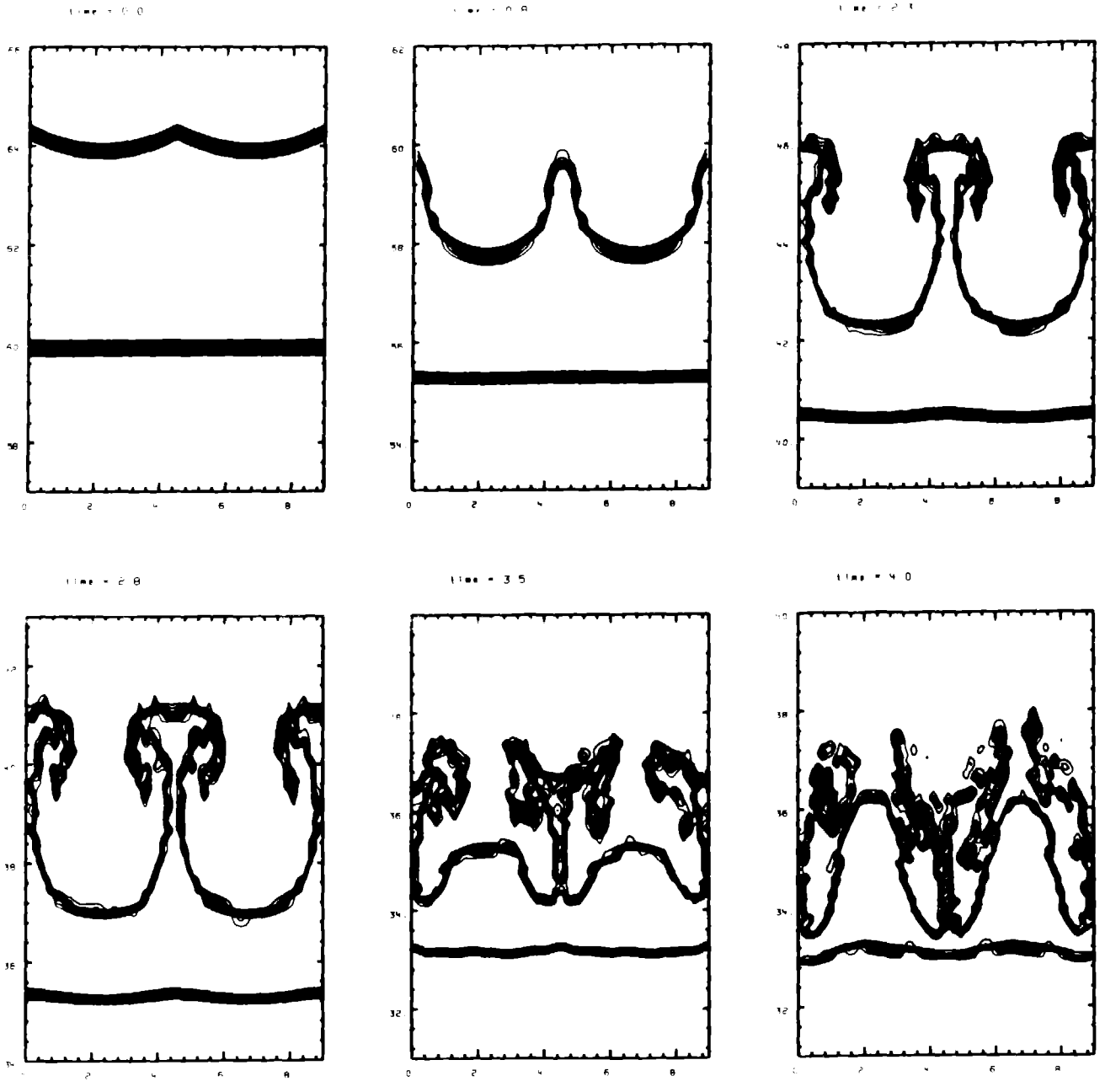

Fig. 18

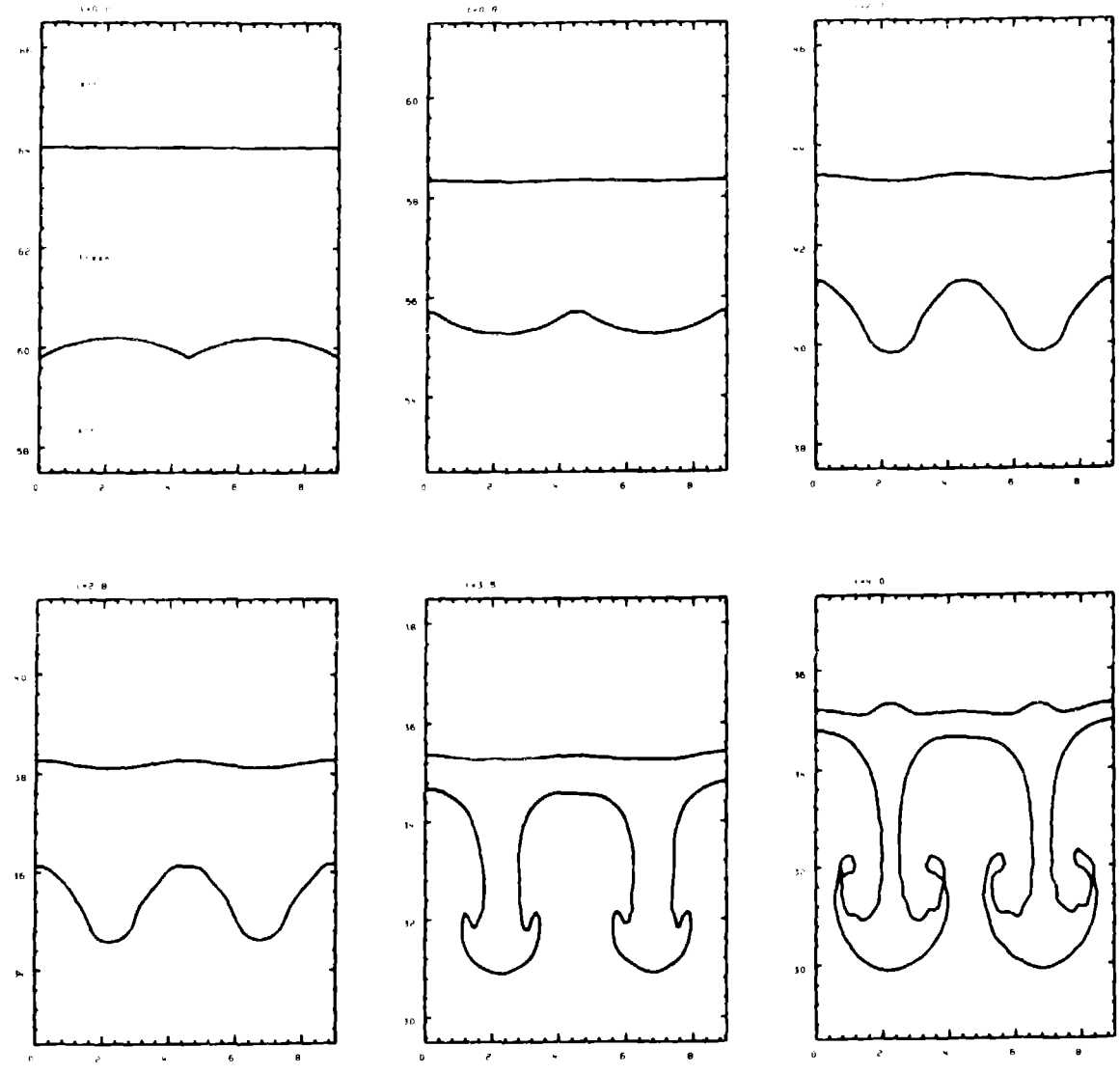

Fig. 19

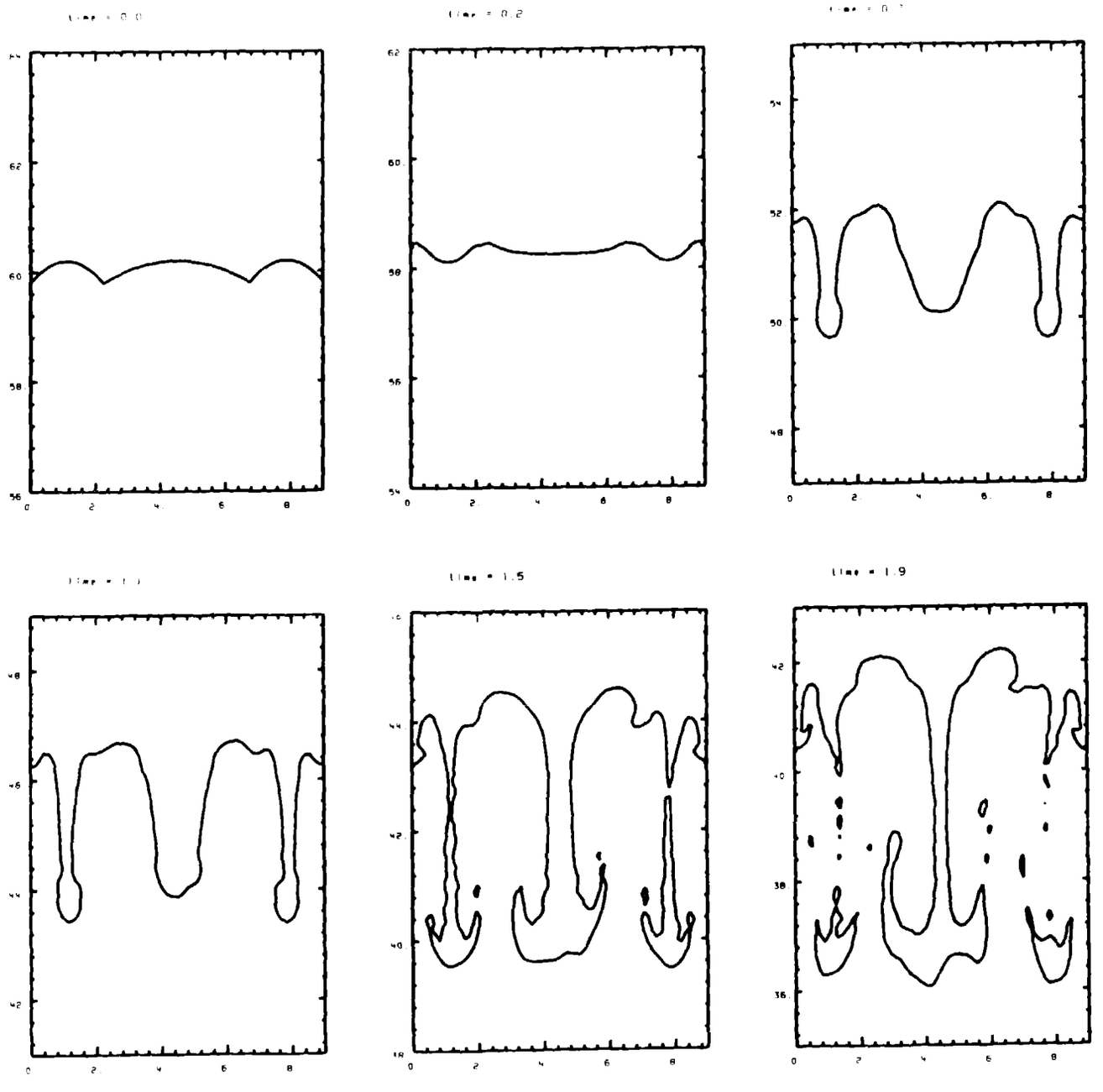

Fig. 20

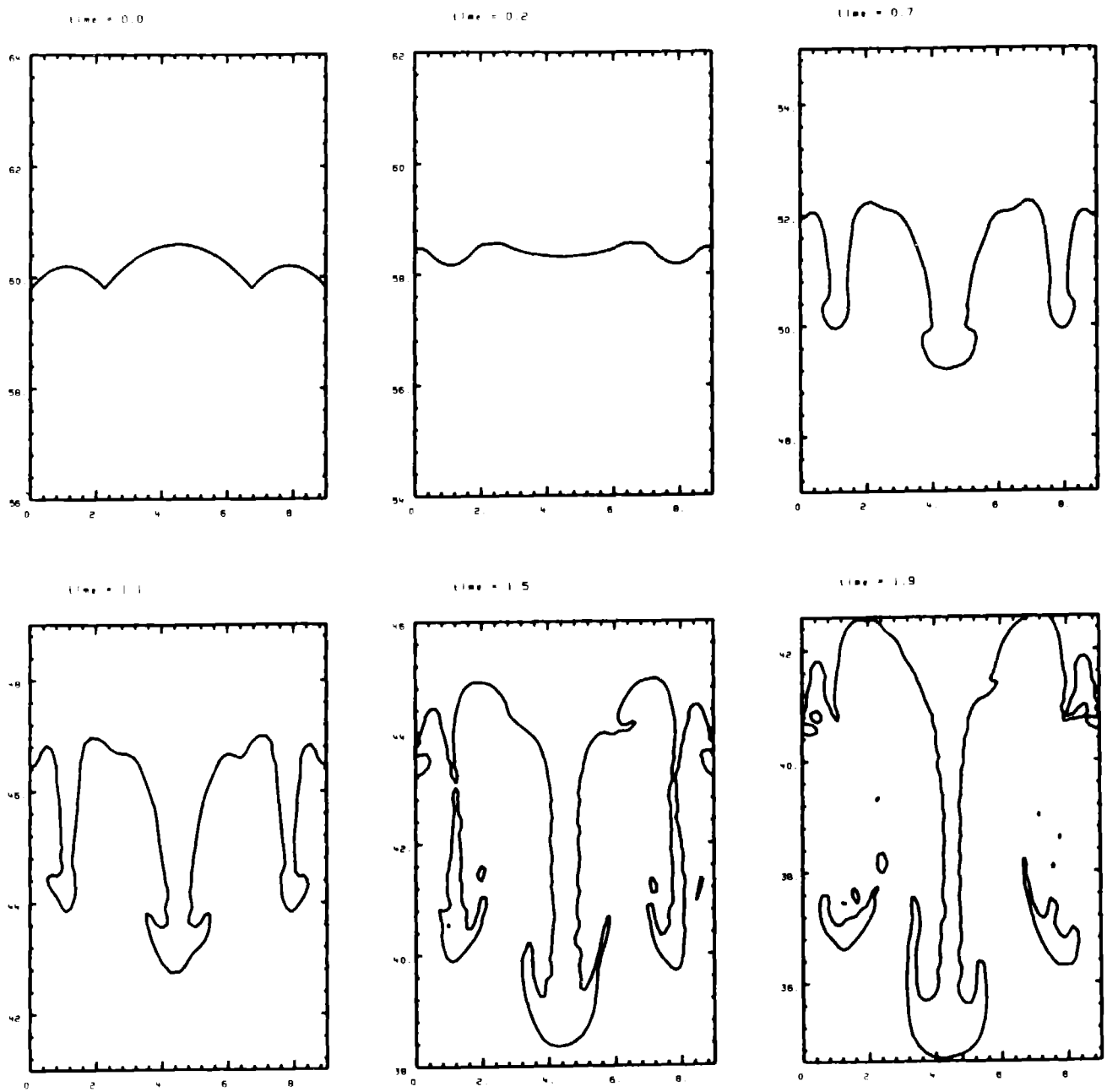

Fig. 21

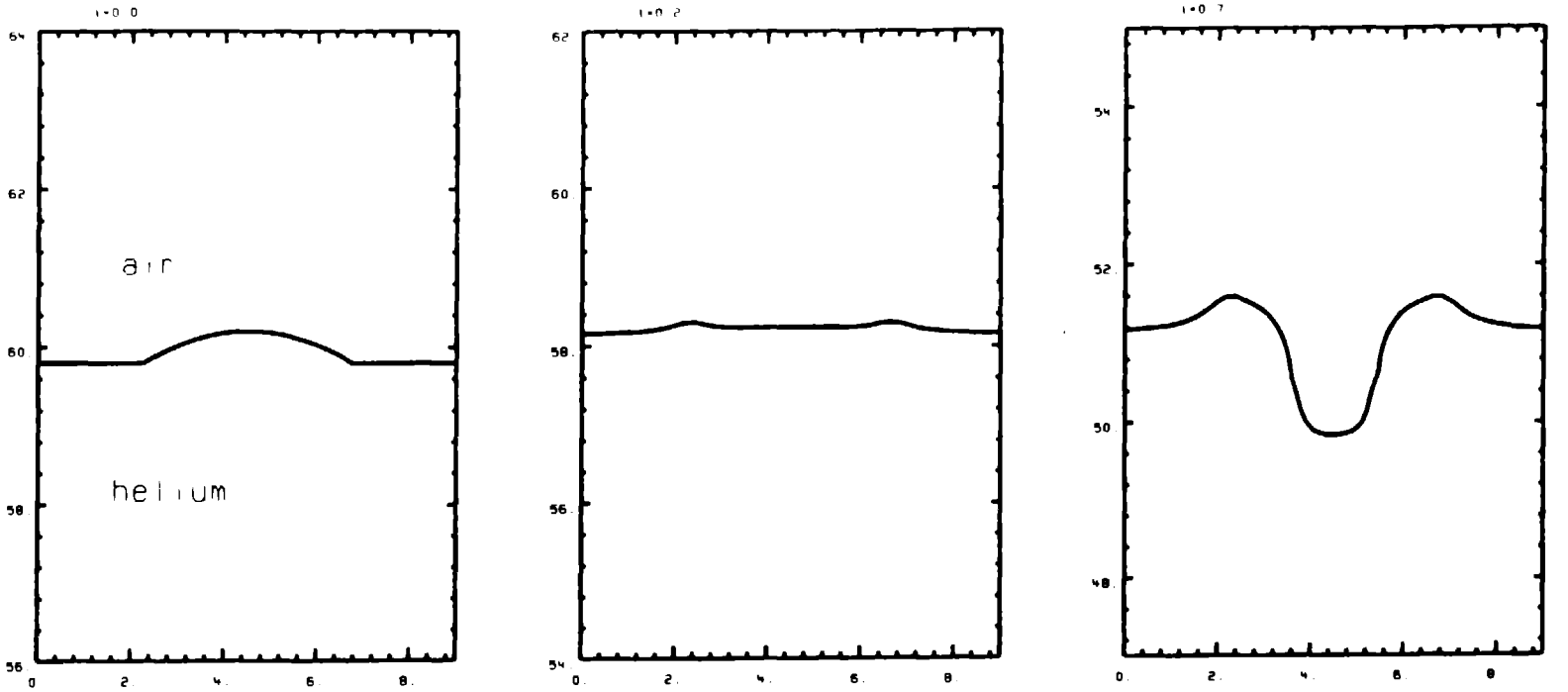

Fig. 22

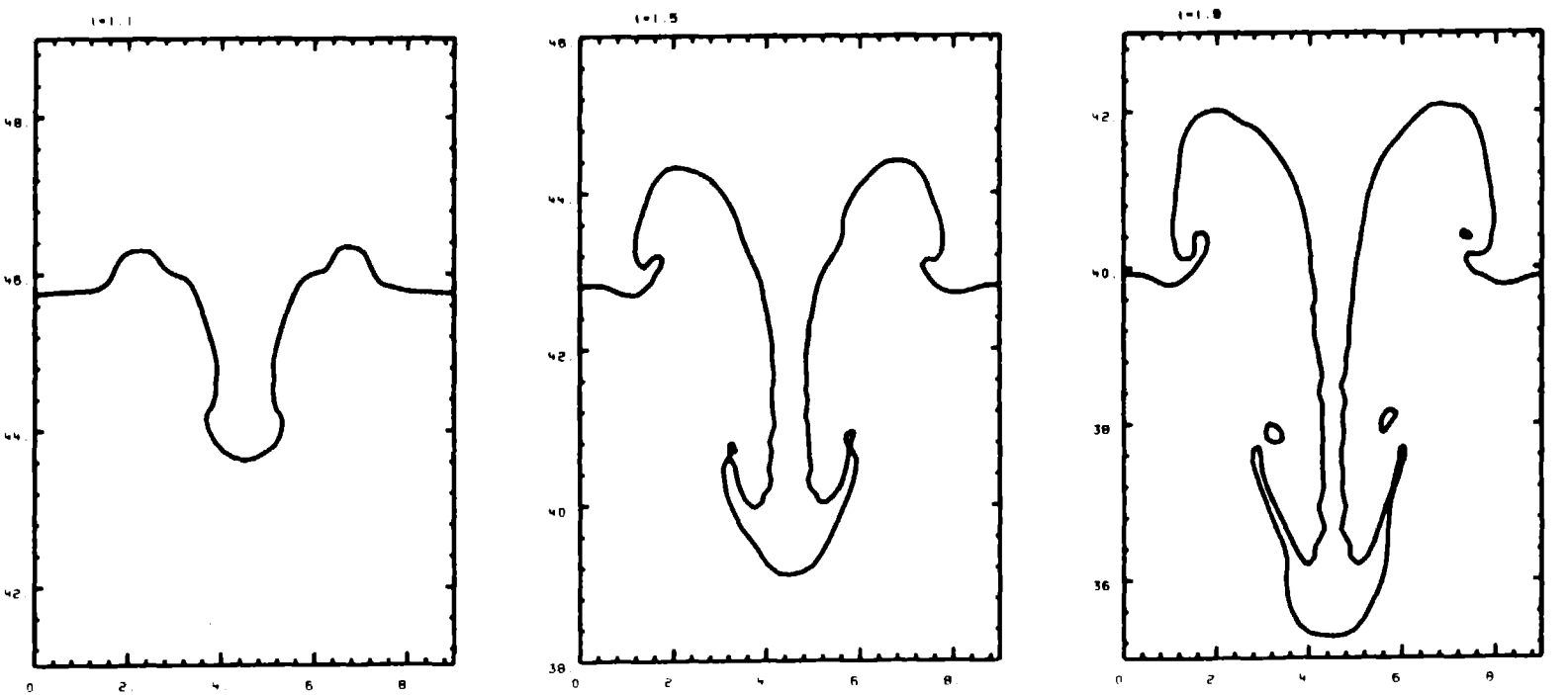

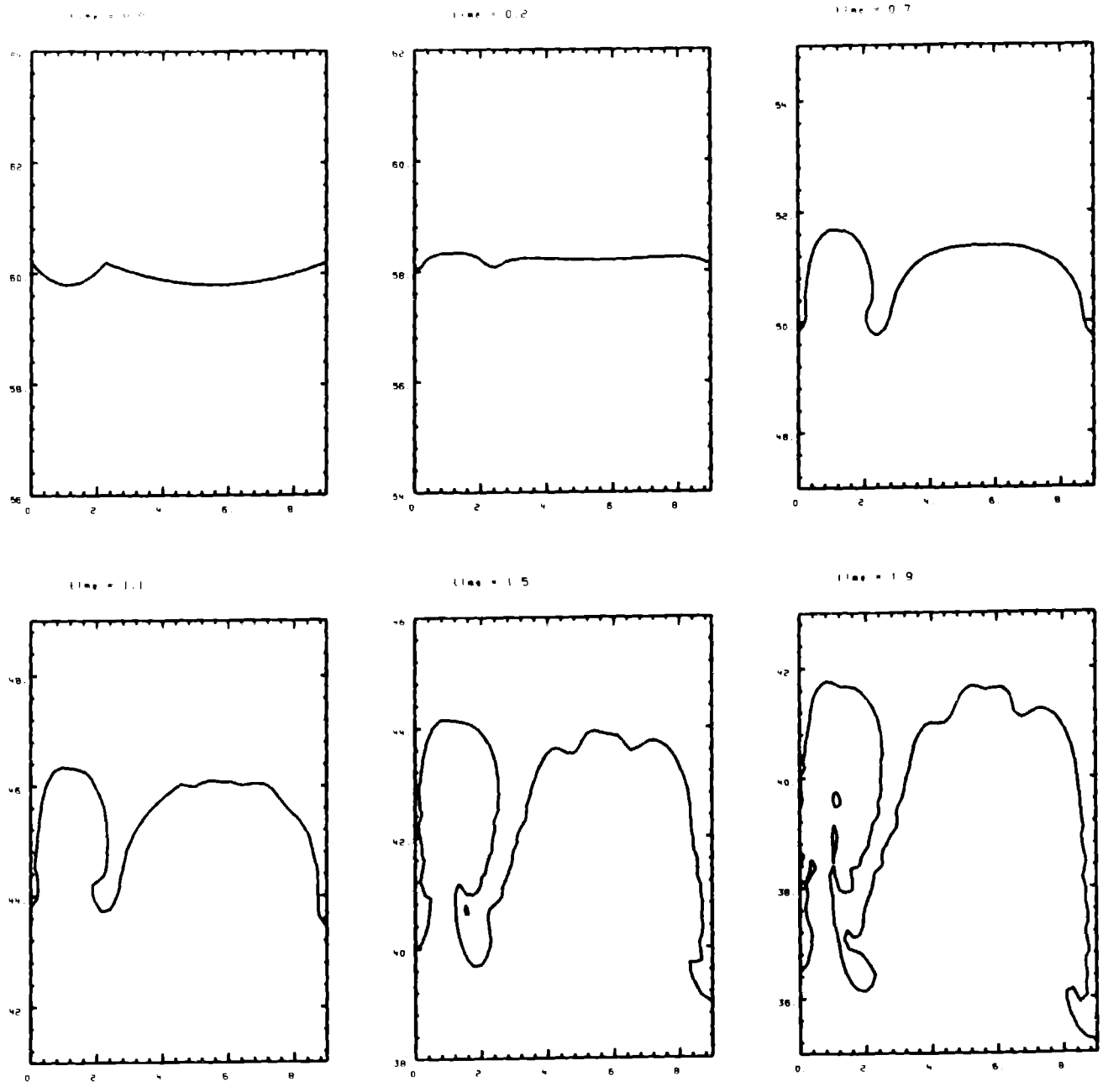

Fig. 23

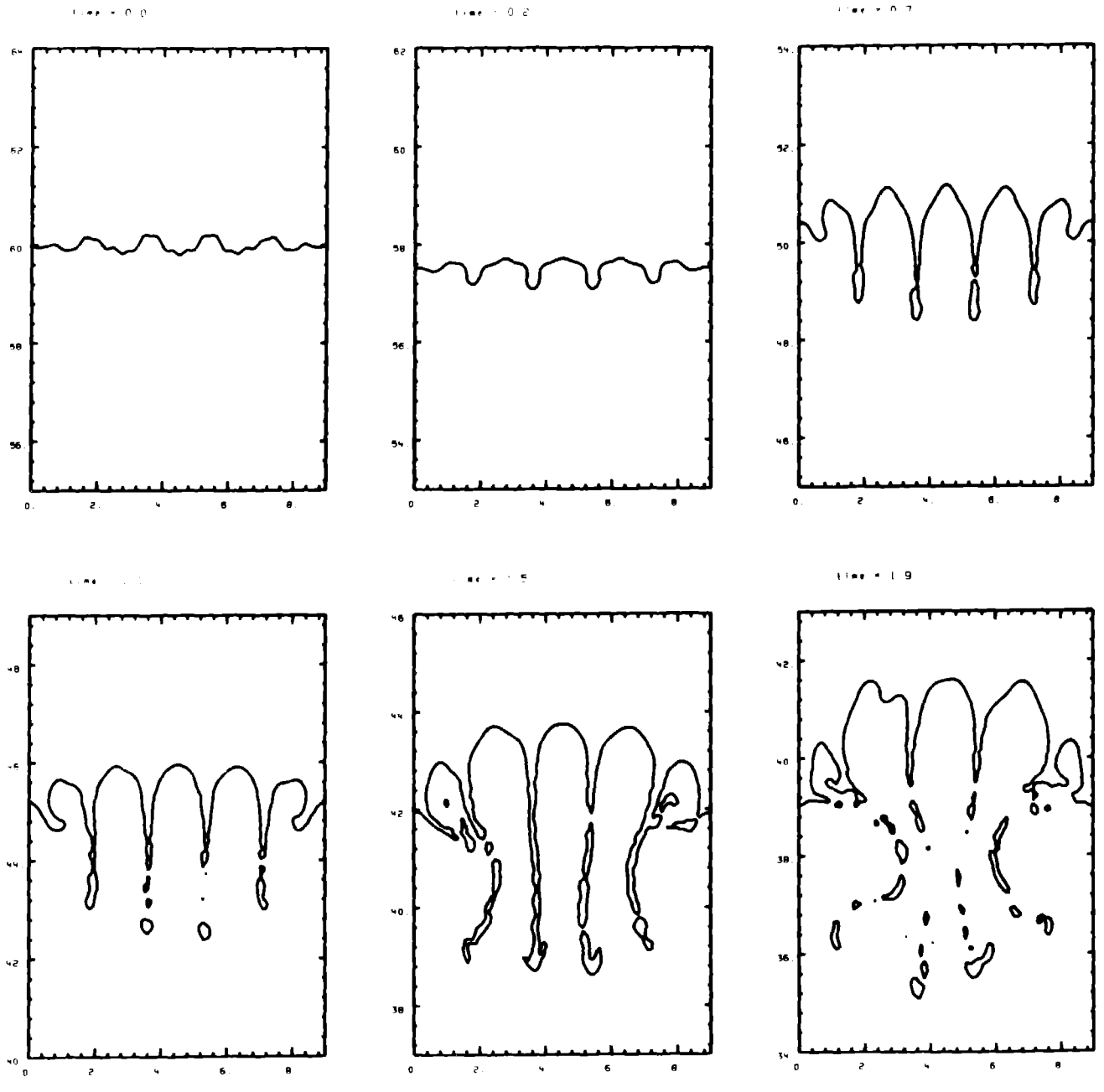

Fig. 24

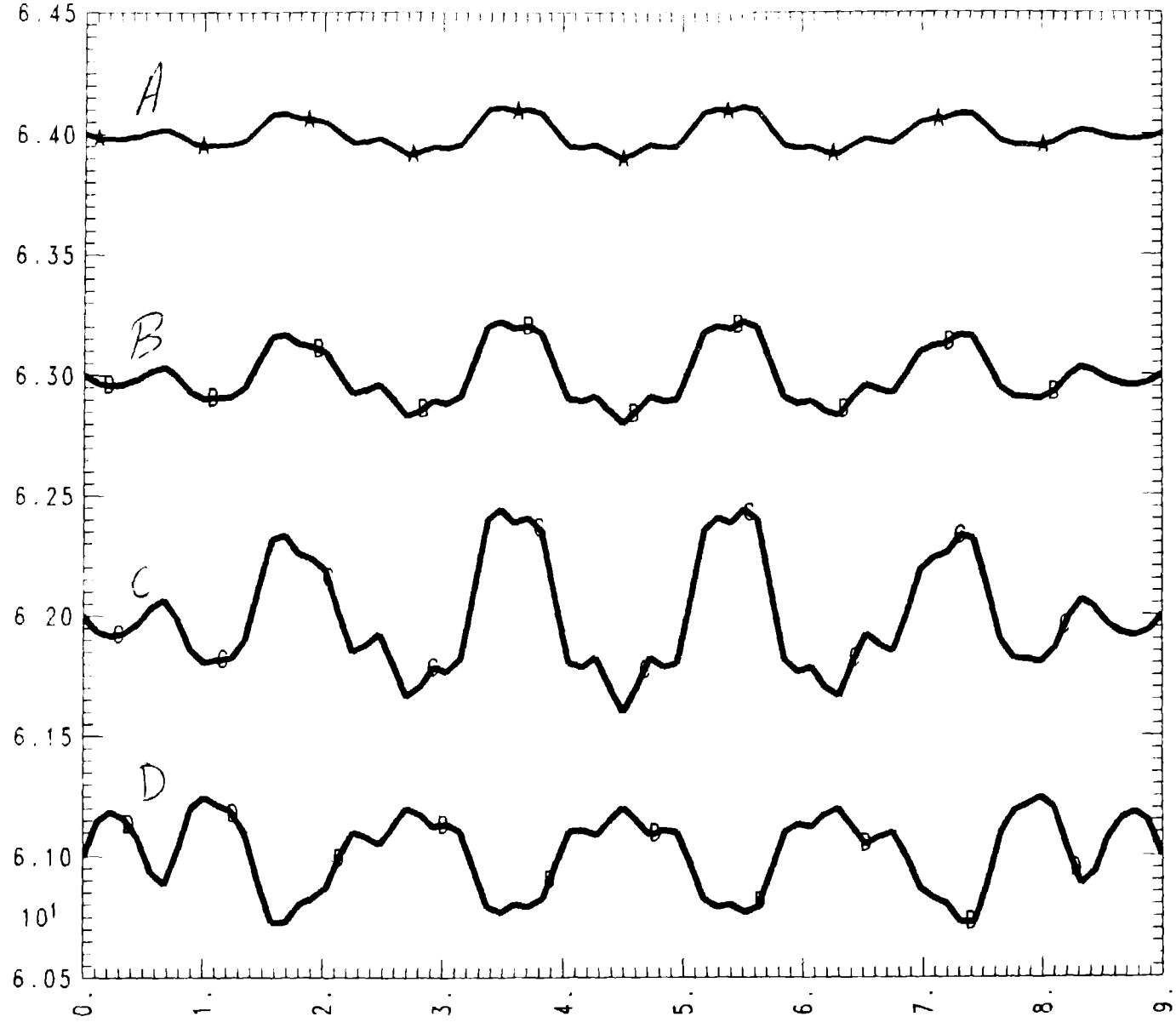

#	Y	X	FILE	XMIN	XMAX	YMIN	YMAX
A	*MW4			0	900+00	639+01	641+01
B	*MW2			0	900+00	628+01	632+01
C	*MW3			0	900+00	616+01	624+01
D	*MW6			0	900+00	607+01	612+01

15:23:2505/12/87 d

Fig. 25

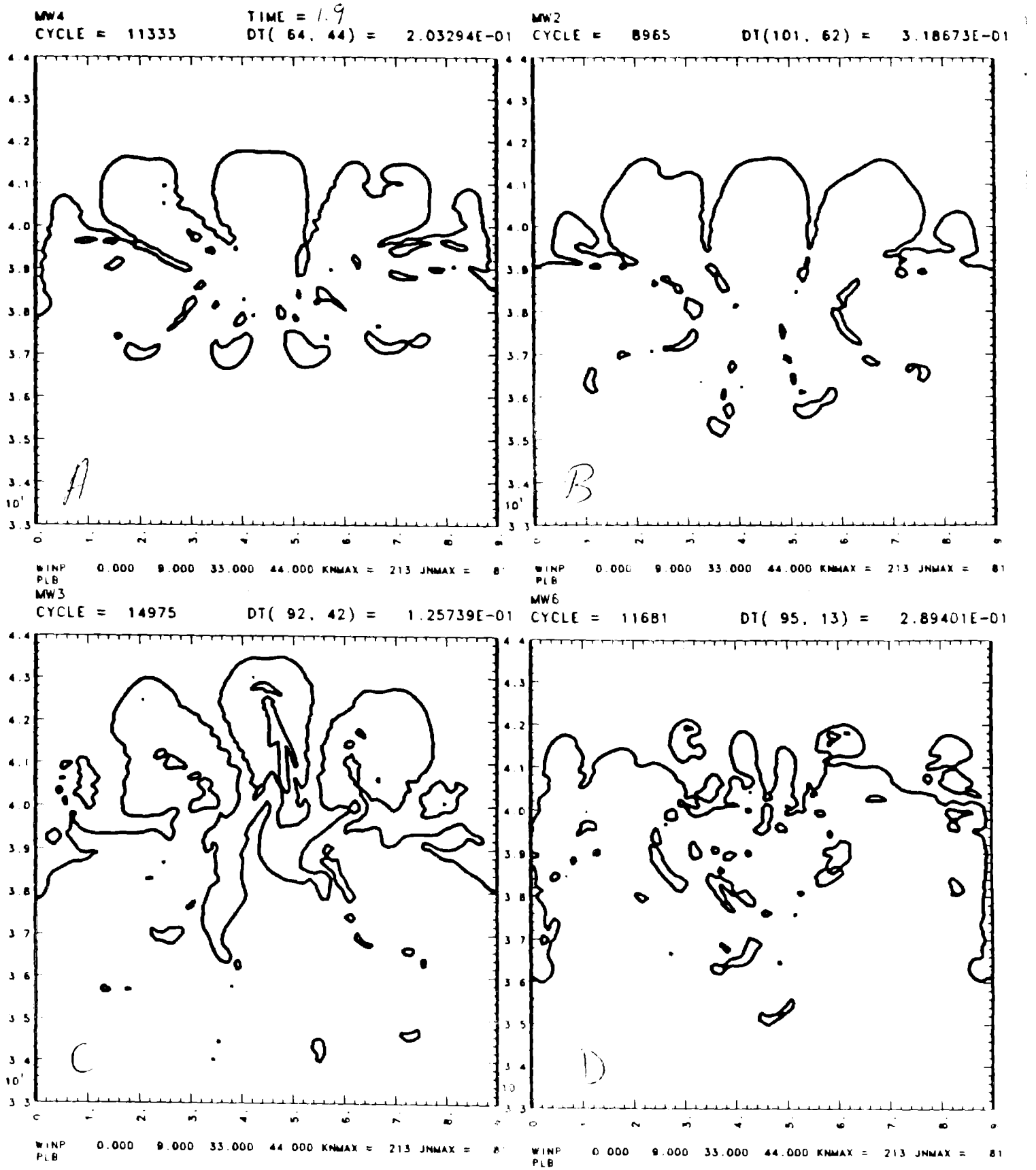
MW4
TIME = 1.9
CYCLE = 11333
DT(64, 44) = 2.03294E-01
A
MW2
CYCLE = 8965
DT(101, 62) = 3.18673E-01
B
MW3
CYCLE = 14975
DT(92, 42) = 1.25739E-01
C
MW6
CYCLE = 11681
DT(95, 13) = 2.89401E-01
D
WINP 0.000 9.000 33.000 44.000 KNMAX = 213 JNMAX = 81
PLB

Fig. 26

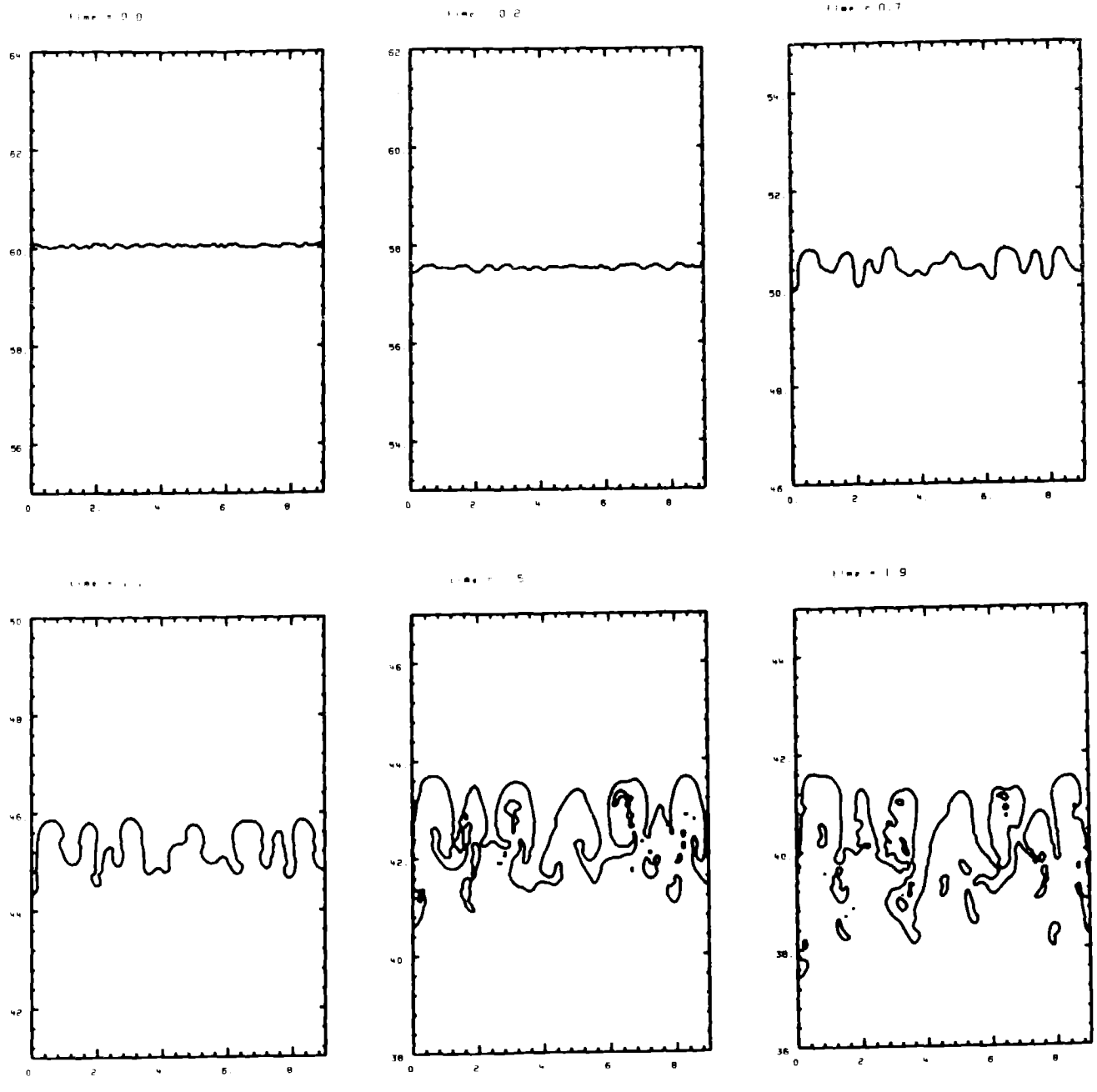

Fig. 27

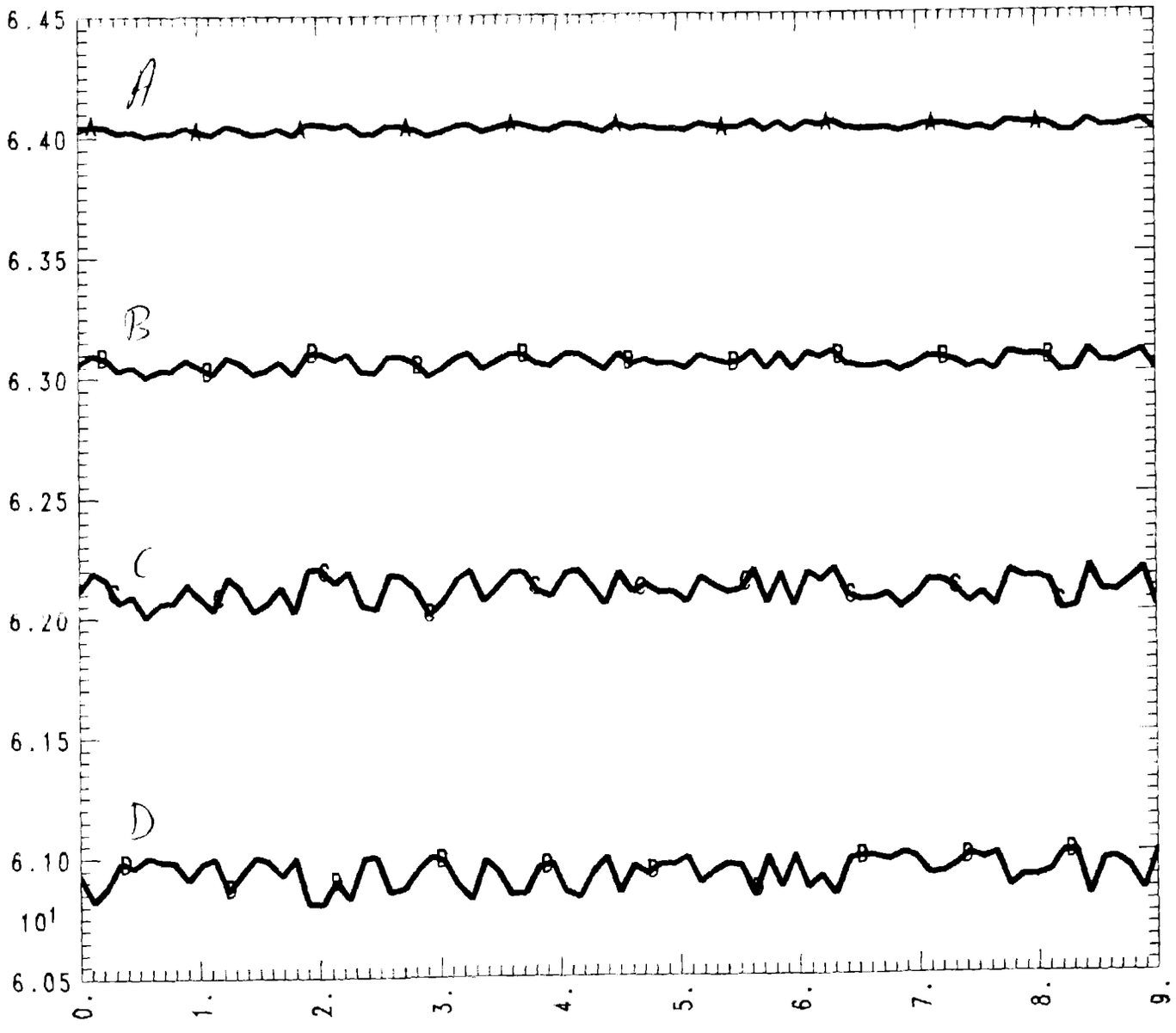

Y X

A*MW34
B*MW33
C*MW35
D*MW36

Fig. 28

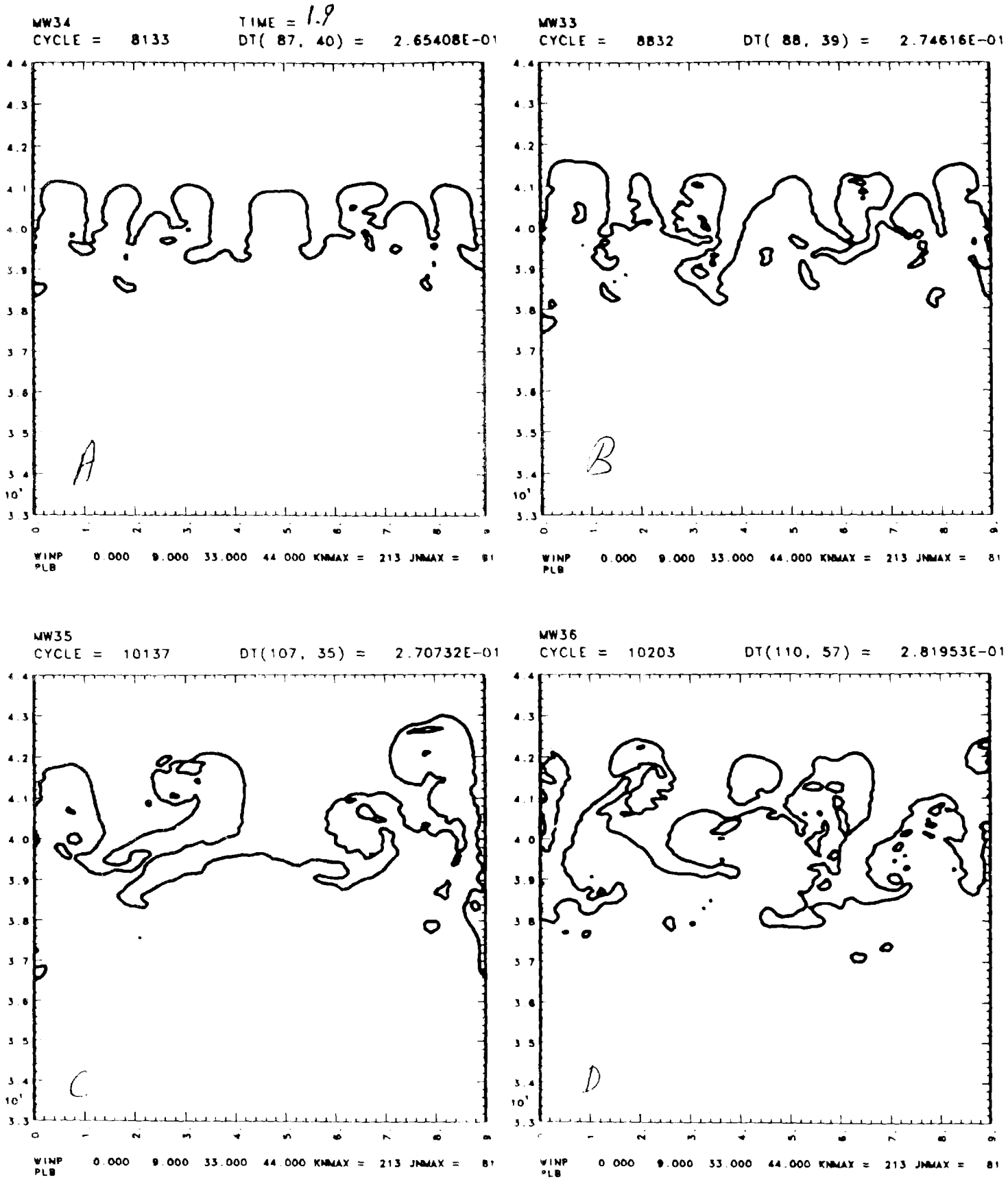
MW34
TIME = 1.9
CYCLE = 8133
DT(87, 40) = 2.65408E-01
A
WINP 0.000 9.000 33.000 44.000 KMAX = 213 JMAX = 81
PLB
MW33
CYCLE = 8832
DT(88, 39) = 2.74616E-01
B
WINP 0.000 9.000 33.000 44.000 KMAX = 213 JMAX = 81
PLB
MW35
CYCLE = 10137
DT(107, 35) = 2.70732E-01
C
WINP 0.000 9.000 33.000 44.000 KMAX = 213 JMAX = 81
PLB
MW36
CYCLE = 10203
DT(110, 57) = 2.81953E-01
D
WINP 0.000 9.000 33.000 44.000 KMAX = 213 JMAX = 81
PLB

Fig. 29

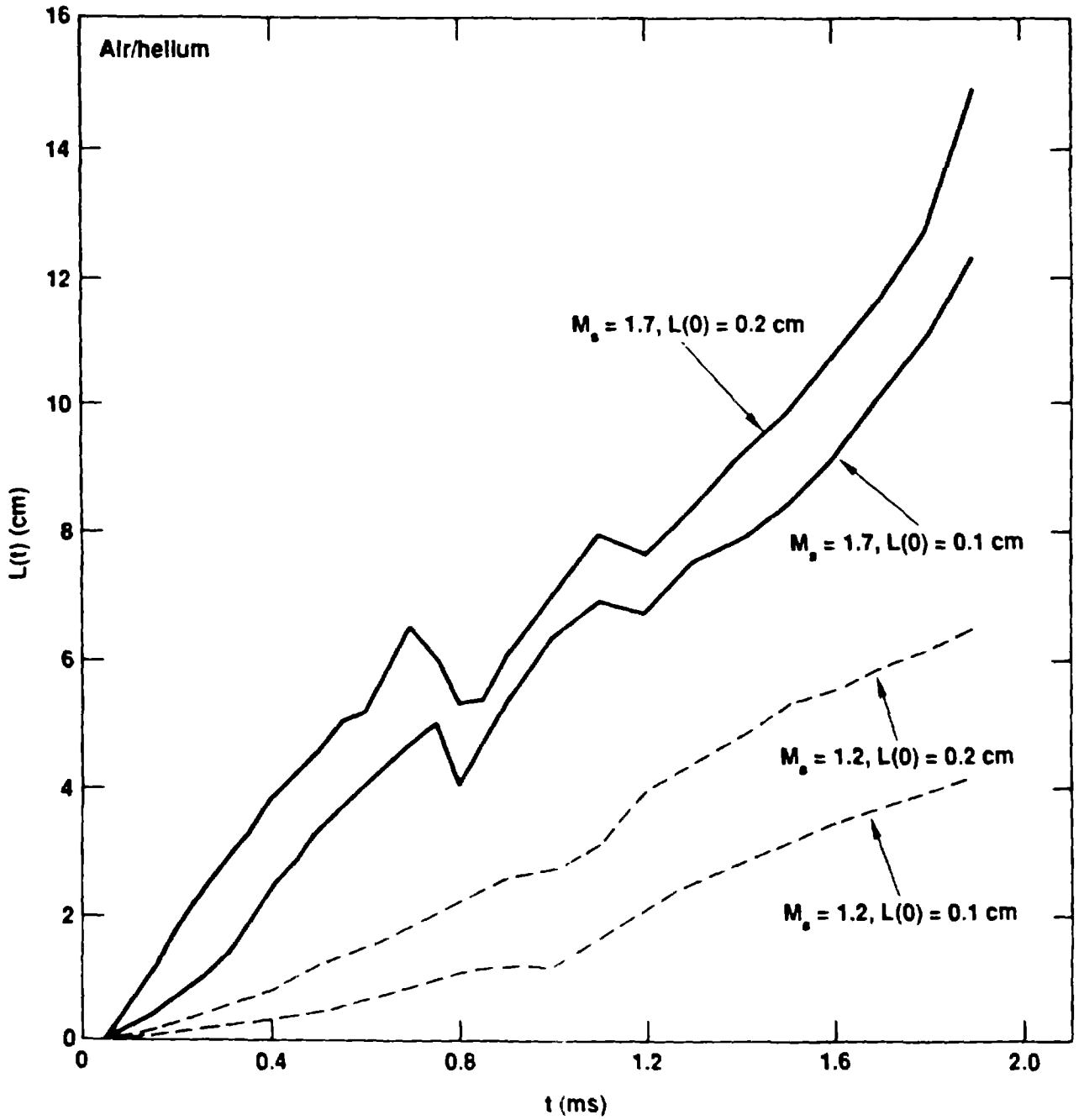
Air/helium
M_s = 1.7, L(0) = 0.2 cm
M_s = 1.7, L(0) = 0.1 cm
M_s = 1.2, L(0) = 0.2 cm
M_s = 1.2, L(0) = 0.1 cm
L(t) (cm)
t (ms)
0
2
4
6
8
10
12
14
16
0
0.4
0.8
1.2
1.6
2.0

Fig. 30

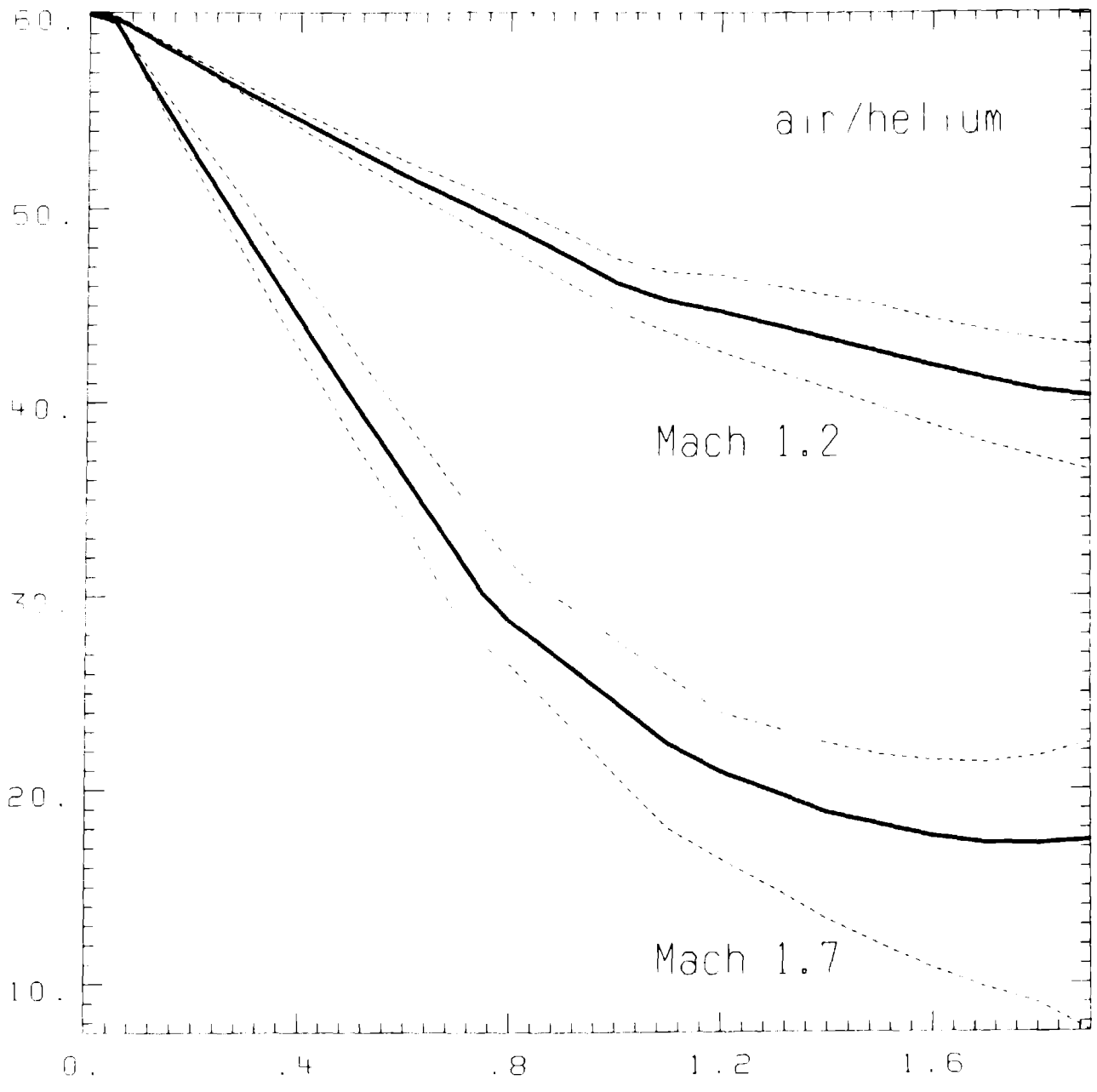

Fig. 31

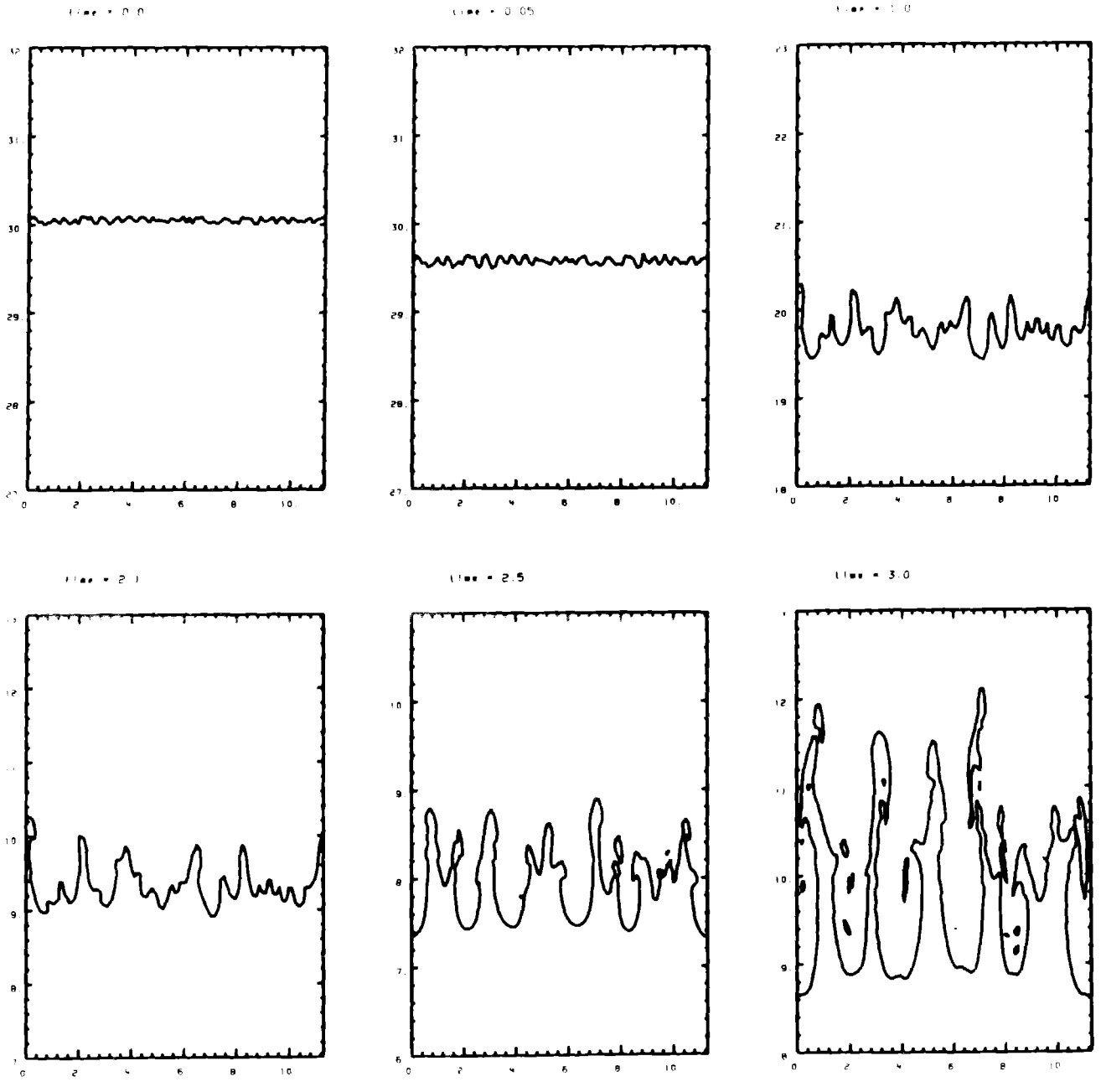

Fig. 32

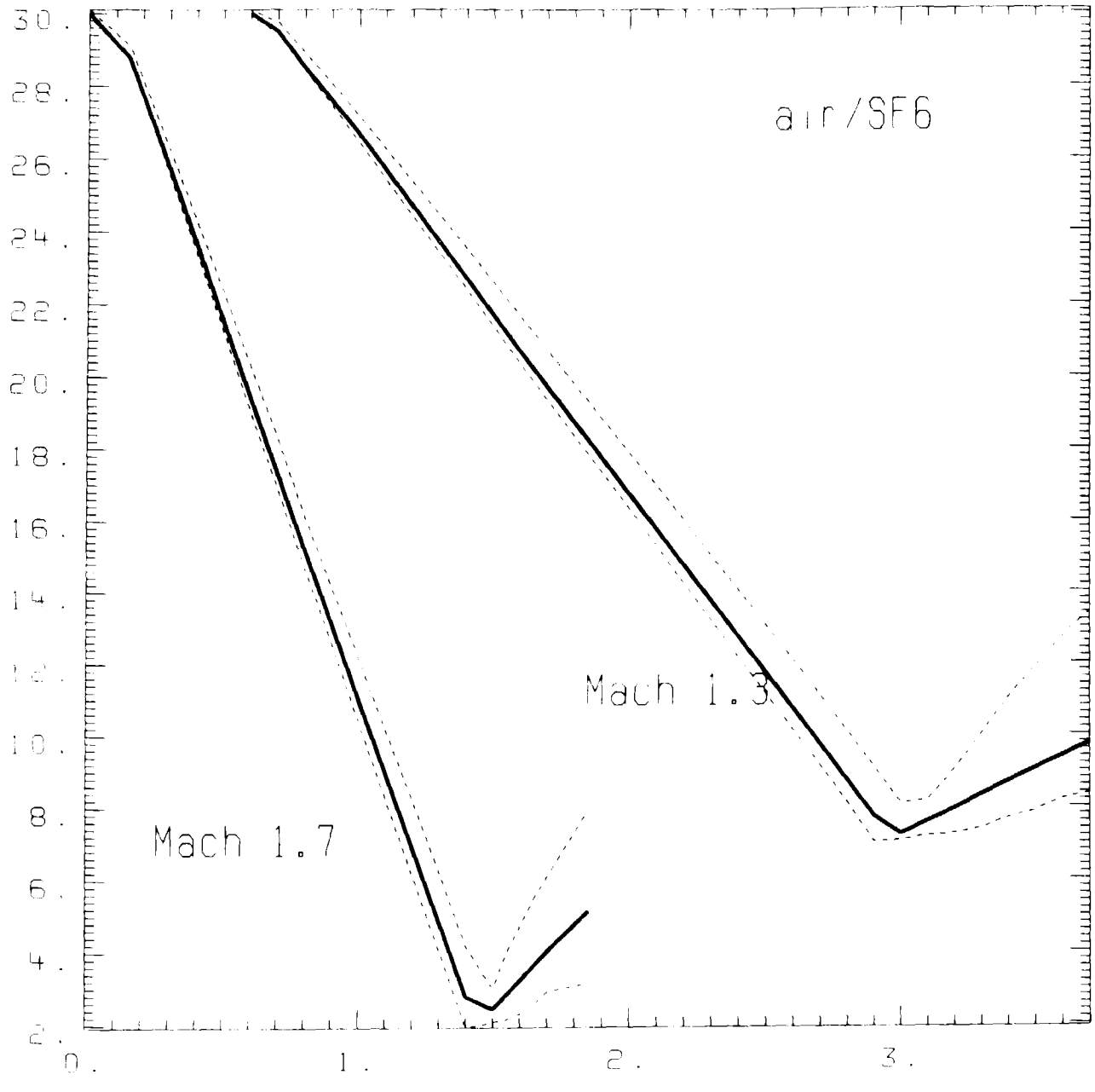

Fig. 33

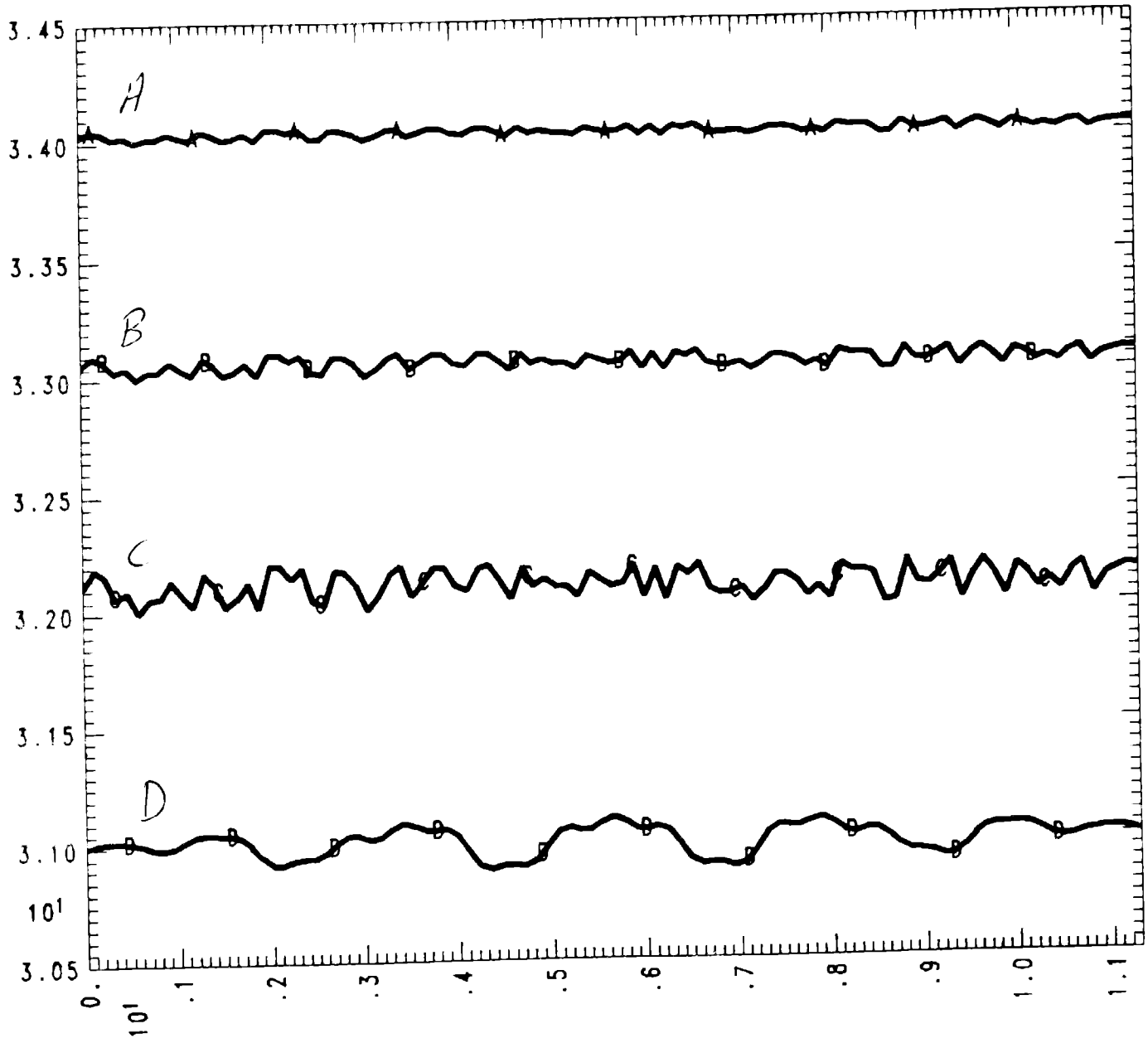
3.45
3.40
3.35
3.30
3.25
3.20
3.15
3.10
3.05
10^1
A
B
C
D
0.
10^1
.1
.2
.3
.4
.5
.6
.7
.8
.9
1.0
1.1
Y X
A*MW31
B*MW29
C*MW32
D*MW28

Fig. 34

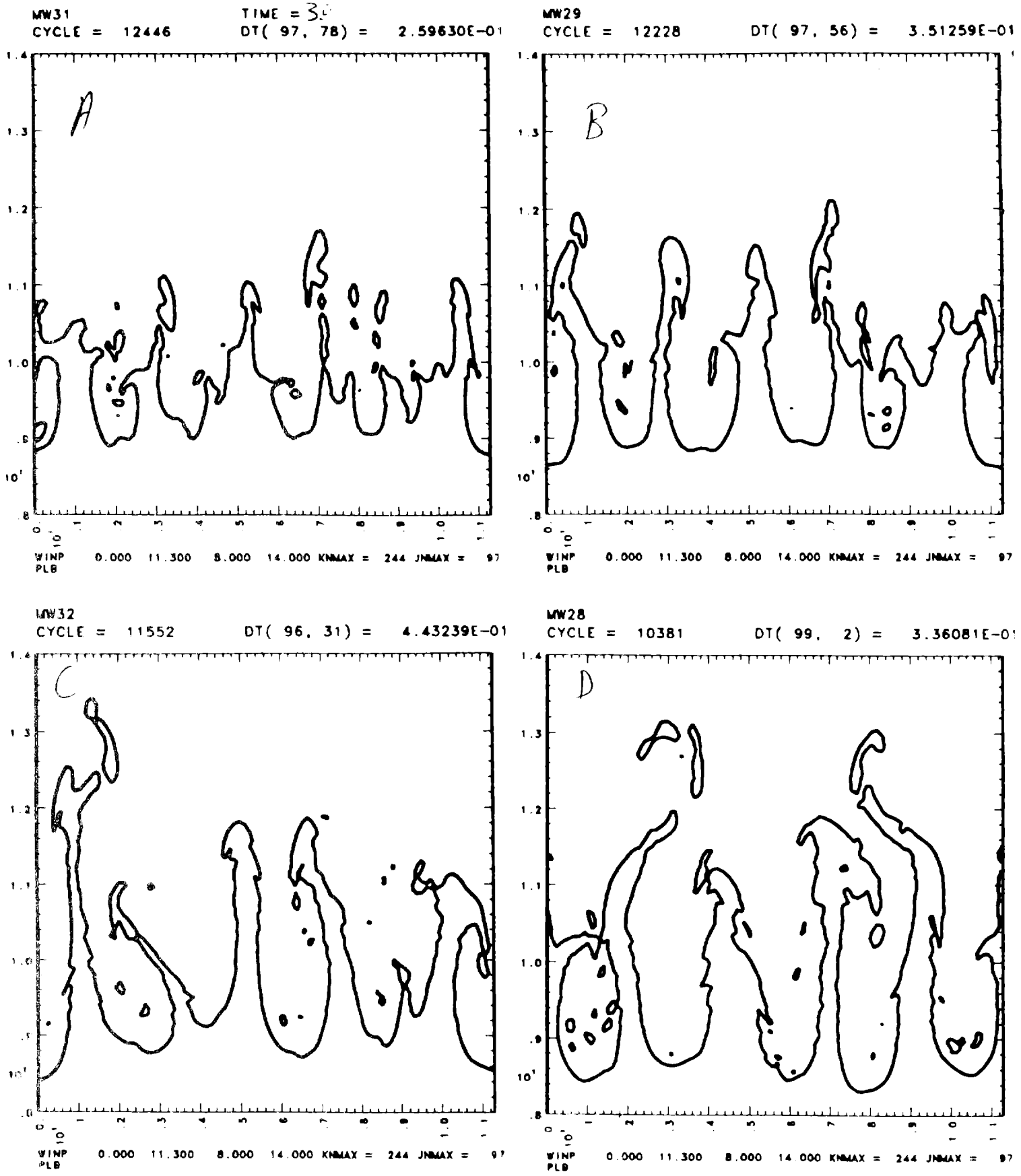
MW31
CYCLE = 12446
TIME = 3.0
DT(97, 78) = 2.59630E-01
A
WINP 0.000 11.300 8.000 14.000 KMAX = 244 JMAX = 97
PLB
MW29
CYCLE = 12228
DT(97, 56) = 3.51259E-01
B
WINP 0.000 11.300 8.000 14.000 KMAX = 244 JMAX = 97
PLB
MW32
CYCLE = 11552
DT(96, 31) = 4.43239E-01
C
WINP 0.000 11.300 8.000 14.000 KMAX = 244 JMAX = 97
PLB
MW28
CYCLE = 10381
DT(99, 2) = 3.36081E-01
D
WINP 0.000 11.300 8.000 14.000 KMAX = 244 JMAX = 97
PLB

Fig. 35

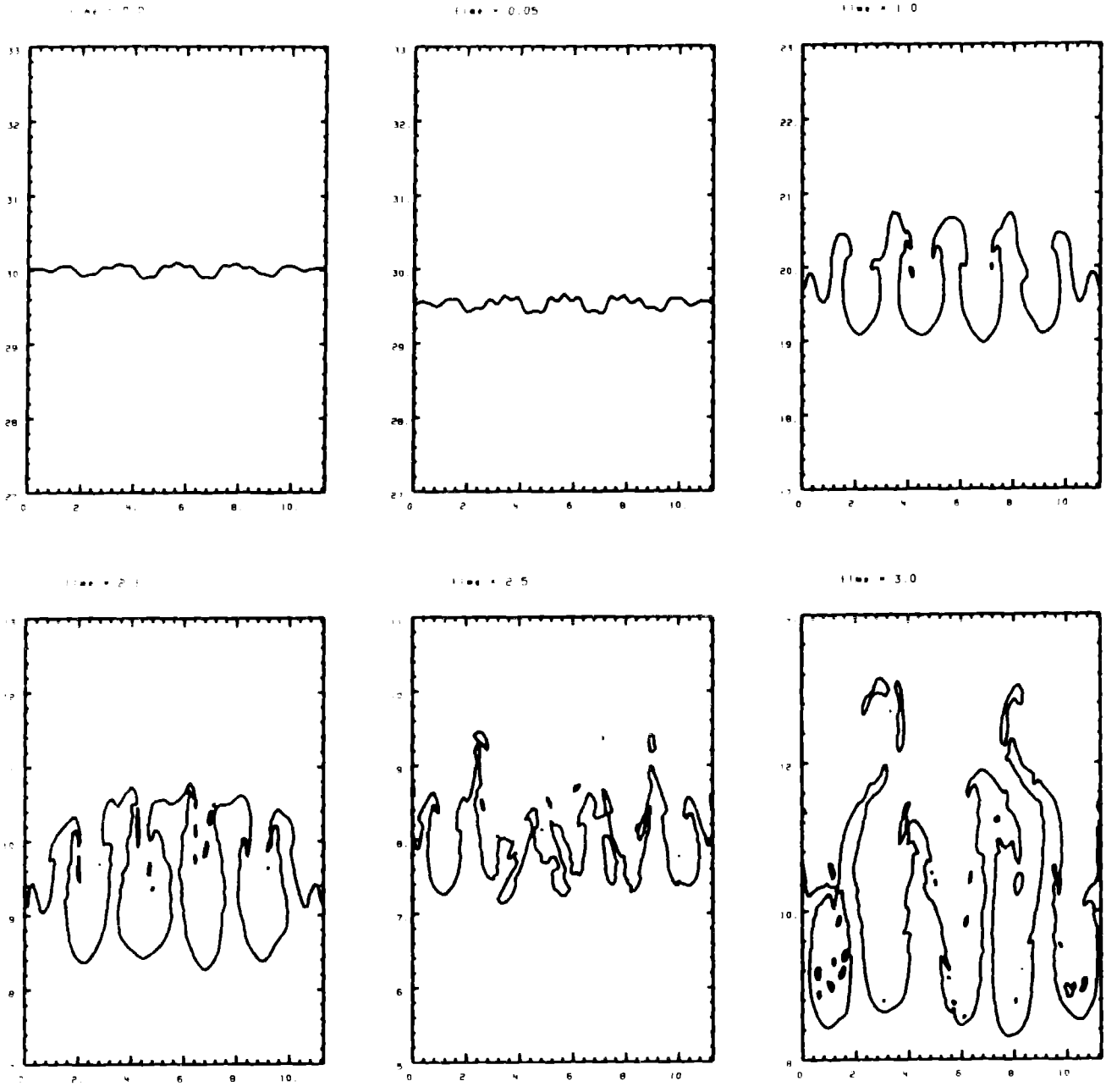

Fig. 36

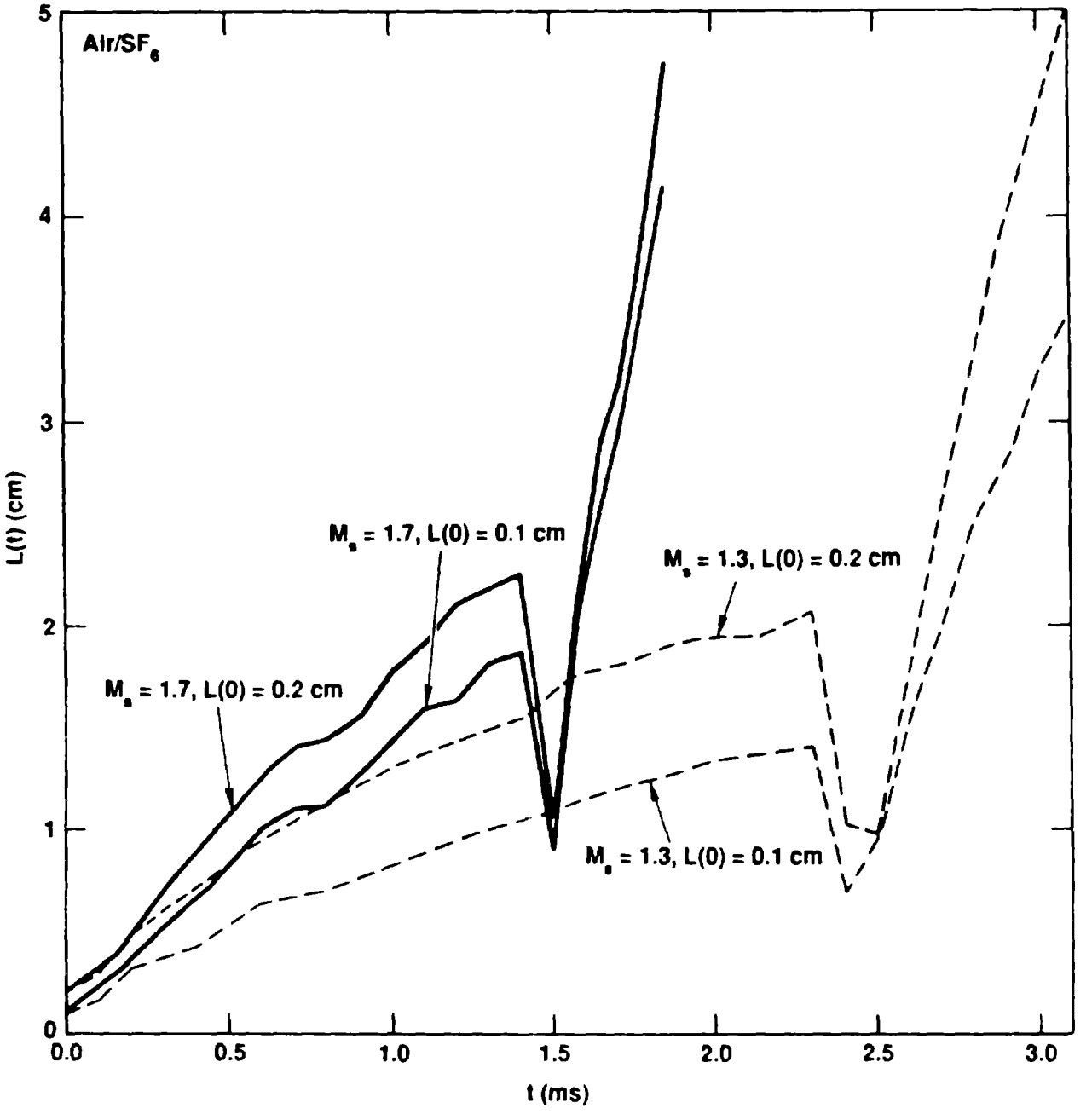
Air/SF6
M = 1.7, L(0) = 0.1 cm
M = 1.3, L(0) = 0.2 cm
M = 1.7, L(0) = 0.2 cm
M = 1.3, L(0) = 0.1 cm
L(t) (cm)
t (ms)
0
1
2
3
4
5
0.0
0.5
1.0
1.5
2.0
2.5
3.0

Fig. 37

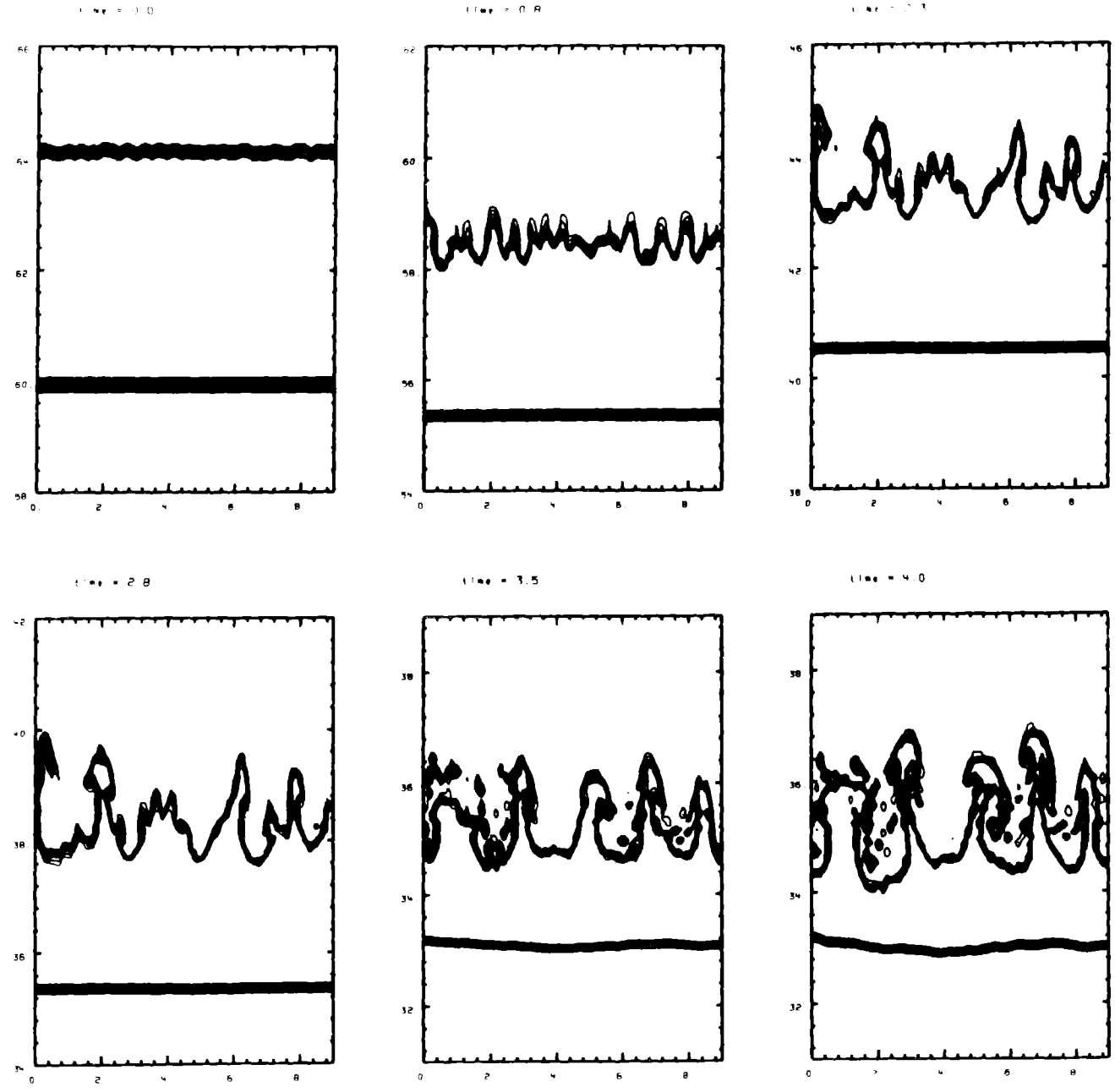

Fig. 38

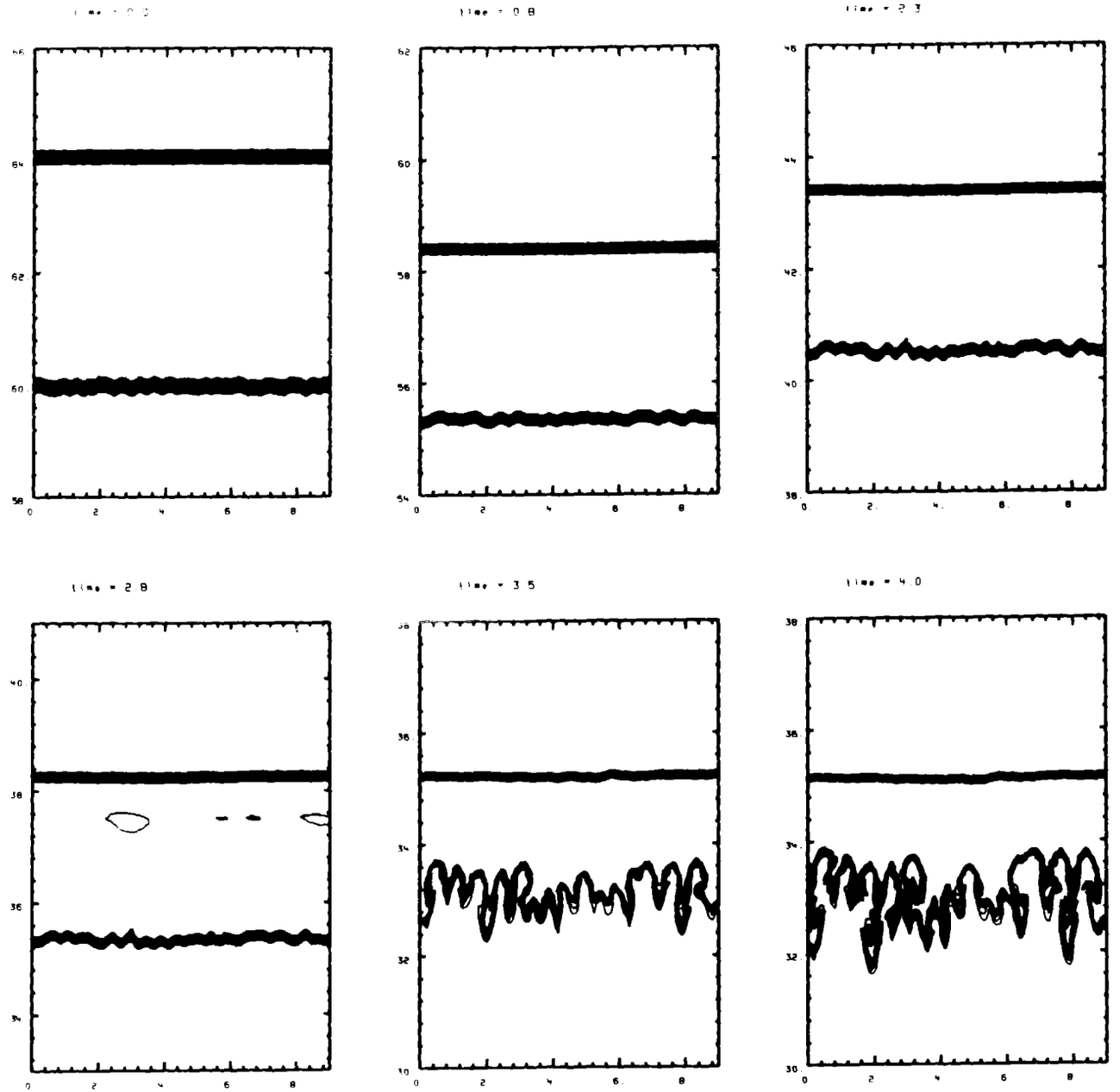

Fig. 39

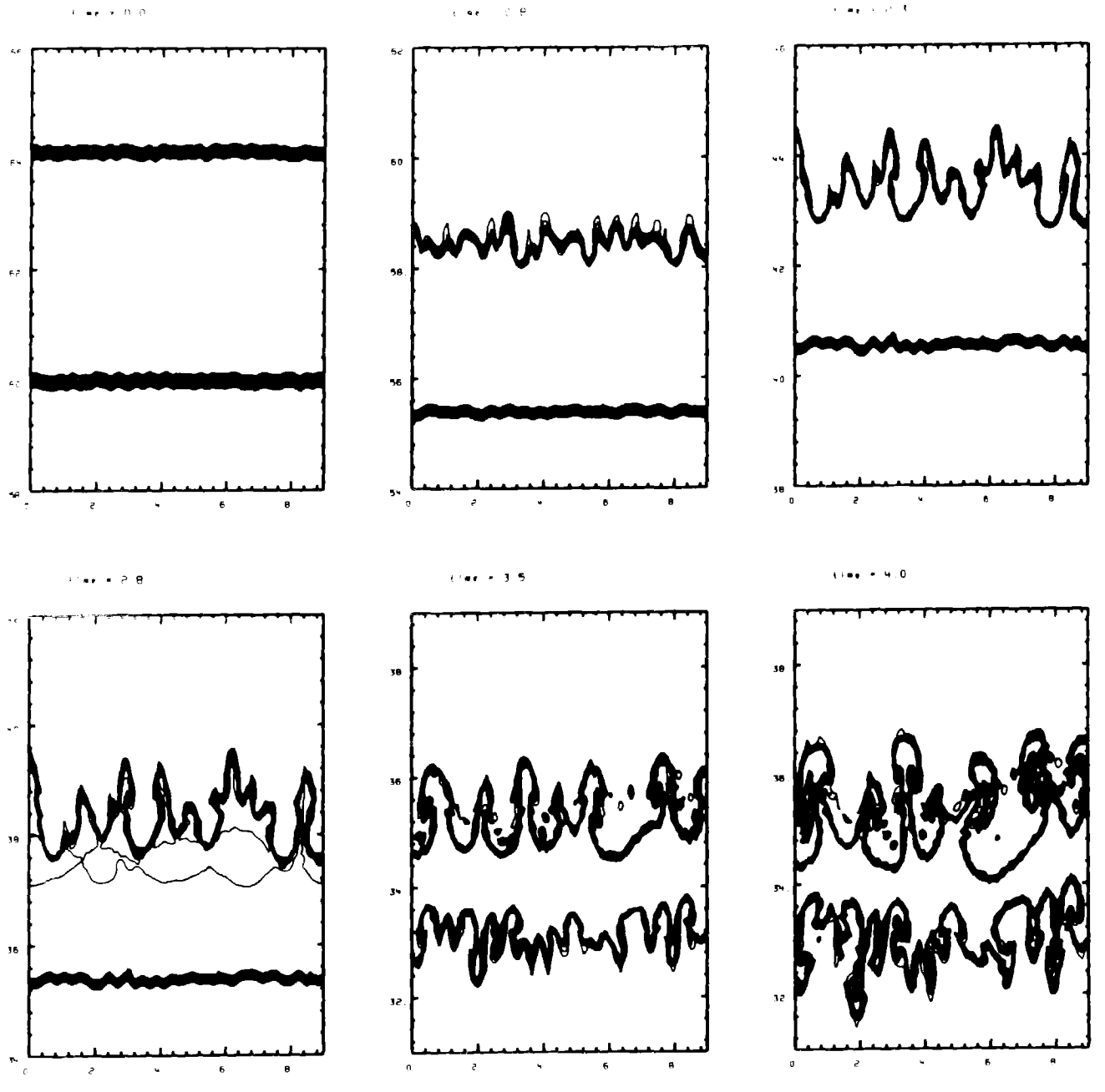

Fig. 40

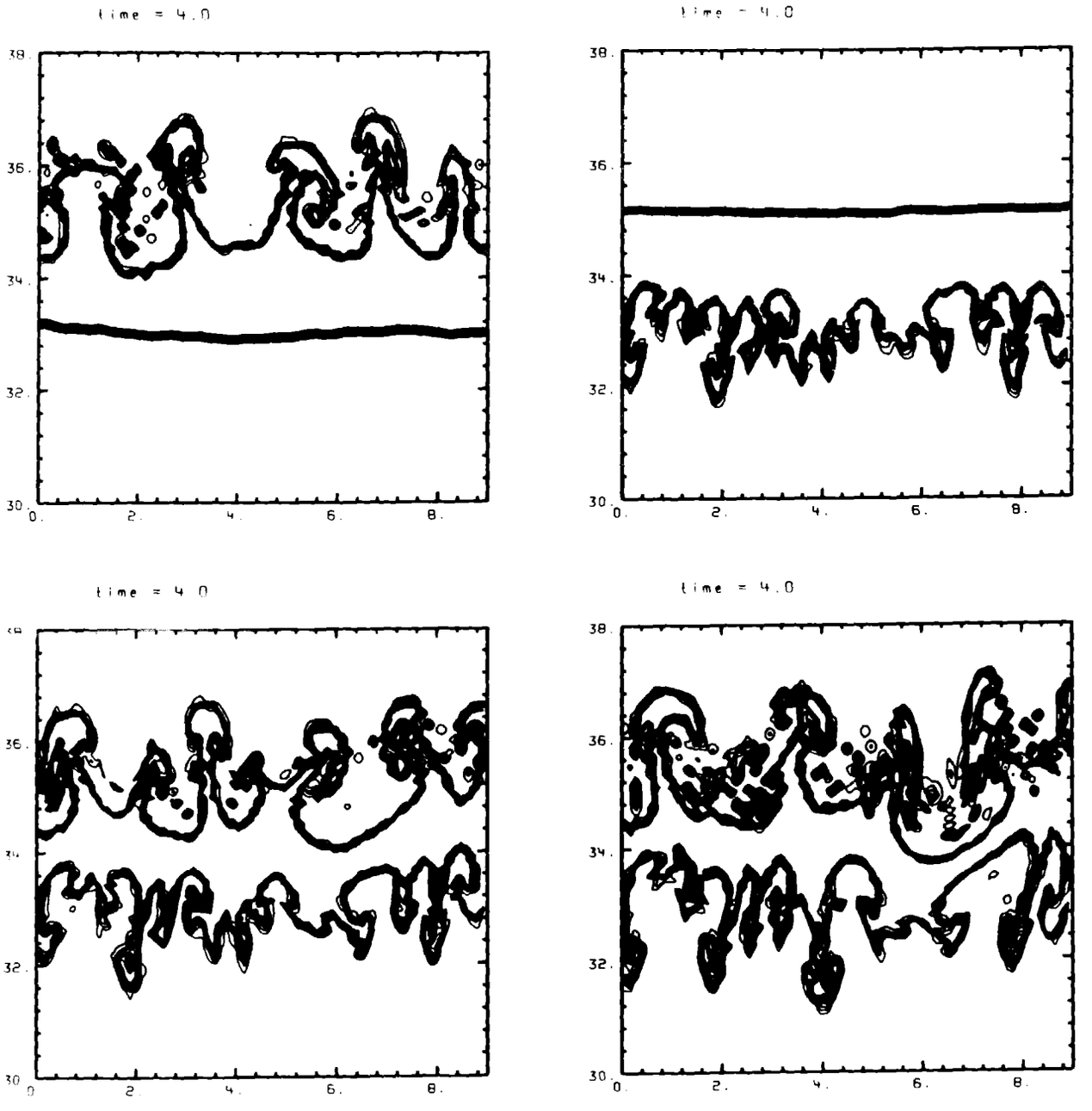
Time = 4.0
38.
36.
34.
32.
30.
0.
2.
4.
6.
8.
Time = 4.0
38.
36.
34.
32.
30.
0.
2.
4.
6.
8.
Time = 4.0
36.
32.
30.
0
2.
4.
6.
8.
Time = 4.0
38.
36.
34.
32.
30.
0.
2.
4.
6.
8.

Fig. 41

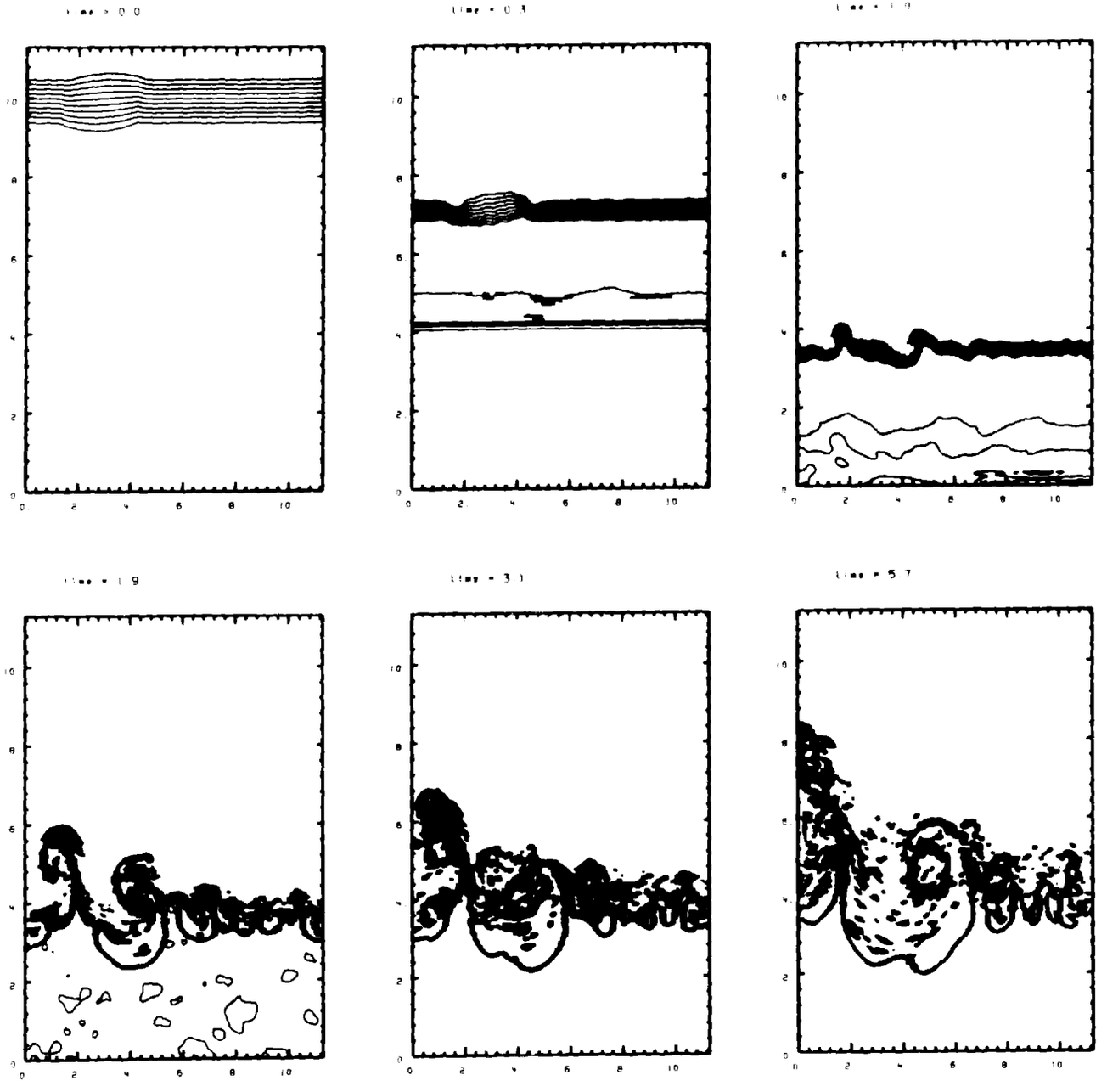

Fig. 42

Our simulations show good agreement with recent shock tube experiments

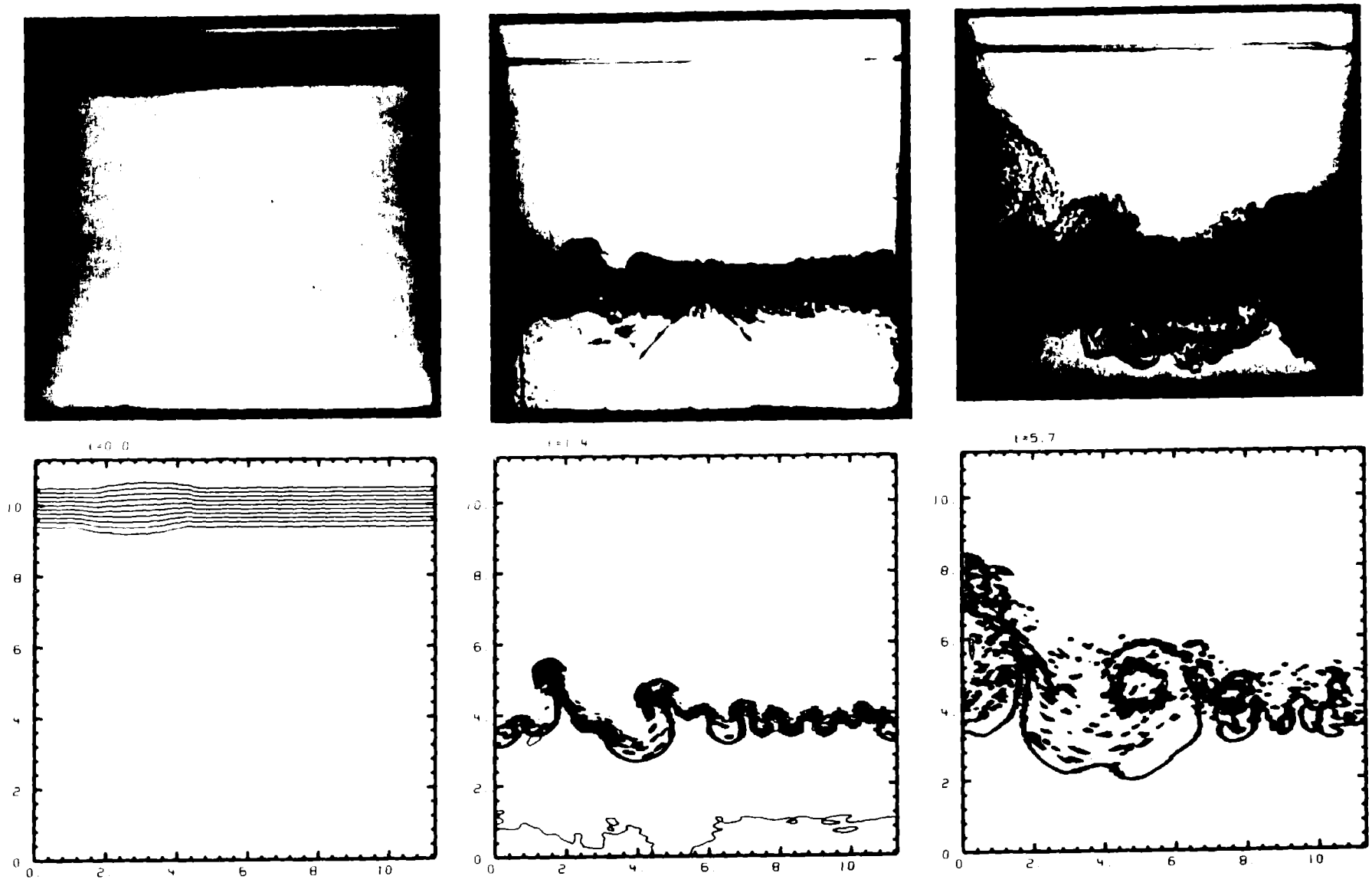

Fig. 43

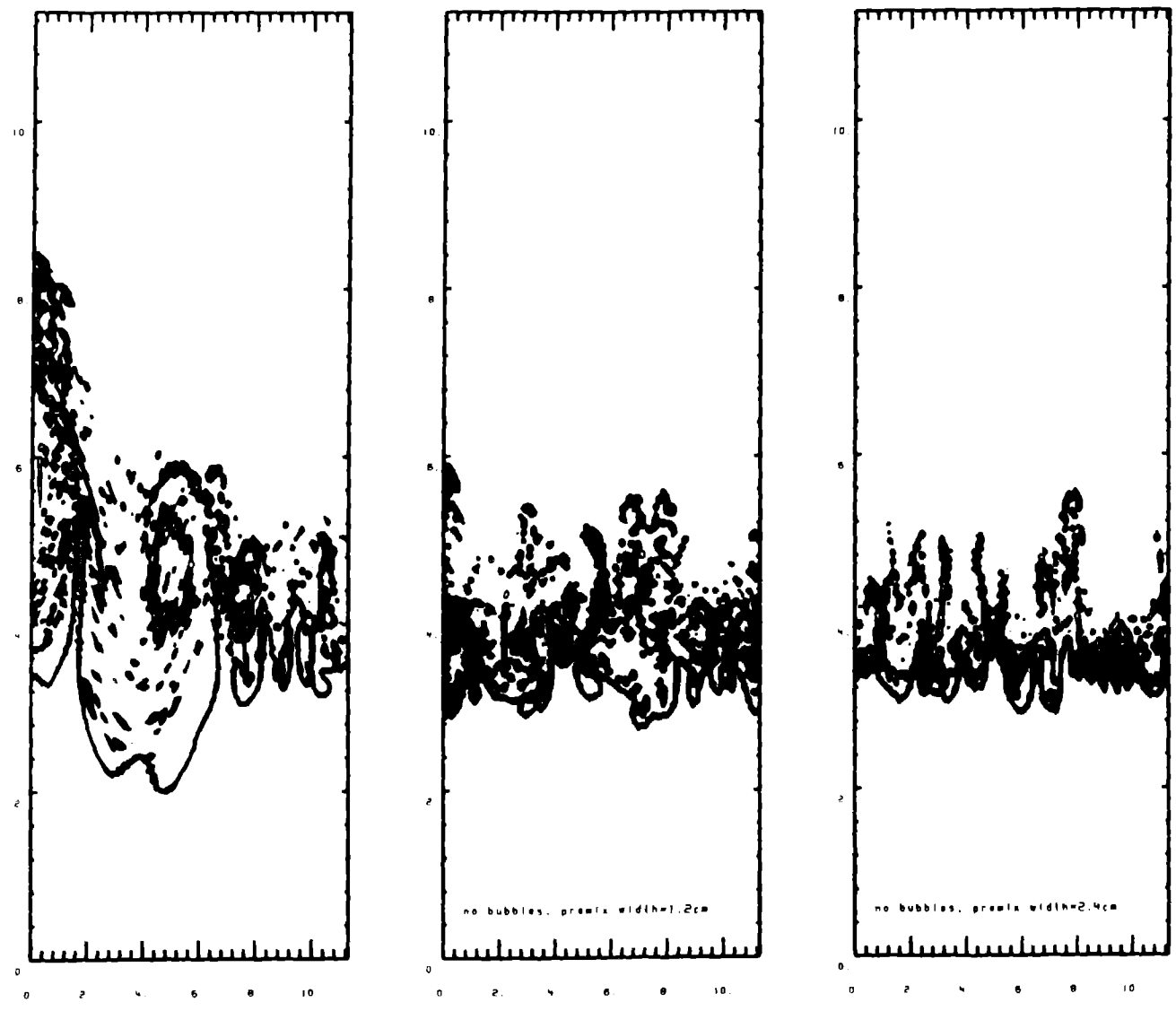

Fig. 44

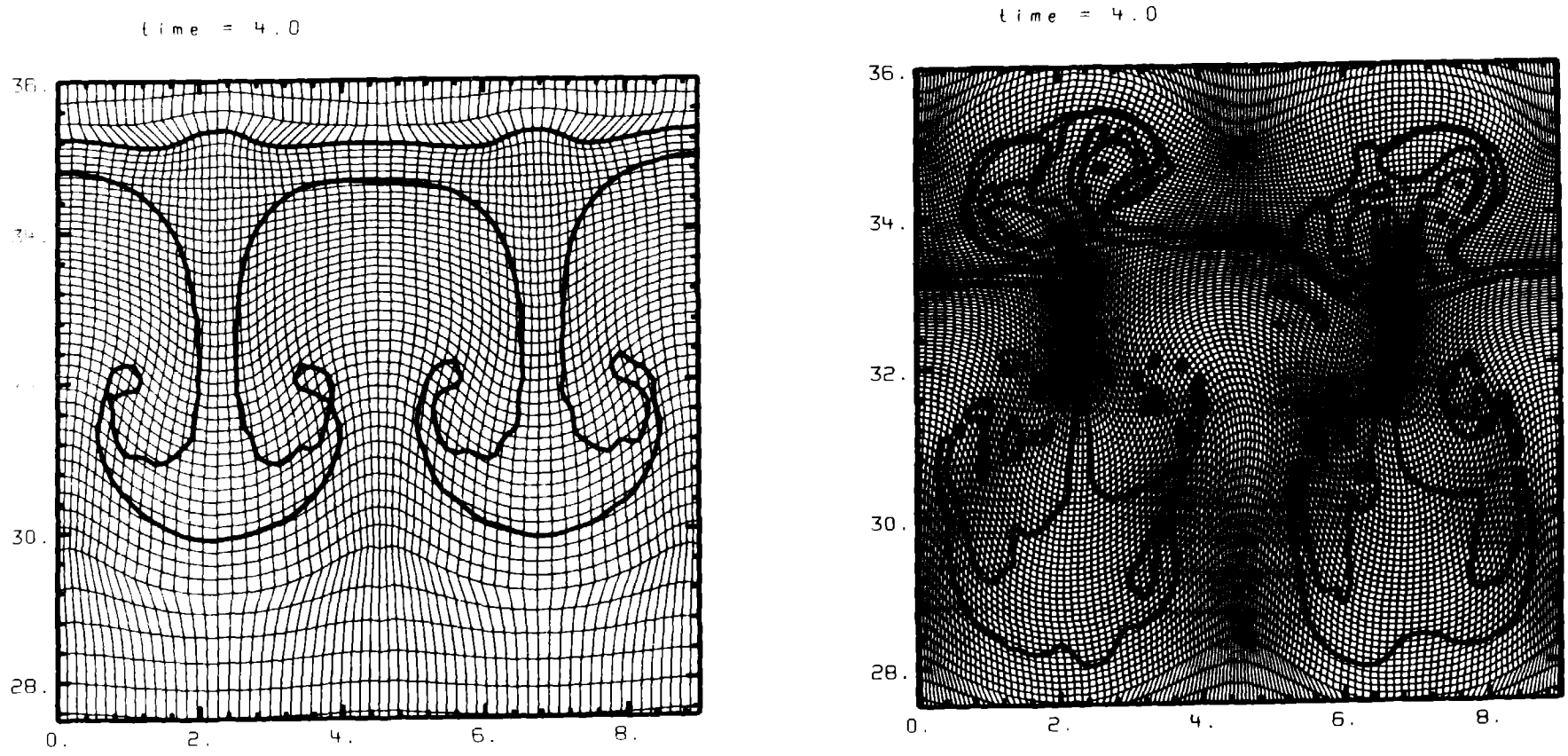

Fig. 45

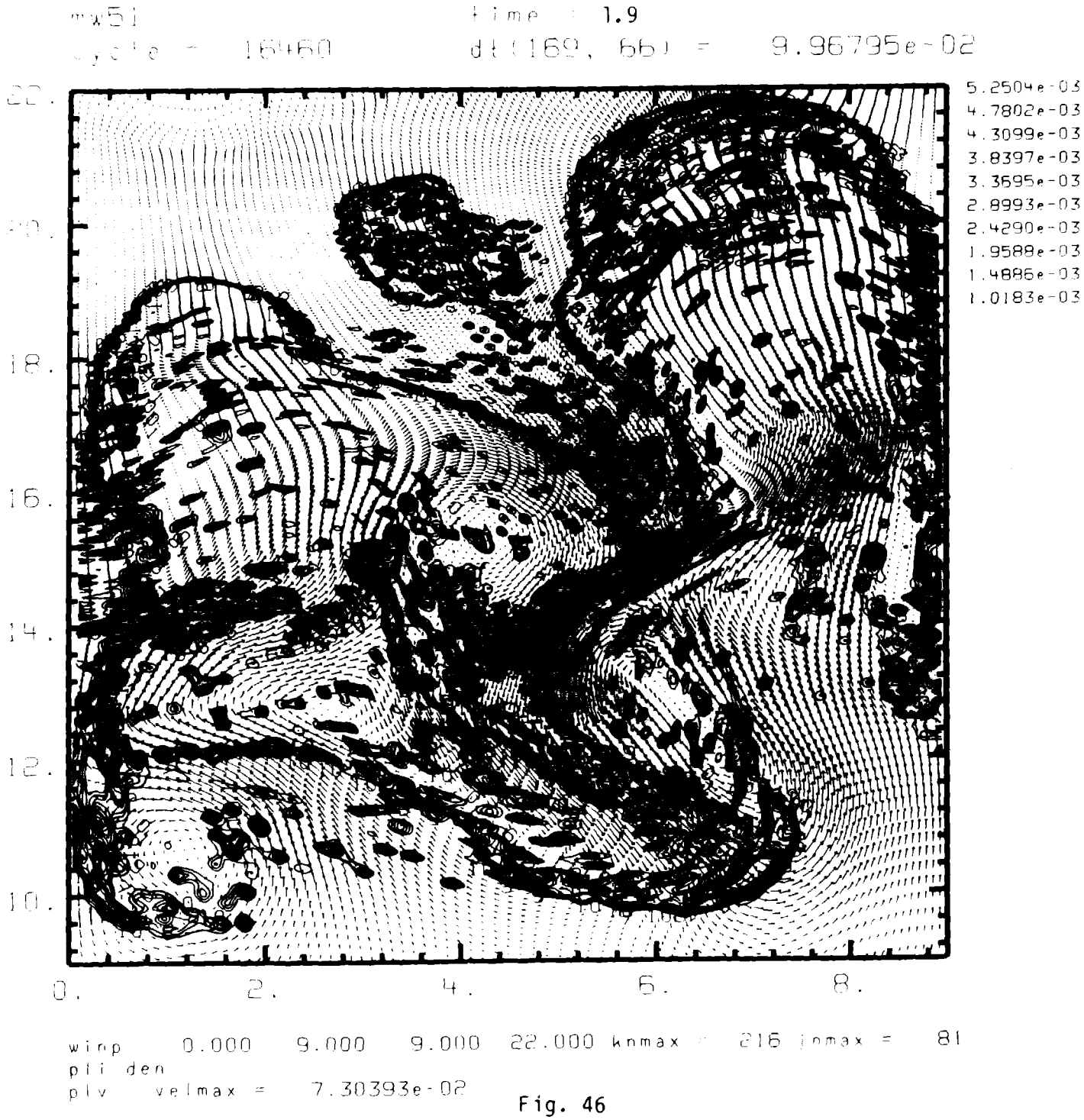
mx51
Time = 1.9
cycle = 16460
dt(169, 66) = 9.96795e-02
5.2504e-03
4.7802e-03
4.3099e-03
3.8397e-03
3.3695e-03
2.8993e-03
2.4290e-03
1.9588e-03
1.4886e-03
1.0183e-03
20.
18.
16.
14.
12.
10.
0.
2.
4.
6.
8.
winp 0.000 9.000 9.000 22.000 knmax = 216 jnmax = 81
pli den
plv velmax = 7.30393e-02

Fig. 46